UNIVERSITY OF PARMA

Department of Civil and Environmental Engineering and Architecture - DICATEA

DOCTORAL THESIS IN CIVIL ENGINEERING

PARTICLE METHOD APPROACH IN MECHANICS OF SOLIDS AND GRANULAR MATERIALS

Author:

Eng. Nicholas Corbari

Supervisor:

Prof. Roberto Brighenti

Head of Doctorate School:

Prof. Gianfranco Forlani

January 2015

ACKNOWLEDEGMENTS

I would like to thank Professor Roberto Brighenti for serving as my Ph.D. advisor. His excellent teaching skills, finite element expertise and constant encouragement have been fundamental aspects during my research work. I would also like to thank Structural Mechanics group for their support, Professor Gianfranco Forlani for his work as PhD coordinator, Professor Alessandro Tasora for his contribution during first steps of this research.

Great thanks to my friends and my work mates of Studiorinnova; Cleb's dinners have been a constant inspiration during these years.

Thanks to my parents and my brother for supporting me during all my graduate studies.

At last, the most important person during these years, my wife Giada, thanks for your support, patience and comprehension, I have a debt with you for the many "lost" weekends.

TABLE OF CONTENTS

CHAPTER 3

SOLID AND FLUID MODELLING WITH PARTICLE METHODS

CHAPTER 4

CONTACT PROBLEMS ANALYSIS IN DEM

CHAPTER 5

THE PROPOSED POTENTIAL BASED INTERPARTICLE MODEL

CHAPTER 6

NUMERICAL APPLICATIONS

CHAPTER 7

CONCLUSIONS

ABSTRACT

It is well recognized that matter has a discrete nature, but this aspect is usually considered only at the nano and microscale, on the other hand at the meso and macroscale levels compact matter is represented with a continuous model. At the macroscopic scales can be usefully adopted a discrete model of solids, without losing accuracy in the description of the main mechanical involved phenomena; when a multiscale study of solids is necessary the discrete approach, tailored to the scale of observation of interest, allows complete and exhaustive descriptions of many phenomena.

This PhD thesis presents a general computational particle method suitable for analyzing the dynamic behaviour of compact solids as well as granular matters. The particle interaction is modelled through proper force functionals related to the nature of the material being analyzed (solid, granular or their interaction); such an approach is also adopted for the boundary and for the particle-particle contacts, so a unified mechanical model can be simply adopted for the simulation of a very wide class of mechanical problems under static or dynamic conditions.

In particular the failure of brittle solids under dynamic dynamic impact can be easily predicted, avoiding the necessity of complex remeshing operations, stress field enrichment or the introduction of discontinuous displacement field, as typically required by numerical continuous approaches such as the finite element method. Moreover the discrete approach allows to simply model mechanical problems involving large displacements, friction or

frictionless interactions with elastic boundaries, fragmentation and clustering of the failed material as well as cohesion in particle-like matters.

Some examples aimed at demonstrating the versatility of the developed approach are finally presented: in particular the problems involving the failure of continuous solid elements under impact loading, confined particle flows and solid-granular materials interaction are simulated through the proposed approach and the related results are critically discussed and, when available, compared with literature data.

NOMENCLATURE

In the following the main symbols used in the present PhD thesis are listed

$a(r_{\text{infl}})$	Function of the influence radius
$A_{ij}, A_{0,ij}$	Cross section area of the truss assumed between particles i and j and its reference value, respectively
c	Coefficient of the force potential
D	Depth of the potential well
$\overline{d} = 2\overline{r} = = (d_i + d_j)/2$	Average diameter of the particles i and j
d^*	Equivalent diameter of two particles in contact
$d_i = 2r_i$	Diameter of the generic particle i
E_i	Elastic modulus of the generic particle i
$\overline{E}$	Equivalent Young modulus of the elastic contact between two particles
$E_{tot}(\mathbf{x}) = \Pi(\mathbf{x})$	Total energy of the particle system
$F(r)$	Generic force acting between a couple of particles at the distance r
$\mathbf{F}_i, \mathbf{F}_d, \mathbf{F}_b, \mathbf{F}_e$	Internal force, damping force, boundary and external force vectors, respectively
$\mathbf{F}_{T;i}$	Vector of the total force acting on the particle i

$K(s)$, K_0	Stiffness of the particles bonding and its value when $F(s)=0$
K_n	Stiffness of the particle-boundary stiffness
m_i, $\mathbf{M}$	Mass of the particle i and mass matrix
n	Exponent of the force potential
$\mathbf{n}$, $\mathbf{t}$	Unit vectors normal and parallel to the tangential plane in the contact point between a generic particle and the boundary surface, respectively
$\mathbf{P}_i$	Force vector acting on article i
$\mathbf{p}$	Unit vector identifying the direction connecting the two particles centres
R	Distance at which the potential reaches its minimum
r_{infl}	Radius of influence of a particle
$r_{ij}=\lvert\mathbf{x}_i-\mathbf{x}_j\rvert$	Generic distance between the centres of the particles *i* and *j*
r_0	Distance between the centres of the particles at which $F(r=r_0)\to-\infty$
s	Effective distance between particles' surfaces
$s'=r-(d_i/2+d_j/2)$	Distance between particles' surfaces
t	Time variable
$\mathbf{T}_n$, $\mathbf{T}_t$	Particle-boundary contact surface forces normal and parallel to the tangential plane in the contact point, respectively

w	Displaced distance of one particle into another or into the contact surface
$\mathbf{x}_i$, $\dot{\mathbf{x}}_i$, $\ddot{\mathbf{x}}_i$	Position, velocity and acceleration vector of the particle *i*, respectively
$\mathbf{x}$, $\dot{\mathbf{x}}$, $\ddot{\mathbf{x}}$	Position, velocity and acceleration vector, respectively
α	Coefficient defining the maximum co-penetration depth
γ	Thickness of a soft layer added to the boundary surface to smooth the contact forces
$\delta = \alpha \cdot \bar{r}$	Maximum co-penetration amount between two particles
Δt	Time integration step amplitude
Φ_{LJ}	Lennard-Jones interatomic potential
$\Phi(\mathbf{x})$, $\Phi_{tot}(\mathbf{x})$	Generic strain energy potential and potential of the particle system, respectively
λ_d	Damping coefficient
η	Viscosity coefficient
$\chi(w)$	Smoothing function for the force particle-boundary contact evaluation
μ_d	Coefficient of dynamic friction between particles and boundaries
μ_{md}	Coefficient of dynamic friction between particles
ν_i	Poissons ratio of the generic particle *i*

Chapter 1

OBJECTIVES AND SCOPE

1.1 Introduction

The discrete nature of matter – typically recognised at the nano and microscale – is usually replaced by a continuous model at the meso and macroscale levels. However the discrete model of solids can be usefully adopted also at the macroscopic scales, still enabling a proper description of the main mechanical involved phenomena; it can be stated that the discrete approach, tailored to the scale of observation of interest, allows the multiscale study of solids, being based on the same common approach.

The discrete element method (DEM), originally developed by Cundall and Strack (1979) has proven to be a powerful and versatile numerical tool for modeling the behavior of granular and particulate systems and also for studying the micromechanics of materials, such as soil, at the particle level. However, the method has also the potential to be an effective tool to model continuum problems, especially those that are characterized by a mechanical behavior involving the transformation from a continuum to a discontinuum (fragmentation). Such problems include failure of concrete structures,

crushing and fragmentation of rock due to blasting, fracture of quasi-brittle materials such as ceramics, etc.

1.2 Objectives

This study presents a general computational particle method suitable for analyzing the dynamic behavior of compact (continuum) solids as well as granular matters. The particle interaction is modelled through proper force functionals, related to the nature of the material being analyzed (solid, granular or their interaction); such an approach is also adopted for the boundary and for the particle-particle contacts, so a unified mechanical model can be simply adopted for the simulation of a very wide class of mechanical problems.

In discrete approaches, complex non-linear interactions between bodies and within bodies (allowed to present different shapes and properties), are numerically simulated in order to get the motion of particles described by non-linear differential equations.

In particular the failure of brittle solids under dynamic conditions can be easily predicted, avoiding the necessity of complex remeshing operations, stress field enrichment or the introduction of discontinuous displacement field, as typically required by numerical continuous approaches such as the finite element method. That is, the developed discrete element method will be used to model the static or dynamic response of materials that are initially solid and continuous, but eventually undergo fracture and become discontinuous due to fragmentation, due to extreme loading conditions.

1.3 Scope and thesis content

After illustrating the basic concepts related to the discrete nature of materials and their mechanical modelling, a unified particle-based approach, suitable for continuum solids as well for discrete incoherent aggregates, will be presented by taking into account for the dynamic nature, large displacements and large strain characteristic of the problem. Finally, some examples related to the failure of brittle solids under impact loading and granular flow will be analyzed in order to underline the capability of the proposed approach.

The obtained results, related to very different problems involving elastic-brittle solids, granular assemblies of particles or mixed cases, have shown the wide capability of the method to capture very different and complex mechanical phenomena in dynamic problems, such as elastic deformation, large strains, elastic impact, material failure, boundary contacts, crack closure, particle-particle and particles-boundary contact friction etc..

The content of this doctoral thesis is organized as follow:

Chapter 2 contains an overview on particles methods; it is a review of recent efforts of researchers in computational science for modelling and simulation of discrete or continuum mechanical behaviors of materials and structures.

In Chapter 3 the theoretical basis of discrete element simulation of solids and fluid is analyzed: the main idea is that fluids or solids can be both represented as a large number of (usually rigid) bodies (particles) that interact via forces exerted at their common contact points.

Chapter 4 describes how the Discrete Element Methods (DEM) can be formulates through a minimal set of contact models as a compromise between

a realistic and an “easy to handle” modeling approach; in some cases a single contact-model allows to simulate various systems and structures and a better and simpler contact models facilitate deeper understanding of the relation between micro and macro-properties.

In Chapter 5 the proposed potential-based inter-particle method is presented; in particular a discrete computational method for continuum materials, granular-like or mixed cases, based on the concept of force potential interaction law, for the assessment of the mutual forces exchanged by particles representing the solid, is derived in detail.

In Chapter 6 several numerical analysis simulating different problems involving compact or granular solids are illustrated.

Finally in Chapter 7 some conclusions and perspectives are drawn.

Chapter 2

OVERVIEW ON PARTICLE METHODS

2.1 Introduction

Solid and fluid mechanics focuses on the materials response to applied external loads and it is concerned with the stressing, deformation, and failure of incoherent solid materials and structures. The mechanics of fluids and solids has traditionally been founded on the principles of continuum mechanics; therefore, the physical quantities necessary to study the kinematics and force-balancing laws within the framework of continuum are displacements, strains, and stresses. The ever-increasing power of modern computers has had a remarkable impact on solid mechanics, indeed more efficient computational methodologies and accurate numerical solution of initial and boundary value problems have been major issues in the research of computational solid mechanics. More realistic and detailed descriptions of materials response, more efficient computational methodologies and accurate numerical solution of initial and boundary value problems, began in the research field of computational solid mechanics [1]. In the last thirty years many new computational methods in the field of solid and structural mechanics has been developed such as the *Finite Element Method (FEM)* [2]

and *Meshfree Particle Methods* also known as the Smoothed Particle Hydrodinamic SPH [3, 4, 5]. The fast development of these models has made them popular numerical techniques widely used in both academia and industry to solve various types of mechanics problems; also continuum-based approaches have been successful by solved for specific nano and macro-mechanics problems [3].

Continuum mechanics does not refer the discrete structure of materials at microscopic length scales; the fundamental postulate of continuum mechanics assumes that materials are continuously divisible and the mechanical deformation and failure of many engineering materials have inherently a multiscale nature, in that processes, which occur on many different length and timescales, govern the observed macroscopic material behavior. At the smallest length scale, quantum mechanical interactions and atomic structure provide an underlying framework for the elastic deformation of materials and, more importantly, for the formation of a wide variety of defects in otherwise crystalline solids. There is an intimate coupling between long-range scale problems defects at the atomic-scale, although theories at higher length scales attempt to subjugate the smaller scale phenomena into ‘effective’ properties or ‘constitutive rules’; however macroscopic phenomena of prime interest in material applications such as fracture and fatigue degradation, strictly depend on the details of smaller scale phenomena. On the other side, full atomistic description of individual defects alone does not permit to understand macroscopic behavior, since the higher scale defect interactions, collectively operate to drive large-scale behavior. Realistic methods and approaches for properly coupling different length scales is a great challenge for computer simulations.

This chapter is a review of recent research efforts in computational science for discrete or continuum based modelling and simulation of mechanical behaviors of materials.

Computational methods related to atomistic/continuum coupling are based on the determination of the total potential energy of a system as a function of its degrees of freedom. It is possible to find the static equilibrium state, by minimizing the total energy or finding the zero force position for every degree of freedom (dof), where the derivative of the total energy with respect to the dof coordinate represents the force related to a dof. Finally, it is worth mention that at the heart of dynamics simulations is the Newton's second law to study the evolutions of the system in the time domain.

2.2 Atomic scale models

Quantum mechanics governs energetics at the atomic-scale; atomistic total energy calculations provide the energy as a function of the collective nuclear coordinates, which are also the degrees of freedom in an atomic-scale calculation. The energy functional is minimized with respect to the electronic degrees of freedom for fixed nuclear coordinates. The force on an individual nucleus can then be obtained by taking the derivative of the total energy with respect to the desired nuclear coordinate. Atomic simulations, such as molecular dynamics (MD) and molecular mechanics (MM) are based on the assumption that atoms are the smallest unit need to be modeled.

The field of molecular dynamics has developed into a sophisticated analysis methodology for simulating atomic-scale processes of different material types. MD Methods provide a mean for simulating those processes involved in material failure, such as void nucleation and dislocation formation

and interaction that form the foundation of a 'bottom-up' multiscale analysis methodology.

MD simulations represent individual atoms as point masses that interact with near atoms through ad hoc force fields. The most refined description utilizes quantum theory that can be applied using some well-known physical constants such as the velocity of light or charges of nuclear particles and differential relationships to directly calculate molecular properties and geometries. Obviously, the computational demands are high and only a relatively small number of atoms can be analyzed.

For larger atomic aggregates, empirical and semi-empirical potential functions have been developed to approximate atomic force fields. This approach to MD replaces quantum mechanics with classical Newtonian mechanics to predict the trajectories of individual atoms. Newton's second law is expressed as:

$$\boldsymbol{F}_{\mathrm{i}} = m_i \boldsymbol{a}_i \tag{2.1}$$

for each atom *i*, in a system constituted by *N* atoms. Here m_i is the atomic mass, $\boldsymbol{a}_i$ is the acceleration vector and $\boldsymbol{F}_{\mathrm{i}}$ is the resultant force acting on the i^{th} atom due to the interactions with other neighboring atoms. The force can also be expressed as the gradient of the potential energy, *V*, as

$$\boldsymbol{F}_{\mathrm{i}} = -\nabla V \tag{2.2}$$

At the atomic-scale, energetic aspects (governed by quantum mechanics), are function of the collective nuclear coordinates, which are the degree of freedom at this length scale. Quantum effects can be best described using, for

example, the Density Functional Theory [6-7] or the Tight Binding Method [8].

2.2.1 The Density Functional Theory

Density Functional Theory, formulated by Hohenberg and Kohn [6] and Kohn and Sham [7] in the 1960's, expresses the total energy of a system as a functional of the total electron density; it calculates the total electronic energy by considering the entire electrons system as a whole. The ground state energy of many-electron system is a unique functional of the electronic density of the type:

$$E = T[\rho(\mathbf{r})] + V_c[\rho(\mathbf{r})] + E_{xc}[\rho(\mathbf{r})] \tag{2.3}$$

where T and V_c are known functionals, corresponding to kinetic energy of electrons and the potential energy of electron-nucleus (or electron-ion) and nucleus-nucleus (or ion-ion) Coulomb interactions, respectively. For large many-electron atoms, only the outer (valence) electrons are usually considered to contribute to the electronic density of interest, while core electrons and the nucleus are treated together as an ion. In this case, the corresponding electron-ion and ion-ion interaction energies are employed for deriving the *Vc* term.

2.2.2 The Tight-Binding Method

Tight-Binding Method, frequently used in mechanical problems, is a semi-empirical method since such application operates by approximations and some parameters need to be well controlled.
This method derives from the method of Linear Combination of Atomic Orbitals (LCAO), proposed by Bloch [8]. The objective of the method is to construct an approximate wave function of a single electron used to obtaining approximate trial functions for the corresponding many-electron systems. Tight-Binding method permits the study of inorganic materials including atomic and electronic structure of surfaces and the interplay between structural and electronic problems.

This method permits to calculate properties of materials, structures, energies, electronic states, charge distributions, spin distributions as ab initio methods do, but it is computational much less demanding; obviously accuracy is reduced by an order of magnitude compared with more precise ab initio methods.

Density Functional Theory and *Tight-Binding Method* are capable of capturing the physics of the problem at the atomic level; in quantum simulations of nano-materials, the force on an individual nucleus is the derivative of the total energy with respect to the desired nuclear coordinate. From a materials nanomechanics point of view, the quantum mechanics total energy calculation is also of central importance because it is possible to study various structural and mechanical properties of materials such as defect structures, grain boundaries, impurities and surfaces.

2.2.3 Empirical Interatomic Potentials

The study of energetic problems at the atomistic scale can be faced adopting classical potentials models, typically used in MD, or quantum mechanics. An important difference between total atomic energy obtained from classical potential and quantum mechanics is that classical potentials models admit the form:

$$E^a = \sum_i E_i \tag{2.4}$$

where E_i is the energy of the i_{th} atom, so the energy is expressed as a sum of individual atom energies. On the other hand, quantum mechanical description of the total energy cannot be partitioned into energies on a per-atom basis. For example fracture problems at atomistic scale, requires an understanding of the bonding between atoms and the simulation must accurately describe the interatomic bonding. Since the bonding is mediated by the valence electrons, a quantum-mechanical (QM) description would be the most accurate, but the computational cost limits such methods to a few thousand atoms for dynamic simulations.

Classical Empirical Potential (EP) simulations, that approximate the interatomic interactions without an explicit QM description, can simulate millions of atoms; obviously, EPs are less accurate than QM to describe the bond breaking process. Most used molecular level continuous potentials are the Morse Potential and the Lennard-Jones Potential.

The Morse – Potential, is an empirical potential that describes covalent bond between a couple of atoms. Its analytic form is:

$$V_M(r) = D_0[1 - e^{-a(r-r_0)}]^2 \tag{2.5}$$

where D_0 is the dissociation energy and r_0 the equilibrium distance, which corresponds to the minimum of the potential function.

This potential is used when interatomic distances are near to equilibrium distance. The research of equilibrium distance, r_0, corresponding of the energy minimum, needs the calculation of the first potential derivative.

$$\frac{dV_M(r)}{dr} = 2D_0[1 - e^{-a(r-r_0)}]^2 a e^{-a(r-r_0)} \tag{2.6}$$

This expression represents the force between atoms obtained by deriving the potential.

First applications of *Lennard – Jones Potential* was in chemistry problems of Van der Waals interactions between atoms. It is an isotropic potential, dependent only by the distance (r) between atoms and is defined as the sum of two terms, one attractive proportional to r^{-6}, one repulsive proportional to r^{-12}.

At shortest interatomic distances ($r \to 0$) repulsive term prevail, while attractive term prevail for long distances ($r \to \infty$); there is an equilibrium distance, r_0, where potential energy is lower and reach the minimum. The classical form of this L-J potential is:

$$V_{LJ}(r) = D_0 \left[\left(\frac{r_0}{r}\right)^{12} - \left(\frac{r_0}{r}\right)^{6} \right] \tag{2.7}$$

where, as for the Morse-Potential, D_0 is the dissociation energy and r_0 the equilibrium distance.

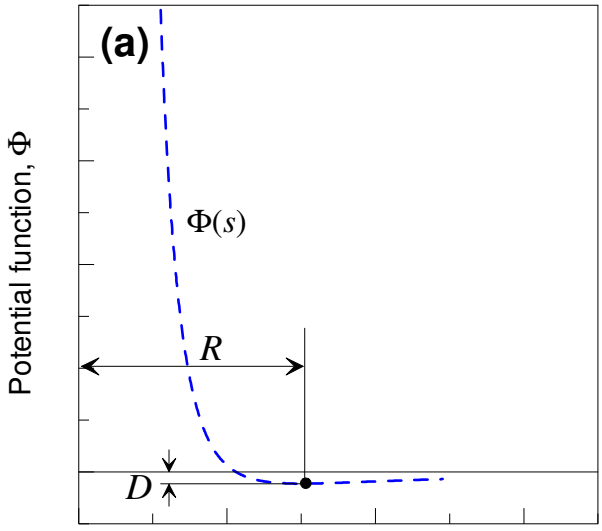

Figure 2.1– Lennard – Jones Potential $\frac{r_0}{r^{12}}$ *represents repulsive term* $\frac{r_0}{r^6}$ *represents attractive term.*

2.3 Mesoscopic models

A widely used mesoscopic model is the discrete element method (DEM). The elementary units of granular materials are mesoscopic grains, which deform under stress. A discrete element simulation consists of a large number of bodies, usually assumed as rigid, that interact via forces exerted at their common contact points. By definition the "discrete element method applies

to a computer program only if it allows finite displacements and rotations of the discrete bodies, including complete detachment, and recognizes new contacts as the calculation progresses."[9]

Recent theoretical models [10] use molecular dynamics approach to study different scale problems, establishing relations between the microscopic quantities of the model and the macroscopic mechanical properties.

DEM is applied in different application fields, ranging from rock mechanics to computer graphics, molecular dynamics (MD) etc, in which classical Newtonian mechanics is the base to predict the dynamic of individual elements. The dynamic behavior of DEM is usually described through time-stepping algorithms; at every time step the movement of every single particle and the contact forces between particles are calculated.

DEM simulations can provide dynamic information, such as the trajectories and transient forces acting on individual particles; most common types of DEMs used are the *soft-particle* and the *hard-particle* approaches.

The *soft-sphere method,* originally developed by Cundall and Strack [11], was the first granular dynamics simulation technique published in the literature; they introduced this method to analyze the behavior of soil by using two dimensional disc elements in the numerical scheme. In such an approach, particles are permitted to suffer minute deformations, and these deformations are used to calculate elastic, plastic and frictional forces between particles. The motion of particles is described by the well-established Newton's laws of motion. A characteristic feature of the soft-sphere models is that they are capable of handling multiple particle contacts, which are of importance when modelling quasi-static systems.

In a *hard-particle simulation*, a sequence of instantaneous collisions is processed and the forces between particles are not explicitly considered.

Therefore, typically, hard-particle method is most useful in rapid granular flows.

In a granular flow, a particle can have two types of motion: translational and rotational. The particle may interact with its neighboring particles or walls and eventually interact with its surrounding fluid during its movement, through which the momentum and energy are exchanged. The particles and fluids of the domain influenced this movement by not only the forces and torques originated from its immediate neighboring particles and eventually the surrounding fluid, but also through the propagation of disturbance waves that involve also particles far away.

In DEM approach, this problem can be solved by choosing a numerical time step less than a critical value so that during a single time step the disturbance cannot propagate from the particle and fluid farther than its immediate neighboring particles and closest region of fluid.

Thus, at all times the resultant forces on a particle can be determined exclusively from its interaction with the contacting particles and neighbor fluid for a coarse particle system. For a fine particle system, non-contact forces such as the van der Waals and electrostatic forces should be also included. Based on these considerations, Newton's second law of motion can be used to describe the motion of individual particles. The governing equations for the translational and rotational motion of particle i with mass m_i and moment of inertia I_i are*:*

$$m_i \frac{d\mathbf{v}_i}{dt} = \sum_j \mathbf{F}_{ij}^c + \sum_k \mathbf{F}_{ik}^{nc} + \mathbf{F}_i^f + \mathbf{F}_i^g \tag{2.8}$$

$$I_i \frac{d\omega_i}{dt} = \sum_j \mathbf{M}_{ij} \tag{2.9}$$

where $\mathbf{v}_i$ and ω_i are the translational and angular velocities of particle *i,* respectively, $\mathbf{F}_{ij}^c$ and $\mathbf{M}_{ij}$ are the contact force and torque acting on particle *i* due to particle *j* or walls, $\mathbf{F}_{ik}^{nc}$ is the non-contact force acting on particle *i* by particle *k* or other sources, $\mathbf{F}_i^f$ is the particle-fluid interaction force on particle *i,* and finally $\mathbf{F}_i^g$ is the gravitational force.

2.4 Multi-scale models

Multi-scale models involve methods from different scientific disciplines to bridge the wide range of time and length scales that are inherent in a number of essential phenomena and processes in materials science and engineering (Fig.2.2). Approaches over many scales a time and space are used to describe a multitude of materials-related phenomena.

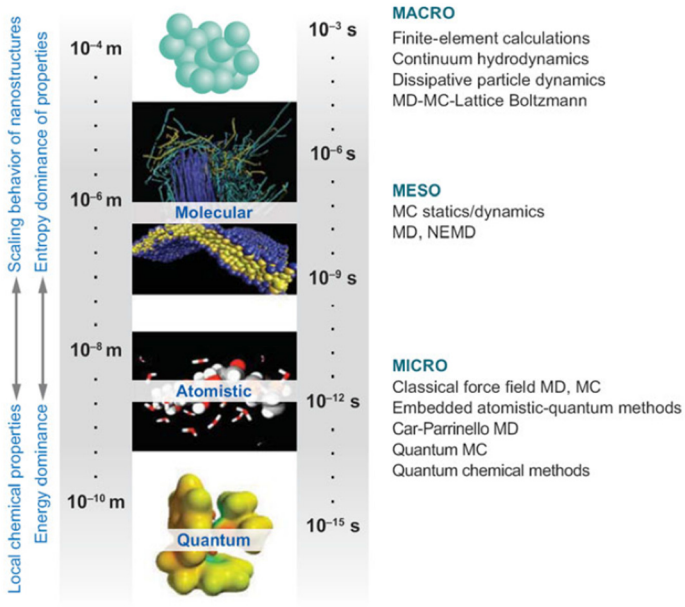

Figure 2.2 –Examples of the different time and space scales in the study of solids (from[12]).

In this approach, models that best simulate the relevant physics at lower length scales are united with models at larger length scales, through information transfer involving averaging, homogenization, or superposition schemes. The ultimate success of this approach is dependent on the accuracy of data linkage and the intrinsic fidelity of the physical models used. Multiscale methodologies relate material over a range of length scales; they are founded on different physics-based models, able to appropriately represent damage mechanisms at each scale, linking larger length scales models with lower length scales(Fig.2.3).

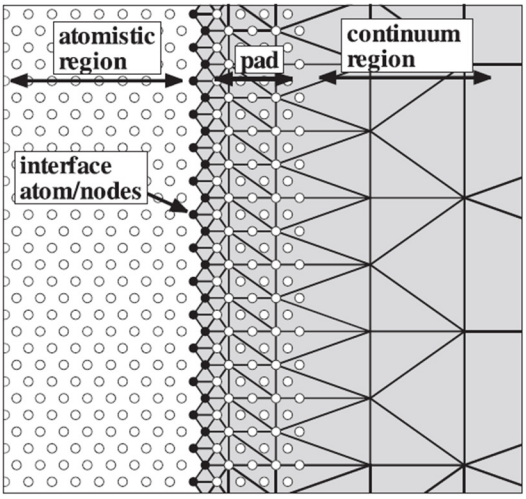

Figure 2.3 –General scheme of coupled atomistic/continuum region (from [12]).

Multiscale approaches usually focus on mechanisms involved in the initiation and evolution of damage and allow a more complete understanding of physics of fracture [4]. Nanoscale methods (*Ab Initio, Tight-Binding TB, Density-Functional Theory DFT, Molecular Dynamics MD, and Molecular Statistics MS* [3]) predict, by using basic physics principles, deformation and fracture processes at the atomistic level. The analysis of a suitable domain in real applications by using only nanoscale methods, in most applications, could reach an upper computational bound for practical analysis. In opposite, continuum methods, like FEM, enable to represent materials behavior at length scale with lower computational cost, but with continuum assumptions.

Multiscale methods may be classified into two categories:

1) *Sequential methods* that use average physical parameters as initial conditions or supply calibrated material constants to another separated

model. Using separated material models, the advantage is that every model has his own length and time scale.

2) *Concurrent methods* are based on the contemporary solution of strongly linked material models. Generally, there exists two domains that describe materials at the atomic level and continuum representation respectively. Between the two domains is collocated an intermediate region where continuum and atomic discretization are overlapped through "pad" atoms/nodes in which different coupling schemes are used. In heterogeneous materials sequential methods the use of different constitutive laws at different scales is adopted; total material deformation, stress and strain con be subdivided in coarse macro-component and fine micro-component. Usually the approach of concurrent methods is to identify a small region of the simulated system where the material is studied at the atomic level; this region is linked with the larger one, where material is represented at the continuum level. To obtain a successful coupling between atomistic and continuum region, it is necessary to refine the continuum representation down to the atomic scale by superposing each node over an atom at the interface region.

2.4.1 The Macroscopic, Atomistic, Ab initio Dynamics methods

The Macroscopic, Atomistic, Ab initio Dynamics (MAAD) procedure was developed by Broughton et al. [13], Abraham et al. [14-17], and Shen et al. [18-19] to simulate fracture; it combines ab initio quantum analysis, molecular dynamics, and finite element continuum models.

For example, in order to study the problem of fracture, bond breakage are predicted at the crack tip by using Ab initio analyses based on Tight-Binding (TB), molecular dynamics (MD) based on empirical force potentials to model the crack wake and surrounding atomic lattice, while finite element (FE) model is used to simulate the far field material. The FE nodes correspond in a one-to-one manner with the interface atoms of the MD region.

Therefore, it was deemed necessary to include a quantum mechanical approach into the simulations for a small region in the immediate neighborhood of the crack tip, where bond breaking is prevalent during fracture, while far away from this region the empirical potential description is adequate.

The spatial decomposition of the computational cell produces five different dynamic regions of the simulation: the continuum FE region at the far-field, where the atomic displacements and strain gradients are small; the atomistic MD region around the crack with large strain gradients but with no bond breaking; the quantum mechanical region (labelled TB because of the use of the tight-binding method) right at the crack tip where atomic bonds are being broken and formed; the FE/MD hand-shaking region; and the MD/TB hand-shaking region. The total Hamiltonian, H_{tot} for the entire system is:

$$\begin{aligned} H_{tot} = {} & H_{FE}(\{\mathbf{u}, \dot{\mathbf{u}}\} \in FE) + H_{MD}(\{\mathbf{r}, \dot{\mathbf{r}}\} \in MD) + \\ & + H_{TB}(\{\mathbf{r}, \dot{\mathbf{r}}\} \in TB) + H_{FE/MD}(\{\mathbf{u}, \dot{\mathbf{u}}, \mathbf{r}, \dot{\mathbf{r}}\} \in FE/MD) + \\ & + H_{FE/MD}(\{\mathbf{r}, \dot{\mathbf{r}}\} \in MD/TB) \end{aligned} \tag{2.10}$$

The degrees of freedom of the Hamiltonian are the atomic positions $\mathbf{r}$ and velocities $\dot{\mathbf{r}}$ for the TB and MD regions, and displacements $\mathbf{u}$ and their time rates of change $\dot{\mathbf{u}}$ for the FE regions. Equations of motion for all the relevant variables in the system are obtained by taking appropriate derivatives of this Hamiltonian.

All variables can then be updated in lock step as a function of time by using the same integrator. Thus, the entire time history of the system may be obtained numerically once an appropriate set of initial conditions is given. Following trajectories dictated by this Hamiltonian leads to the evolution of the system with conserved total energy, which ensures numerical stability.

This kind of discretization has two main problems: one is the expensive computational cost and the other is the lack of damping, needed to remove spurious reflections at the interface between the three regions.

2.4.2 The Finite Element-Atomistic method

The Finite Element-Atomistic (FEAt) method developed by Kohlhoff et al. [20], Gumbsch and Beltz [21], and Gumbsch [22] is a methodology similar to MAAD approach that links atomistic representation to a continuum finite element discretization.

This method is based on the decomposition of a crystal into a (generally) three different domains: a lattice region with fully atomistic resolution, where interatomic potentials are employed; a continuum region discretized by finite elements; between continuum domain and atomistic domain a region, called "*pad region"*, in which individual atoms are directly linked to finite element nodes (Fig.2.4).

In FEAt, the coupling condition is on the force level, whereas other concurrent multiscale methods perform the coupling on the energy level. To define these coupling conditions in a consistent fashion, the elastic energy $E = \hat{E}(\varepsilon)$ is expanded into a Taylor series about the state of zero strain under the assumption of zero stress,

$$E(\varepsilon) = E(0) + \frac{\partial E}{\partial \varepsilon_{ij}} + \frac{1}{2}\frac{\partial^2 E}{\partial \varepsilon_{ij}\partial \varepsilon_{kl}}\partial \varepsilon_{ij}\partial \varepsilon_{kl} + \\ + \frac{1}{6}\frac{\partial^3 E}{\partial \varepsilon_{ij}\partial \varepsilon_{kl}\partial \varepsilon_{mn}}\partial \varepsilon_{ij}\partial \varepsilon_{kl}\partial \varepsilon_{mn} + \ldots.. \tag{2.11}$$

For the stresses continuity, the strains and all coefficients in this series must be equal in the atomistic region and in the continuum. Since the strains have been made equal by means of the strong compatibility of displacements, equality of the stresses implies, that the elastic constants of the continuum are equal to those defined by the interatomic potential in the atomistic region ,

$$\mathbb{C}_{ij} = \frac{\partial E}{\partial \varepsilon_{ij}} \quad , \quad \mathbb{C}_{ijkl} = \frac{\partial^2 E}{\partial \varepsilon_{ij}\partial \varepsilon_{kl}} \quad , \quad \mathbb{C}_{ijklmn} = \frac{\partial^3 E}{\partial \varepsilon_{ij}\partial \varepsilon_{kl}\partial \varepsilon_{mn}} \tag{2.12}$$

Since the reference state of the series in Eq.(2.11) is a homogeneous deformation, $\varepsilon = 0$, it is indeed permissible to assign to the continuum the second and higher order elastic constant as defined by Eq.(2.12), derived from the interatomic potential. The first-order elastic constants in the continuum are zero by definition, which imposes the restriction on the potential that must provide zero stress in a perfect lattice. Within the framework of local and linear elasticity theory, equilibrium between the lattice and the FE continuum is fulfilled, if terms up to the second order are matched. FEAt accounts for elastic nonlinearity in that, additionally, elastic constants of third order, are adopted as well.

These approaches have been successfully applied to the problem of crack propagation but the direct atom to node linkage at the MD-FEM interface gives rise to undesirable phonom reflection.

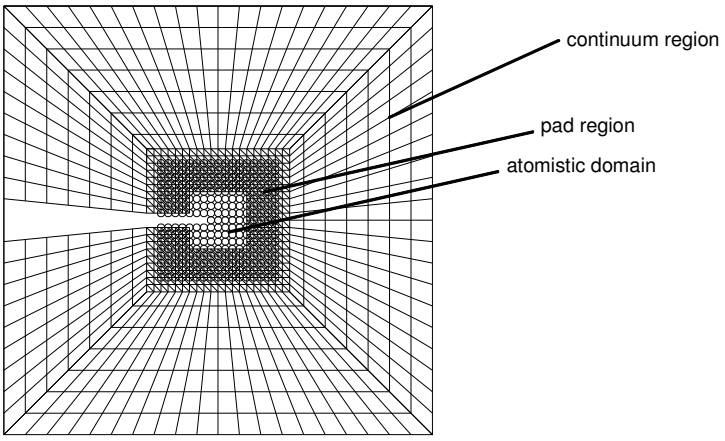

Figure 2.4 – FEAt model of a crack tip in an fcc crystall (from Gumbsch and Beltz [21]*)*

2.4.3 The Coarse Grained Molecular Dynamics method

A generalized formulation of conventional FEM utilizes FEM nodes superposed over the entire material domain to develop another computational scheme for atomistic-continuum coupling called Coarse Grained Molecular Dynamics (CGMD) developed by Rudd and Broughton [23,24].

According to this method, in the molecular dynamics (MD) refined region, atoms and nodes correspond in a one-to-one fashion; in the coarse-grained (CG) finite element region the finite element mesh is coarsened with individual nodes associated with many atoms. In this way, the computational cost of representing the entire material is reduced. Dynamic problem in the MD region is solved by using the integrated equations of motion for each atom, while the kinematics of the nodal degrees of freedom in the CG region are obtained by using the standard equations of continuum FEM approach.

The key point of this effective model is that the equations of motion for the nodal (mean) fields are *not* derived from the continuum model, but from

the underlying atomistic model. The nodal fields represent the average properties of the corresponding atoms, and equations of motion (in this particular case the Hamilton's equation) are constructed to describe the mean behavior of underlying atoms.

One important principle of CGMD is that the classical ensemble must obey the constraint that the position and momenta of atoms are consistent with the mean displacement and momentum fields. To be specific, let the displacement of atom μ be $\mathbf{u}_\mu = \mathrm{x}_\mu - \mathrm{x}_{\mu 0}$ where $\mathrm{x}_{\mu 0}$its equilibrium position is. The displacement of mesh node j is an average of the atomic displacements

$$\mathbf{u}_j = \sum_\mu f_{j\mu} \mathbf{u}_\mu \tag{2.13}$$

where $f_{j\mu}$ is a weighting function, a microscopic interpolating functions analog to the FE approach. Note that Latin indices, $j,\ k$ denote mesh nodes and Greek indices, $\mu,\ \nu$, denote atoms; a similar relation holds for the momenta $\mathbf{p}_\mu$. Since the nodal displacements are less than or equal to the number of atomic positions, fixing the nodal displacements and momenta, does not necessarily determine the atomic positions entirely. Therefore some subspace of phase space remains not sampled, which corresponds to the degrees of freedom that are missing from the mesh points. The coarse-grained energy is defined as the average energy of the canonical ensemble on this constrained phase space:

$$E(\mathbf{u}_k, \dot{\mathbf{u}}_k) = \langle H_{MD} \rangle_{\mathbf{u}_k, \dot{\mathbf{u}}_k} = \int d\mathrm{x}_\mu d\mathrm{p}_\mu H_{MD} e^{-\beta H_{MD}} \Delta / Z$$

$$\Delta = \prod_j \delta\left(\mathrm{u}_j - \sum_\mu \mathrm{u}_j f_{j\mu}\right) \delta\left(\dot{\mathrm{u}}_j - \sum_\mu \frac{\mathrm{p}_\mu f_{j\mu}}{m_\mu}\right) \tag{2.14}$$

where $\beta = 1/(k_B T)$ is the inverse temperature and Z is the partition function. The 3-D delta function $\delta(\mathbf{u})$ enforce the mean field constraint (Eq. 2.14). When the mesh nodes and the atomic sites are identical, the CGMD equations of motion agree with the atomistic equations of motion. As the mesh size increases some short-wavelength degrees of freedom are not supported by the coarse mesh. Nevertheless, these degrees of freedom not neglected entirely, because their thermodynamic average effect has been retained. This approximation is expected to be good if the system is initially in thermal equilibrium, and the missing degrees of freedom only produce adiabatic changes of the system.

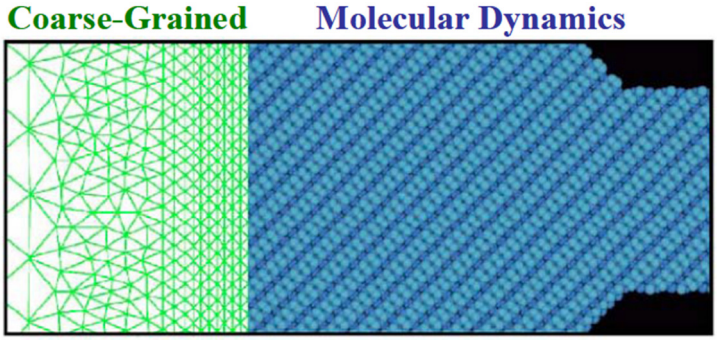

Figure 2.5 –GC and MD regions in the CGMD approach (from Rudd and Broughton [23]*).*

2.4.4 The Quasicontinuum method

The Quasicontinuum (QC) method was originally formulated by Tadmor et al. [25] to provide a direct coupling of an atomistic region to a continuum domain; additional developments to the model have been presented by Knap and Ortiz [26].

The essential building blocks of the static quasicontinuum model are: (1) the constrained minimization of the atomistic energy of the solid; (2) the use of summation rules to compute the effective equilibrium equations; and (3) the use of adaptation criteria in order to tailor the computational mesh to the structure of the deformation field. An extension of the method to finite-temperature has also been proposed [27].

The material domain is fully described at the atomistic scale by introducing "representative atoms" or "repatoms"; this kind of atoms have a dual role in defining either "nonlocal" individual atoms that are subjected to a force environment of neighboring atoms, or "local" atoms that operate similarly to continuum finite element nodes. The partitioning of the QC region into local continuum regions and MD domains is shown in Fig. 2.6. Deformation gradients over local atomistic domains are calculated and, if small enough, allow the application of the Cauchy-Born rule [28] to be performed in which kinematic constraints, similarly to finite element shape functions are enforced on clusters of atoms that are considered as a local continuum. Remeshing is constantly performed to update the model in order to resolve atomic scale detail and to redefine continuum atomic subdomains, where deformation gradients are small and can be grouped to minimize computational cost.

The quasicontinuum model starts from a conventional atomistic description that computes the energy of the solid as a function of the atomic positions. The configuration space of the solid is then reduced to a subset of

representative atoms. The positions of the remaining atoms are obtained by piecewise linear interpolation of the representative atom coordinates, in the same manner as displacements field is constructed in the FE method. The effective equilibrium equations are then obtained by minimizing the potential energy of the solid over the reduced configuration space. A direct calculation of the total energy in principle requires the evaluation of sums that are extended over the full collection of atoms, namely,

$$E_{tot} = \sum_{i=1}^{N} E_i, \tag{2.15}$$

where N is the total number of atoms in the solid. The full sums may be avoided by the introduction of approximate summation rules; for example, the lattice quadrature analog of Eq.(2.15) can be written as

$$E_{tot} \approx \sum_{i=1}^{N_r} n_i \overline{E}_i, \tag{2.16}$$

where n_i is the quadrature weight that signifies how many atoms a given representative atom stands for the description of the total energy, and $\overline{E}_i$ is the energy of *i*-th representative atom. Note that in this case the sum is over N_r representative atoms only. In the quasicontinuum approach, the FE method serves as the numerical tool for determining the displacement fields, while an atomistic calculation is used to determine the energy of a given displacement field. The positions of the coarsegrained atoms are needed because the energy of the representative atoms depends on them. This approach is in contrast to standard FE schemes, where the constitutive law is introduced through a phenomenological model. The selection of the representative atoms may be

based on the local variation of the deformation field. The method can be used in 2D problems.

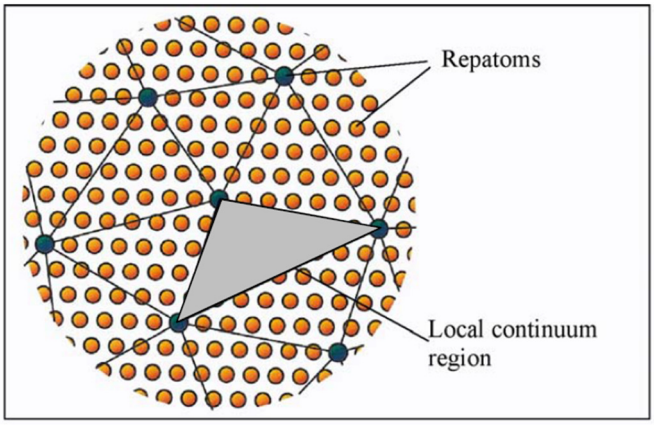

Figure 2.6 – Repatoms used to define individual atoms and local continuum regions in the QC method. (from Knap and Ortiz [26])

Spurious "ghost forces" are present at the interface and special treatments are necessary to remove them.

2.4.5 The Coupled Atomistic/Discrete Dislocation method

The Coupled Atomistic/Discrete Dislocation (CADD) method developed by Shilkrot et al. [29,30], Curtin and Miller [31], Shilkrot et al. [32], and Shiari et al. [33] can be used for problems in which dislocation formation and interaction are the physical mechanisms of interest and persist over long distances.

The interface region between MD and FEM is similar to the MAAD and FEA methods; a detection band is created near MD-FEM interface to determine the type of dislocation entering the continuum. The detection scheme is shown in Fig.2.7 where, for 2D dislocations, active slip planes are separated by relative angles equal to $\pi/3$.

Because the material is assumed to be linear elastic, a superposition can be made to decompose the continuum into an infinite domain that contains the long–range singular dislocation stress fields, represented by dislocation dynamics methods and a finite domain region that contains smooth displacement fields represented by FEM.

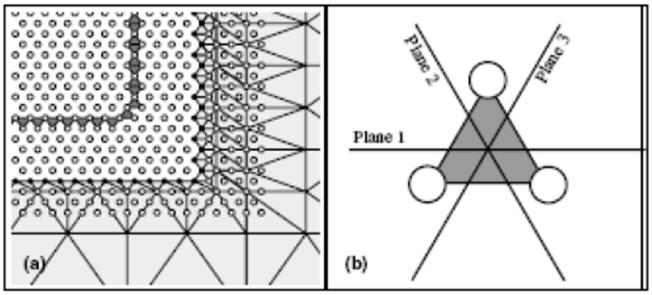

Figure 2.7 – Close-up of dislocation detection and near interface (from Shilkrot et al. [32]).

Full atomic simulation is not required because the dislocations are represented analytically, and it allows a significant improvement in modeling efficiency. A one-to-one node-atom linking is used in the transition between the atomic and continuum finite element domains; this method links directly the interface atoms to the nodes in the continuum. Pad atoms are superposed with continuum elements and are connected to nodal displacements in an extension of the atomic region into the continuum. The atoms in the extension minimize the effect of the free surface on the interface atoms, but they contribute to increase a modelling error by introducing nonphysical stiffness along the interface.

The interatomic interactions in the one-dimensional chain of atoms are assumed to be represented by linear springs connecting first and second neighbors along the chain. The presence of second-neighbor interactions

constitutes the non-locality of the atomic problem. The stiffness constant for first-neighbor interactions is denoted as k_1 and that for second-neighbor interactions as k_2 A zero-force spring length a is assumed for the near neighbor springs and $2a$ for the second neighbor springs. Thus, the unstressed reference crystal corresponds to a chain of atoms with lattice constant a. The energy functional for the chain of atoms can be written in terms of the displacements u_i of the atoms measured from their original lattice sites as

$$E^a = \sum_i E_i^a \tag{2.17}$$

where $E_i^a = \frac{1}{2}\left[\frac{1}{2}k_1(u_i - u_{i-1})^2 + \frac{1}{2}k_1(u_{i+1} - u_i)^2 + \frac{1}{2}k_1(u_i - u_{i-2})^2\right]$ with factor ½ accounting for double counting of spring energies in the sum over Eq. (2.15).

An appropriate continuum model of the one-dimensional chain is constructed by considering elastic energy density functional of the form

$$W = \frac{1}{2}C_c\varepsilon^2 \tag{2.18}$$

where C_c is the appropriate elastic constant and ε is the strain. In the one-dimensional chain with each atom corresponding to a continuum node, the strain between nodes i and $i-1$ is $\varepsilon = (u_i - u_{i-1})/a$, so the energy of element i can be written

$$E_i^C = \frac{1}{2}k_c(u_i - u_{i-1})^2 \tag{2.19}$$

where k_c is the effective stiffness of the element. To determine a proper value for k_c, considering a state of uniform deformation, the energy of the continuum system is matched to that of the fully atomistic system. So we can get

$$k_c = k_1 + k_2 \tag{2.20}$$

By using the stiffness k_c, the continuum model can predict perfectly the behavior under any uniform applied load. The total continuum energy is then

$$E^c = \sum_i E_i^C \tag{2.21}$$

In the CADD model, the transition region contains the pad atoms $I+1$ and $I+2$ are not connected to the corresponding continuum nodes $I+1$ and $I+2$; they are extra degrees of freedom in the problem. The energy for the entire problem is written as

$$E_{CADD} = \sum_{i \le I+2} E_i^a + \sum_{i \ge I} E_i^c \tag{2.22}$$

which is minimized with respect to the real atoms positions, the two pad atoms, and all the continuum nodes

CADD is currently restricted to simulating dislocations in two dimensions.

2.4.6 The Equivalent Continuum Model

A combined MD and Equivalent Continuum Model (ECM) method has been developed by Shen and Atluri [18], it is similar to the Quasi-continuum methods, but uses the meshless local Petrov-Galerkin (MLPG) representation to link the MD and ECM regions.

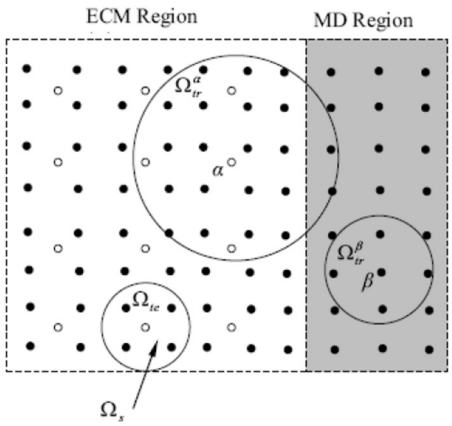

Figure 2.8 – Depiction of ECM and MD region in the MLPG approach MD-FEM cupling (from Shen and Atluri [18]).

Generally, the Finite Element Method has some disadvantages as the need for remeshing in large deformation problems or the need to interpolate discontinuous secondary variables across interelement boundaries; to overcome this kind of problems, meshless method has been developed. The Cauchy-Born hypothesis is applied in the ECM region for determining the elastic properties of the continuum from the atomistic description of the system.

As shown in Fig. 2.8, in the MD region the solid points represent atoms, while in the ECM region, the solid points represent atoms and the open points represent nodes used in the MLPG method. Thus, in the ECM region, atoms and nodes do not have to be coincident. The ECM method has been demonstrated to be suitable in one-dimensional chain models and in the two-dimensional analysis of graphene sheets.

2.5 Continuum models

Under the traditional continuum framework, materials are assumed to be composed of a divisible continuous medium, with a constitutive relation that remains the same for a wide range of system sizes. There are a large variety of numerical methods that can be used for solving continuum problems described by partial differential equations, the most popular being the finite element method (FEM) [34]. It is a numerical method that permits to obtain an approximate solution of a system of partial differential equations that are transformed in an algebraic system of equations. Dividing the continuum into a number of elements, each one connected to the next by nodes, it is possible to obtain a discretization (mesh). FEM's discretization process converts continuum equations, that are typically in the form of deterministic or stochastic partial differential equations (PDE's), into a set of coupled ordinary equations that are solved at the nodes of the FE mesh and interpolated throughout the interior of the elements using shape functions. Total potential energy is the sum of two parts, the internal energy U, that is the strain energy caused by the deformation of the body, and external work W associated by the applied surface and body forces.

The total potential energy under the FE frameworks written as:

$$\Pi = U - W \tag{2.23}$$

The internal energy is the strain energy caused by deformation of the body and can be explicitly written under the linear elastic hypothesis as

$$U = \frac{1}{2}\int_{\Omega} \{\sigma\}^T\{\varepsilon\}\, d\Omega = \frac{1}{2}\int_{\Omega} \{\varepsilon\}^T[D]\{\varepsilon\}\, d\Omega \tag{2.24}$$

where $\{\sigma\} = \{\sigma_{xx}\sigma_{yy}\sigma_{zz}\tau_{xy}\tau_{yz}\tau_{zy}\}^T$ denotes the stress vector, $\{\varepsilon\} = \{\varepsilon_{xx}\varepsilon_{yy}\varepsilon_{zz}\gamma_{xy}\gamma_{yz}\gamma_{zy}\}^T$ denotes the strain vector, $[D]$ is the elastic matrix, and Ω indicates that integration must be performed over the entire domain.

A recent computational technique, known as element-free Galerkin method (EFG), proposed initially by Belytschko et al. [35, 36] for the solution of elasticity problems doesn't suffer of the typical drawbacks of the finite element method.

The EFG method is a Galerkin discretization technique based on the concept of moving least-square approximation, proposed by Lancaster and Salkauskas [37] that has been used first in the diffuse element method by Nayroles et al. in [38] and has some features in common with the Smoothed Particle Hydrodynamics (SPH) method.

It can be considered as a generalisation of the finite element method since in the EFG method local approximation does not depend only on nodal values of nodes belonging to a particular element, as happens in the FEM, but on the weighted values of a "cloud" of nodes in the neighbourhood of the point of

interest. It has been successfully applied to different engineering problems such as elasticity [39], elastoplasticity [40], dynamic and fatigue fracture problems [41], and so on.

The description of the moving least-square interpolant $u^h(\mathbf{x})$ of a generic field function $u(\mathbf{x})$ is the key for the comprehension of the element-free Galerkin method.

The moving local approximation (instead of *interpolation* as usually done with finite elements) is written by using a linear combination of a base of functions p_j (usually monomials) in the space coordinates $\mathbf{x} = [x, y, z]$:

$$u^h(\mathbf{x}) = \sum_{j=1}^{m} p_j(\mathbf{x}) \cdot a_j(\mathbf{x}) = \mathbf{p}^T(\mathbf{x}) \cdot \mathbf{a}(\mathbf{x}) \tag{2.25}$$

For instance linear and quadratic monomials bases in 3 dimensions are the following:

$$\begin{aligned} &\mathbf{p}^T(\mathbf{x}) = [1, x, y, z] && , \ m = 4 \\ &\mathbf{p}^T(\mathbf{x}) = [1, x, y, z, x^2, y^2, z^2, xy, yz, xz] && , \ m = 10 \\ &..... \end{aligned} \tag{2.26}$$

Once the vector of the coefficients $\mathbf{a}(\mathbf{x})$ has been determined at the point (which position is given by the vector $\mathbf{x}$) where the approximation is sought, the local approximation is completely known. Such a vector $\mathbf{a}(\mathbf{x})$ can be determined by minimising the discrete weighted square difference $\left[u^h(\mathbf{x}) - u(\mathbf{x})\right]$ between the approximate and the real solution. This can be obtained by the minimisation of the norm L defined by:

$$L = \sum_{1}^{n} w(d_I) \cdot \left[u^h(\mathbf{x}) - \hat{u}_I\right]^2 = \sum_{1}^{n} w(d_I) \cdot \left[\mathbf{p}^T(\mathbf{x}) \cdot \mathbf{a}(\mathbf{x}) - \hat{u}_I\right]^2 \qquad (2.27)$$

where $\hat{u}_I$ are the fictitious nodal values (and not the actual nodal values $u(\mathbf{x}_I)$ of the unknown displacement field at $\mathbf{x} = \mathbf{x}_I$, $w(d_I = \|\mathbf{x} - \mathbf{x}_I\|)$ is a weight function (depending on some parameters such as the relative Euclidean distance between points $\mathbf{x}$ and $\mathbf{x}_I$, $d_I = \|\mathbf{x} - \mathbf{x}_I\|$) and n is the total number of nodes in the neighbourhood of $\mathbf{x}$ where $w(\mathbf{x} - \mathbf{x}_I) \neq 0$ (i.e. inside the domain of influence of the considered point $\mathbf{x}$).

The condition of minimum of L with respect the unknown vector $\mathbf{a}(\mathbf{x})$, $\partial L / \partial \mathbf{a}(\mathbf{x}) = 0$, leads to a system of linear equations with the solution:

$$\mathbf{a}(\mathbf{x}) = \mathbf{A}^{-1}(\mathbf{x})\, \mathbf{B}(\mathbf{x})\, \hat{\mathbf{u}} \qquad (2.28)$$

where the matrices $\mathbf{A}(m \times m), \mathbf{B}(m \times n)$ and the vector $\hat{\mathbf{u}}$ can be written:

$$\begin{aligned} &\mathbf{A}(\mathbf{x}) = \sum_{1}^{n} w(d_I) \cdot \mathbf{p}(\mathbf{x}_I) \cdot \mathbf{p}^T(\mathbf{x}_I) \quad , \quad \hat{\mathbf{u}}^T = \left[\hat{u}_1 \quad \hat{u}_2 \quad \ldots \quad \hat{u}_n\right] \\ &\mathbf{B}(\mathbf{x}) = \left[w(d_1) \cdot \mathbf{p}(\mathbf{x}_1) \quad w(d_2) \cdot \mathbf{p}(\mathbf{x}_2) \quad \ldots \quad w(d_n) \cdot \mathbf{p}(\mathbf{x}_n)\right] \end{aligned} \qquad (2.29)$$

By substituting eqn. (2.28) into (2.25) the approximate solution $u^h(\mathbf{x})$ of the filed variable can be obtained:

$$u^h(\mathbf{x}) = \mathbf{p}^T(\mathbf{x}) \cdot \left[\mathbf{A}^{-1}(\mathbf{x})\, \mathbf{B}(\mathbf{x})\, \hat{\mathbf{u}}\right] = \boldsymbol{\Phi}(\mathbf{x})\, \hat{\mathbf{u}} \qquad (2.30)$$

where the vector $\mathbf{\Phi}(\mathbf{x})$ of the shape functions can be recognised:

$$\mathbf{\Phi}(\mathbf{x}) = \left[\mathbf{\Phi}_1(\mathbf{x}) \quad \mathbf{\Phi}_2(\mathbf{x}) \quad .... \quad \mathbf{\Phi}_n(\mathbf{x})\right] = \mathbf{p}^T(\mathbf{x}) \cdot \mathbf{A}^{-1}(\mathbf{x})\, \mathbf{B}(\mathbf{x}) \tag{2.31}$$

It is important to note that, at the location $\mathbf{x} = \mathbf{x}_I$, the obtained shape functions depend only on the polynomial basis, on the local node arrangement and on the weight function used $w(d_I)$.

The EFG method requires that the support of the weight function associated with the *I-th* point involves a sufficient numbers of nodes to ensure the invertibility of the matrix $\mathbf{A}(\mathbf{x})$. On the other hand, such a support should not be too large in order to keep the local character of the approximation necessary in the EFG method and not producing ill-conditioned system matrices.

Since the shape functions do not fulfil the so-called Kroneker delta condition (i.e. $\Phi_J(\mathbf{x}_I) \neq \delta_{IJ}$), as usually happens for the shape functions in the FE or boundary elements methods, the enforcement of Dirichlet boundary conditions is not simple as in classical computational technique.

Different techniques have been proposed to this end: the most common can be considered the Lagrange multiplier method, modified variational principles [43], the penalty method [44], etc. In other words, in the EFG method the boundary conditions cannot be enforced by simply writing $\hat{\mathbf{u}} = \overline{\mathbf{u}}$ due to its approximation property; the following relation must be considered instead:

$$\mathbf{u}^h(\mathbf{x}) = \boldsymbol{\Psi}(\mathbf{x})\,\hat{\mathbf{u}} = \bar{\mathbf{u}} \tag{2.32}$$

where $\boldsymbol{\Psi}$ is the matrix of shape functions.

By adopting for the penalty method [44], the functional governing the equilibrium problem must be modified as follows:

$$\Pi^* = \frac{1}{2}\int_{\Omega} \boldsymbol{\varepsilon}^T \boldsymbol{\sigma}\, d\Omega - \int_{\Omega} \mathbf{b}^T \mathbf{u}\, d\Omega - \int_{\Gamma_t} \bar{\mathbf{t}}^T \mathbf{u}\, d\Gamma_t - \frac{\alpha}{2}\int_{\Gamma_u} (\mathbf{u}-\bar{\mathbf{u}})(\mathbf{u}-\bar{\mathbf{u}})\, d\Gamma_u \tag{2.33}$$

where α is the penalization term; when the boundary conditions are exactly satisfied, the added term in eqn. (2.33) is zero and the functional Π^* is therefore identical to the standard one, Π.

By using the approximation of the displacement field, $\mathbf{u}^h(\mathbf{x}) = \boldsymbol{\Psi}(\mathbf{x})\,\hat{\mathbf{u}}$ (Eq. (2.33)), the stationariness of the modified functional becomes:

$$\delta\,\Pi^* = (\mathbf{K} + \mathbf{K}_\alpha)\,\hat{\mathbf{u}} - \mathbf{f} - \mathbf{f}_\alpha = 0 \tag{2.34}$$

where $\mathbf{K} = \int_{\Omega} \mathbf{B}^T \mathbf{D}\mathbf{B}\, d\Omega$ and $\mathbf{K}_\alpha = \alpha \int_{\Gamma_u} \boldsymbol{\Psi}^T \mathbf{S}\boldsymbol{\Psi}\, d\Gamma_u$ represent the standard stiffness matrix and the contribution to stiffness matrix due to constraints, respectively; $\mathbf{f} = \int_{\Omega} \boldsymbol{\Psi}^T \mathbf{b}\, d\Omega + \int_{\Gamma_t} \boldsymbol{\Psi}^T \bar{\mathbf{t}}\, d\Gamma_t$, and $\mathbf{f}_\alpha = \alpha \int_{\Gamma_u} \boldsymbol{\Phi}^T \bar{\mathbf{u}}\, d\Gamma_u$ are the vector of nodal forces and the contribution to vector of nodal forces given by constraints, respectively, while $\mathbf{B} = \partial\boldsymbol{\Psi}$ is the compatibility matrix and $\mathbf{S}$ is a 3x3 (in 3-D problems) diagonal matrix in which the term S_{jj} is equal to 1 if the *j-th* degree of freedom is prescribed on Γ_u and equal to 0 otherwise.

2.6 Macroscale DEM

Macroscale DEM is becoming an effective method of investigating engineering problems in sold, liquid, granular and heterogeneous materials, especially in granular flows, powder mechanics, advanced ceramics, and rock mechanics.

DEM at the macroscale in geomechanics is a widespread method to study many kind of problems. The behavior of bulk granular materials is usually difficult or sometimes impossible to measure and the performance of equipment that handles or processes these materials can often only be determined by making measurements on the outputs from physical prototypes. DEM simulation to the discrete manufacturing industry can simulate and analyze the bulk behavior of granular materials, providing the means to reduce dependency on physical prototyping shorten design cycles and leverage design know-how in the simulation environment. Other industries within the discrete manufacturing sector use DEM in the design of steelmaking plants, asphalt production plants, pharmaceutical processing equipment, high-speed printers, electronics, aircraft and automotive components.

Examples of processes where DEM is being used at the macroscale to improve designs and optimize process configuration include: dry and wet mixing of powders, drying – drum, cross-flow and counter-flow, comminution – crushing, grinding, mixing and blending of pharmaceutical powders, drying and coating of pharmaceutical tablets, aggregates, food products, granulation and agglomeration of powders, mixing and extrusion melting of plastics.

Another field of application for macroscale DEM is the modeling or simulation of fluid-solids or fluid-particles systems.

These concepts will be treated accurately in the Chapter 3, considering different theories and studies presented in literature.

References

[1] M. M. Carroll (1985), Mechanics of Geological Materials, *Appl. Mech. Rev*, 38, 1301.

[2] T. J. R. Hughes (2012), Finite Element Method - Linear Static and Dynamic, *Courier Dover Publications*.

[3] S. Li and W. K. Liu (2002), Meshfree and particle methods and their applications, *Appl. Mech. Rev*. 55, 1-34.

[4] S. Li and W. K. Liu (2004), Meshfree Particle Methods, *Springer,* New York.

[5] Monaghan JJ (1985), Particle methods for hydrodynamics, *Comput.Phys. Rep.* **3**, 71–124.

[6] W. Kohn and L. J. Sham, (1965), Self-Consistent Equations including exchange and correlation effects, *Phys. Rev.*, 140, A1133.

[7] P. Hohenberg and W. Kohn , Inhomogeneous Electron Gas, *Phys. Rev*., 136, B864.

[8] F. Bloch (1928), Über die Quantenmechanik der Elektronen in Kristallgittern, *Zeitschrift fur Physik* 52, 555.

[9] Cundall, P. and Hart, R. (1989), Numerical modeling of discontinuation*, DEM 1st U.S. Conference*, Denver, Colo., USA.

[10] A. M. Krivtsov. (2004), Molecular dynamics simulation of plastic effects upon spalling, Fiz. Tverd. Tela (St. Petersburg) 46(6), 64 [Phys. Solid State] 46, 6 .

[11] Cundall, P. A. and Strack, D. L. (1979), A discrete numerical model for granular assemblies. *Geotechnique,* , 29, 47-65.

[12] Saether E., (2008), A multiscale method for simulating fracture in polycrystalline metals. *Faculty of Virginia Polytechnic Institute and State University.*

[13] Broughton, J. Q., Abraham, F. F., Bernstein, N., and Kaxiras, E (1999), Concurrent Coupling of Length Scales: Methodology and Application *Phys. Rev. B*, 60, pp. 2391-2403.

[14] Abraham, F.F., Brodbeck, D., Rafey, R.A., and Rudge, W.E. (1994), Instability Dynamics of Fracture: A Computer Simulation Investigation, *Phys. Rev. Lett.,* 73, pp. 272-275.

[15] Abraham FF, Broughton JQ, Bernstein N, and Kaxiras E. (1998), Spanning the Continuum to Quantum Length Scales in a Dynamics Simulation of Brittle Fracture, *Europhysics Letters*, 44, p. 783.

[16] Abraham, F.F., Bernstein, N., Broughton, J.Q., and Hess, D. (2000), Dynamic Fracture of Silicon: Concurrent Simulation of Quantum Electrons, Classical Atoms and the Continuum Solid, *Materials Research Society Bulletin,* 25, pp. 27-32.

[17] Abraham, F.F. (2001), The Atomic Dynamics of Fracture, *J. Mech. Phys. Solids*, 49, pp. 2095-2111.

[18] Shen, S. and Atluri, S.N. (2004), Computational Nano-Mechanics and Multi-Scale Simulation, CMC*: Computers, Materials, & Continua*, 1, pp. 59-90.

[19] Shen, S. and Atluri, S.N. (2004), Multiscale Simulation based on the Meshless Local Petrov-Galerkin (MLPG) Method, *Computer Modeling in Engineering & Sciences*, 5, pp. 235-255.

[20] Kohlhoff, S., Gumbsch, P., and Fischmeister, H.F. (1991), Crack Propagation in BCC Crystals Studied with a Combined Finite-Element and Atomistic Model, *Phil. Mag. A*, 64, pp. 851-878.

[21] Gumbsch, P. and Beltz, G.E (1995), On the Continuum Versus Atomistic Descriptions of Dislocation Nucleation and Cleavage in Nickel, *Mod. Sim. Mat. Sci. and Engrg.*, 3, pp. 597-613.

[22] Gumbsch, P. (1995), An Atomistic Study of Brittle-Fracture - toward Explicit Failure Criteria from Atomistic Modeling, *J. Mat. Res.*, 10, pp. 2897-2907.

[23] Rudd R.E., and Broughton J.Q. (1998), Coarse-Grained Molecular Dynamics and the Atomic Limit of Finite Elements, *Phys. Rev. B*, 58, p. R5893.

[24] Rudd R.E., and Broughton J.Q.. (2005), Coarse-Grained Molecular Dynamics: Nonlinear Finite Elements and Finite Temperature, *Phys. Rev. B*, 72, p.144104.

[25] Tadmor, E. B., Ortiz, M., and Phillips, R. (1996), Quasi-Continuum Analysis of Defects in Solids, *Phil. Mag. A,* 73, pp. 1529-1563.

[26] Knap, J. and Ortiz, M. (2001), An Analysis of the Quasicontinuum Method, *J. Mech. Phys. Solids*, 49, pp. 1899-1923.

[27] V. Shenoy, V. Shenoy, and R. Phillips(1999), in *Multiscale Modeling of Materials*, edited by V.V. Bulatov, T. Diaz de la Rubia, R. Phillips, E. Kaxiras, and N. Ghoniem (Mater. Res. Soc. Symp. Proc. 538, Warrendale, PA,), p.465.

[28] Born, M., and Huang, K. (1954), Dynamical Theory of Crystal Lattices, Oxford University Press.

[29] Shilkrot, L.E., Curtin, W.A. and Miller (2002), R.E., A Coupled Atomistic/Continuum Model of Defects in Solids, *J. Mech. and Phys. Solids*, 50, pp. 2085-2106.

[30] Shilkrot, L.E., Miller, R.E. and Curtin, W.A. (2003), Coupled Atomistic and Discrete Dislocation Plasticity, *Phys. Rev. Lett.*, 89, p. 025501-1.

[31] Curtin, W.A. and Miller, R.E. (2003), Atomistic/Continuum Coupling in Computational Materials Science, *Mod. Sim. Mat. Sci. and Engrg.*, 11, pp. R33-R68.

[32] Shilkrot, L.E., Miller, R.E., and Curtin, W.A. (2004), Multiscale Plasticity Modeling: Coupled Atomistics and Discrete Dislocation Mechanics, *J. Mech. and Phys. Solids* 52, pp. 755-787.

[33] Shiari, B., Miller, R.E., and Curtin, W.A. (2005), *Coupled Atomistic/Discrete Dislocation Simulations of Nanoindentation at Finite Temperature*, J. Engrg. Mat. and Tech. Transactions of the ASME, 127, pp. 358-368.

[34] Zienkiewicz, O.C. and Taylor, R.L. (2000), *The finite element method*. 5th Edition, 3 Volumes, Butterworth–Heinemann.

[35] Belytschko T, Lu YY, Gu L. (1994), Element-free Galerkin methods. *Int J. Num. Meth. Engng* ; 37: 229-256.

[36] Belytschko T, Krongauz Y, Organ D, Fleming M, Krysl P(1996), Meshless methods: an overview and recent developments. *Computer Methods Applied Mechanics Engng* ; 139: 3-47.

[37] Lancaster P, Salkauskas K. (1991), Surface generated by moving least square methods. *Math of Comp* ; 37: 141-158.

[38] Nayroles B, Touzot G, Villon P. (1992), Generalizing the finite element method: diffuse approximation and diffuse elements. *Computational Mechanics* ; 10: 307-318.

[39] Krysl P, Belytschko T(1996), Analysis of thin shells by the element-free Galerkin method. *Int J. Solids and Structures*; 33: 3057-3080.

[40] Barry W, Saigal (1999)S, A three dimensional element-free Galerkin elastic and elastoplastic formulation. *Int J. for Numerical Meth in Engng* 46: 671-693.

[41] Belytschko T, Lu YY, Gu L, Tabbara M. (1995), Element-free Galerkin methods for static and dynamic fracture. *Int J. Solids and Structures*; 32: 2547-2570.

[42] Yu X, Saigal S (1998), An element free Galerkin formulation for stable crack growth in an elastic solid, *Computer Meth in Appl Mech and Engng*; 154(3-4): 331-343.

[43] Gu YY, Belytschko T, Gu L (1994), A new implementation of the element free Galerkin method. *Computer Methods Applied Mechanics Engineering*; 113: 397-414.

[44] Mukhejee YX, Mukhejee S (1997), On boundary conditions in the element-free Galerkin method. *Computational Mechanics*; 19: 264-270.

Chapter 3

SOLID AND FLUID MODELLING WITH PARTICLE METHODS

3.1 Introduction

Since the invention of the finite element method (FEM) in the 1950s, it has become a widely used method in engineering computations. A salient feature of the FEM is that it divides a continuum into discrete elements connected together by a topological map, which is usually called “mesh”.

However, this procedure is not always advantageous, because the numerical compatibility condition is not the same as the physical compatibility condition of a continuum.

Today, some kind of problems like simulations of impact/penetration, explosion/fragmentation, flow pass obstacles, and fluid-structure interaction problems, involve adaptive remeshing procedures that often introduces numerical errors, and thus is not desirable from a computational point of view. Therefore, the so-called Arbitrary Lagrangian Eulerian (ALE) formulations have been developed [1-5].

The objective of the ALE formulation is to make the mesh independent of the material so that the mesh distortion can be minimized. In computer

simulations of very large deformation and/or high-speed mechanical and structural systems, even with the ALE formulation, a distorted mesh introduces important errors in numerical computations. Furthermore, the convective transport effects in ALE often leads to spurious oscillation that needs to be stabilized by artificial diffusion or through a Petrov-Galerkin stabilization.

Another way it would be to subdivide a continuum by only a set of nodal points, or particles, without mesh constraints, with the aim to have a method computationally efficient; this is the *leitmotif* of contemporary meshfree Galerkin methods. Indeed, the meshfree particle methods can easily handle very large deformations, since the connectivity among nodes is generated as part of the computation and can change with time; the discretized domain can be linked more easily with a CAD database than finite elements do. Since it is not necessary to generate an element mesh, it is possibly to study the damage of the components, such as fracture, which should prove very useful in modeling of material failure and accuracy can be controlled more easily, since in regions where more refinement is needed, nodes can be added quite easily (h-adaptivity).

According to computational modeling, particle methods may be categorized into two different types: those serving as approximations of the strong forms of partial differential equations (PDEs) and those serving as approximations of the weak forms of PDEs.

To approximate the strong form of a PDE by using a particle method, the partial differential equation is usually discretized by a specific collocation technique. Examples are Smoothed Particle Hydrodynamics (SPH) [6–10], the vortex method [11-16], the e generalized finite difference method [17,18].

It is worth mentioning that some particle methods, such as SPH and vortex methods, were initially developed as probabilistic methods [8,12], and it turns out that both SPH and the vortex method are most frequently used as deterministic methods today. Nevertheless, the majority of particle methods in this category are based on probabilistic principles, or used as probabilistic simulation tools. Methods in this category are molecular dynamics (both quantum molecular dynamics [19-20] and classical molecular dynamics [21-22]), direct simulation Monte Carlo (DSMC), or Monte Carlo method based molecular dynamics, such as quantum Monte Carlo methods [23-24] and the lattice gas automata (LGA), or lattice gas cellular automata [25–26].

Therefore, a discrete element simulation of solids consists of a large number of bodies, usually rigid, that interact via forces exerted at their common contact points. For example in the DEM models of cemented material the bonding agent is often represented by breakable bonds between particles. Some of the bond models are based on a transfer of tensile and tangential forces until there is bond breakage [27-28] while others use additionally torque transfer to account for the finite extent of the cementation [29-30].

In this context, it is useful to cite some sentences about the discrete nature of solids taken from [31]: "*Primarily, Cauchy and Navier considered a rigid body as a system of material particles. They assumed that the material particles in each pair are mutually connected by interaction forces that are directed along the line connecting them and linearly depend on the distance between the particles. On the level of the physical science at the beginning of the nineteenth century, it was impossible to describe the elastic properties of actual bodies. Nowadays, there are rigorous physical theories that permit determining the elastic properties of crystal of various structure, starting*

from the consideration of the interatomic interaction forces in the crystal lattice. A simpler way accepted in the modern theory of elasticity is to consider the distribution of the body matter over the entire volume, which permits, considering the displacements of material points, as continuous functions of the coordinates".

From the above considerations, it appears as the discrete nature of solids can be exploited for their modelling in computational approaches.

3.2 Discrete model strain and stress evaluation

The model of elastic strain of a continuum medium is constructed following the simple way mentioned above. In the theory of elasticity the principal postulates are based on the assumption that the medium is continuum and infinitely divisible, the displacements and strains are relatively small, and the stresses and strains are related by a linear law. Under these conditions, considering an infinitely small cube cut from the continuum, the equilibrium condition can be written as:

$$\frac{\partial \sigma_{ij}}{\partial x_j} + X_i = 0 \ \ (i,j = 1,2,3) \tag{3.1}$$

where σ_{ij} are the stresses acting on the faces perpendicular to the axes Ox_i in the direction of the axes Ox_j, and the X_i are the components of the body force in the principal coordinates; summation from 1 to 3 over repeated indices are assumed. The stress tensor σ_{ij} is symmetric

$$\sigma_{ij} = \sigma_{ji} \tag{3.2}$$

The notion of relative variations in the distance between points of the continuum can be introduced by the formula

$$\varepsilon_{ij} = \frac{1}{2}\left(\frac{\partial u_i}{\partial x_j} + \frac{\partial u_j}{\partial x_i}\right) = 0 \;\; (i,j = 1,2,3) \tag{3.3}$$

where ε_{ij} are the strains. At this point, the tensor law relation between the stresses and strains (Hooke's law) can be written:

$$\sigma_{ij} - \; K\theta\delta_{ij} = 2G\,(\varepsilon_{ij} - \frac{1}{3}\theta\delta_{ij}) \tag{3.4}$$

These are the classical equations of Cauchy-Navier theory of elasticity. The displacements of the points of the continuum medium after the application of the loads are indicated as $u_i = u_i(x_1, x_2, x_3)$, while K and G are constants characterizing the elastic medium resistance to uniform compression (tension) and shear (shape variation); $\theta = \varepsilon_{11} + \varepsilon_{22} + \varepsilon_{33}$ is the bulk or volumetric strain and δ_{ij} is the Kronecker symbol. It is assumed that the displacements and strains in formulas (3.1,), (3.3) and (3.4) are small.

The expression (3.3) cannot be used if the displacements and strains are not small and it is necessary to study the medium properties in the framework of the so-called geometrically nonlinear theory of elasticity. Hooke's law is not appropriate for many materials even for small strains ($\varepsilon_{ij} \cong 5 - 10$ %); for these situations were developed numerous physically non-linear models of continuum.

Another case of particular interest concerns anisotropic materials that have different behavior in different directions; for this reason the physical

properties of the medium are described by the corresponding generalization of Hooke's law (3.4).

When only the displacements are considered as unknown variables, it is possible to obtain a system of three partial differential equations in the form:

$$G\Delta u_i + (\lambda + G)\frac{\partial \theta}{\partial x_i} + X_i = 0, \quad i = 1,2,3 \tag{3.5}$$

$$\Delta = \frac{\partial^2}{\partial x_1^2} + \frac{\partial^2}{\partial x_2^2} + \frac{\partial^2}{\partial x_3^2}, \quad \lambda = K - \frac{2}{3}G > 0 \tag{3.6}$$

To solve the system composed by (3.5) and (3.6) it is necessary to define the corresponding boundary conditions.

3.2.1 General basis of the discrete method

Some authors [32] try to return to the Cauchy-Navier idea and to construct a model of deformable continuum as a system of mutually interacting material particles. The basic idea is to divide the medium into material particles or points interacting each other by forces depending on the relative distance between them. The interaction can be studied considering not only the simple Hooke's law but also the physical non linear properties of the continuum.

The total mass of the matter is distributed over discrete interrelated points; for example in 2D problems, the material system is subdivided in some cases using circles or triangular elements of various shape interacting each other with springs. In 3D problems cubes, spheres or tetrahedral elements can be used. Once the continuum discretization scheme and the law of interaction between particles are chosen, it is assumed that all the particles

(with mass m_i) obey Newton's second law, eventually by taking into account the attenuation force usually proportional to the particle motion velocity:

$$m_i\ddot{u}_i + \alpha_i\dot{u}_i + \sum_{j=1}^{k} \beta_{ij}\left(u_i - u_j\right) = F_i(t), \quad \alpha_i > 0, \qquad \beta_{ij} > 0, \qquad i = 1,2,\dots,n \tag{3.7}$$

where n is the number of discrete particles into which the deformable continuum is divided, α_i is the attenuation coefficient, β_{ij} characterize the rigidity of interaction between particles *i* and *j* when a relative displacement occurs, *k i*s the number of particles surrounding a given particle, and $F_i(t)$ is the nodal force (for example the gravity force for internal particles or the external force for the boundary particles).

As mentioned above an important aspect is the domain of influence of every particle; it is typically assumed as a volume, such as a sphere centered on every element of discretization, such that particles inside this space interact with the particle under consideration, while other particles do not exchange forces with it.

3.2.2 Interactions between particles

Basic DEM interaction is usually defined by two stiffnesses: normal stiffness K_N and shear (tangent) stiffness K_T. It is desirable that K_N be related to fictitious Young's modulus of the particles' material, while K_T is typically determined as a given fraction of computed K_N. The $\frac{K_T}{K_N}$ ratio can be associated to the macroscopic Poisson's ratio of the arrangement as can be

shown by dimensional analysis: elastic continuum has two parameters (E and ν) and basic DEM model also has two parameters with the same dimensions K_N and $\frac{K_T}{K_N}$; macroscopic Poisson's ratio is therefore determined solely by $\frac{K_T}{K_N}$ and macroscopic Young's modulus is then proportional to K_N and affected by $\frac{K_T}{K_N}$.

The commonly formulated algorithms use normal interaction stiffness represented by two springs in serial configurations with lengths equal to sphere radii (Fig.3.1).

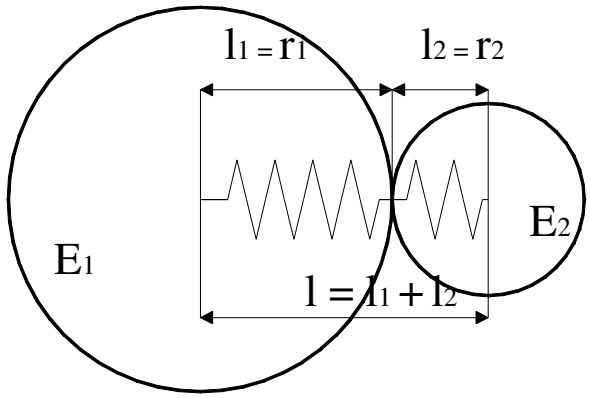

Figure 3.1 – Stiffness between two particles represented by a couple of spings in series configuration.

The normal contact stiffness between two spheres is thus represented by a series of two springs; defining l_i as the distances between the contact point and spheres centers, it is possible to calculate the distance $l = l_1 + l_2$.When the distance between particles centers change, a length variation of the springs takes place, $\Delta l = \Delta l_1 + \Delta l_2$, i.e. the sum of deformations of both spheres, that is proportionally to their compliances.

The displacement change Δl generates the force $F_i = K_i \Delta l_i$, where the term $K_i = K_N$ represent stiffness; it can be related to the sphere's material elastic modulus E_i and to an equivalent cross-section A_{eq},

$$K_i = E_i \frac{A_{eq}}{l_i} \tag{3.8}$$

3.2.3 Relation between the parameters of the discrete-truss dynamic model and the basic parameters of the theory of elasticity

In the mathematical model of the classical elasticity theory, Young modulus and the Poisson ratio play a key role; the Young modulus is usually considered as the rigidity coefficient between the stress (force per unit area) and the strain (relative elongation) of the specimen:

$$E = \frac{\sigma}{\varepsilon} \tag{3.9}$$

where $\sigma = F/S$, F is the tensile force, S is the cross-section (after tension), and $\varepsilon = \Delta l/l$ is the specimen strain. Usually E is assumed the same in case of tension or compression, otherwise different moduli can be adopted for some materials.

It follows that, in two-dimensional problems of elasticity where the medium is discretized according to a rectangular scheme, the rigidity of interaction between material particles under tension or compression, can be considered to correspond to the Young modulus. A specimen under tension somewhat decreases its dimension in the transverse direction because of

tension of diagonal springs, which means that it is similar to the Poisson ratio effect for this model [32].

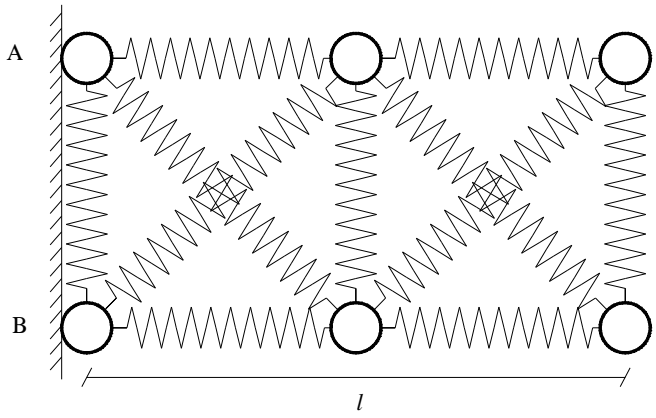

Figure 3.2 – Truss Model of particles in 2D elastic problems.

It is assumed that the fixation points A e B move freely along the vertical axis. In actual experiments, to determine the Young modulus, it is necessary to take a sufficiently long specimen, because, according to the Saint-Venant principle, the specimen fixation does not affect its strain at a sufficiently large distance, so the relations are:

$$\sigma = \frac{F}{S}, \qquad \varepsilon = \frac{\Delta l}{l}, \qquad \sigma = \tilde{E}\varepsilon \tag{3.10}$$

where $\tilde{E}$ is the total Young modulus of the discretized material with the stretched springs taken into account, including diagonal ones.

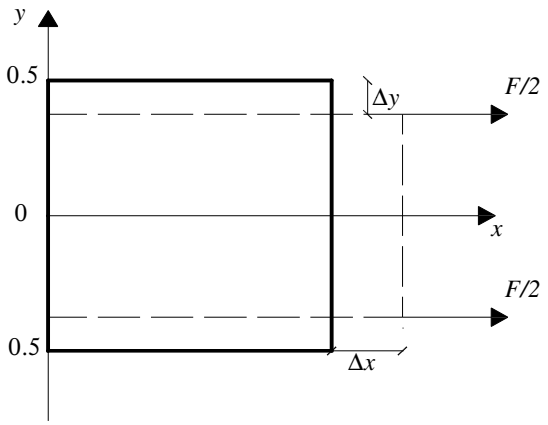

Figure 3.3 - Square Lattice deformation

It is possible to obtain the Young Modulus $\tilde{E}$ in case of small strains for the square lattice. In Fig. 3.3 the square shaped continuum has side length $l = 1$. The quantities Δx and Δy are the longitudinal elongation and the transverse compression of the stretched specimen. The diagonal length increment in case of small strains is equal to:

$$\begin{gathered}\Delta l = \sqrt{(1+\Delta x)^2 + (1-2\Delta y)^2} - \sqrt{1^2+1^2} = \\ \sqrt{2+2\Delta x - 4\Delta y} - \sqrt{2} = \sqrt{2}\left(\sqrt{1+\Delta x - 2\Delta y} - 1\right) = \\ \sqrt{2}\left(\frac{\Delta x}{2} - \Delta y\right)\end{gathered} \tag{3.11}$$

where the second order terms have been neglected. The diagonal strain is thus:

$$\varepsilon_d = \frac{\Delta l}{\sqrt{2}} = \frac{\Delta x}{2} - \Delta y \tag{3.12}$$

If the spring rigidity in the direction *Ox* is equal to k_1 and the rigidity of diagonal springs is k_2, respectively, then we obtain the obvious classical equilibrium condition

$$2k_1\Delta x + 2k_2\left(\frac{\Delta x}{2} - \Delta y\right)cos45 = F \tag{3.13}$$

Taking into account the relation between Δx, Δy and the strains ε_{11}, ε_{22}, $\varepsilon_{11} = \Delta x$, $\varepsilon_{22} = 2\Delta y$, we have:

$$2k_1\varepsilon_{11} + \sqrt{2}k_2\left(\frac{\varepsilon_{11}}{2} - \frac{\varepsilon_{22}}{2}\right) = F \tag{3.14}$$

By the definition of the Poisson ratio as the transverse contraction coefficient, it is possible write out the following relation between the strain absolute values ε_{11} and ε_{22} in two directions:

$$\varepsilon_{22} = \nu\varepsilon_{11} \tag{3.15}$$

Then, finally, formulas (3.12) and (3.14) imply that

$$\left[2k_1 + \frac{\sqrt{2}}{2}(1-\nu)k_2\right]\varepsilon_{11} = E\varepsilon = \sigma \tag{3.16}$$

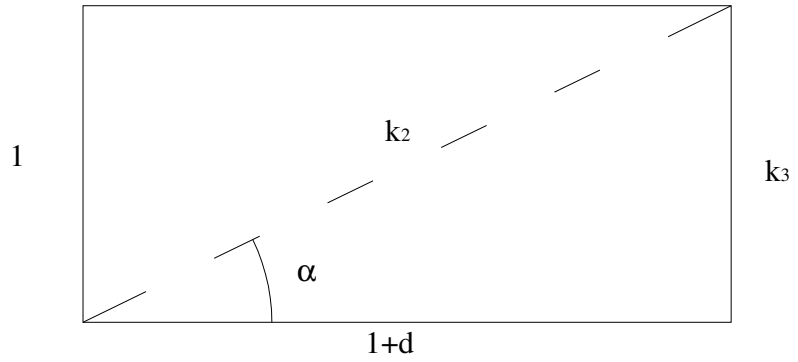

Figure 3.4 – Different Stiffnesses

Thus the total Young modulus in the model is determined by the coefficient of longitudinal rigidity of the spring in the direction *Ox* (k_1) and by the diagonal rigidity (k_2) by the formula

$$E = 2\left[k_1 + \frac{\sqrt{2}}{4}(1-\nu)k_2\right]\sigma \tag{3.17}$$

If $k_1 = k_2 = k$, then, according to (3.17), the Young modulus becomes

$$E = 2k\left[1 + \frac{\sqrt{2}}{4}(1-\nu)\right] \tag{3.18}$$

Thus, in the classical theory of elasticity formula (3.18) relates the Young modulus to the rigidity coefficient *k* of the constraints between particles.

The formulas obtained above also permit calculating an analog of the Poisson ratio for the model under study. Obviously, the diagonal springs

compress the elastic edges of the square in the direction *Oy*. The equilibrium force condition readily implies the relation

$$2k_1 cos45 \left(\frac{\varepsilon_{11}}{2} - \frac{\varepsilon_{22}}{2}\right) = k_3 \varepsilon_{22} \tag{3.19}$$

Taking to account (3.15), it is possible to derive the following expression for the Poisson ratio of the model from (3.19):

$$\nu = \frac{k_2 cos45}{k_3 + k_2 cos45} = \frac{k_2}{\sqrt{2}k_3 + k_2} \tag{3.20}$$

It follows from (3.19) that $\nu \approx 0.4$ for $k_3 = k_2$, which corresponds to the Poisson ratio for a large class of materials.

For an isotropic material ($k_2 = k_3$):

$$\nu = \frac{sen\alpha}{1 + sen\alpha} \tag{3.21}$$

Note that $0 \leq \nu \leq 0.5$ if $0 \leq sen\alpha \leq 1$.

The above equilibrium considerations enables to relate explicitly the mechanical parameters of the material to the stiffnesses of the springs connecting the particles. However, for more complex arguments of particles or for 3D assemblies the above theoretical equations become very difficult to be determined and numerical analysis are thus necessary to this end.

Such numerical approach will be adopted in section 3.3 where the mechanical parameters of the 3D particle arrangements considered in this thesis are prospected.

3.3 DEM applied to solid materials

In the last decades computer calculation power increase very fast, so simulation methods of material behavior allow more realistic modeling of the microstructure (particles, phases, and the bonds between them). In the last years researches on solid models at the macroscale have been oriented towards transition from the finite element method (with the classical hypothesis of continuum mechanics) to discrete particle models and lattice models in which the continuum is approximated by a system of discrete elements in contact.

The discrete element method (DEM) discretizes a material by using rigid elements of simple shape that interact with neighboring elements according to interaction laws that are applied at points of contact. This kind of approach is not so different from molecular dynamics; the most important differences between DEM and MD are the interelement potentials and scale analysis, micro for molecular dynamics and meso or macro for DEM.

Obviously, this method is ideal for problems not accessible to traditional continuum-based methods such as concrete structural failure, rock-blasting operations, fra cture of brittle materials involving great deformations, presence of discontinuity in the material structure as voids, imperfections and heterogeneities.

The elementary units of DEM methods are usually mesoscopic grains or spherical particles, which deform under stress. Frequently the realistic modeling of the deformations of the single elements is too much complicated, so the interaction force is strictly related to the overlap δ of two particles or grains (this is an assumption of the proposed model, see Chapter 5).

To calculate the deformation field all forces f_i acting on every single particle i, caused from boundaries, other particles or external forces are needed. The solution of the discretized problem is reduced to the integration of Newton's equations of motion for the translational and rotational degrees of freedom:

$$m_i \frac{d^2}{dt^2}\boldsymbol{r}_i = \boldsymbol{f}_i + m_i\boldsymbol{g}, \quad \text{and} \quad I_i \frac{d}{dt}\boldsymbol{\omega}_i = \boldsymbol{t}_i \tag{3.22}$$

where m_i is the mass m_i of particle i, position vector $\boldsymbol{r}_i$, total force acting on it $\boldsymbol{f}_i = \sum_c \boldsymbol{f}_i^c$ (due to contacts with other particles or with the walls), inertia forces responsible for volume forces like gravity $\boldsymbol{g}$, spherical particles moment of inertia I_i, angular velocity $\boldsymbol{\omega}_i$ and total torque $\boldsymbol{t}_i = \sum_c(\boldsymbol{l}_i^c \times \boldsymbol{f}_i^c \times \boldsymbol{q}_i^c)$, where $\boldsymbol{q}_i^c$ are torques/couples contacts other than due to a tangential force (due to rolling and torsion).The equations of motion are thus a system of coupled ordinary differential equations.
Another fundamental aspect is the interaction range between particles in order to regularize the internal lattice with the solid material; for instance for granular materials short-range interactions are considered, in opposite to solid materials where long-range interactions exist.

As mentioned above the interaction between two generic particles of the model is strictly related with their overlap δ (the nature and the evolution of the contact will be analyzed in the following Chapter 4). This superposition causes a force on particle i from particle j that can be decomposed into a normal and a tangential part representing normal stiffness and tangential stiffness.

$$\boldsymbol{f}_i^c = f^n \boldsymbol{n} + f^t \boldsymbol{t} \tag{3.23}$$

Where the normal contact force is usually expressed as:

$$f_n = k\delta + \gamma_0 v_n \tag{3.24}$$

with k the spring stiffness, γ_0 the viscous damping coefficient, and v_n the relative velocity in normal direction.

For the tangential degrees of freedom, there are three different force- and torque- laws to be implemented: friction, rolling resistance and torsion resistance.

Some authors [33] use the relative velocity as input, compute either sliding, rolling or torsion resistance and return the respective forces as function of accumulated deformations.

Remaining at the macroscopic level, a consistent model has to consider the following forces in macroscopic simulations: contact plasticity, or recoil (when necessary), attractive forces, such as cohesion, adhesion, liquid bridging, electrostatic attraction. Note that, because of the overhead from determining nearest neighbor pairs, exact resolution of long-range (compared with particle size) forces, can increase the computational cost or require specialized algorithms to resolve these interactions.

3.4 Solid and Fluid Interaction

In the last years, there has been an increasing interest in the development of efficient numerical methods for the analysis of engineering problems involving the interaction of fluids and structures [34], accounting for large motions of the fluid free surface and the existence of fully or partially submerged bodies. Ship hydrodynamics, offshore structures, spillways in dams, free surface channel flows, liquid containers, stirring reactors, mould filling processes are examples of fields applications of this numerical methods.

A classical approach to study moving solids in fluid is the finite element method (FEM)[35] based on the Lagrangian-Eulerian (ALE) formulation [36]; in ALE the movement of the fluid particles is decoupled from that of the mesh nodes; as a consequence the convective velocity in the momentum equations is the relative velocity between mesh nodes and particles.

Some numerical procedures for fluid-structure interaction (FSI) analysis use ALE formulation in conjunction with stabilized finite element methods; for instance the Deforming Spatial-Domain/Stabilized space-time (DSD/SST)[37] proposed for computation of fluid-structure interaction and free-surface flow problems, the Mixed Interface-Tracking/Interface-Capturing Technique (MITICT) [38] used for computation of problems that involve both fluid-structure interactions and free surfaces. The MITICT can in general be useful for classes of problems that involve both interfaces that can be tracked with a moving-mesh method and interfaces that are too complex or unsteady to be tracked and therefore require an interface-capturing technique.

Common problems in FSI analysis based on the use of FEM with both the Eulerian and ALE formulation are:

- the treatment of the convective terms and the incompressibility constraint in the fluid equations,
- the modelling and tracking of the free surface in the fluid,
- the transfer of information between the fluid and solid domains via the contact interfaces, the modelling of wave splashing,
- the possibility to deal with large rigid body motions of the structure within the fluid domain,

Most of this problems can be eliminated formulating the governing equations of both solid and fluid domain by using a *Lagrangian description;* in this way the finite element mesh of solids can be considered as moving "particles", and following the individual motion of them, is possible to study the transient solution of the total domain.

This method called Particle Finite Element Method (PFEM), considers the mesh nodes in the fluid and solid domains as particles, which can freely move and even separate from the main fluid domain representing, for instance, the effect of water drops. A finite element mesh connects the nodes defining the discretized domain where the governing equations are solved in the standard FEM fashion [39].

An obvious advantage of the Lagrangian formulation is that the convective terms disappear from the fluid equations, but the need of properly treating the incompressibility condition in the fluid remains.

3.4.1 Basic concepts of Particle Finite Element Methods

In a domain containing both fluid and solid subdomains, the moving fluid particles interact with the solid boundaries thereby inducing the deformation of the solid, which in turn affects the flow motion and, therefore, the problem, is fully coupled. FSI problems traditionally are solved using an arbitrary Eulerian-Lagrangian description (ALE) for the flow equation whereas the structure is modeled with a full Lagrangian formulation [34].

In the PFEM approach, both the fluid and the solid domains are modelled using an updated Lagrangian formulation and the finite element method (FEM) is used to solve the continuum equations in both domains. Hence, a mesh discretizing these domains must be generated in order to solve the governing equations for both the fluid and solid problems in the standard FEM fashion.

A typical solution with PFEM follows these steps:

a) Discretize the fluid and solid domains with a finite element mesh. The mesh generation process can be based for example on a standard Delaunay discretization;
b) Identify the external boundaries for both the fluid and solid domains;
c) Solve the coupled Lagrangian equations of motion for the fluid and the solid domains. Velocities, pressure and viscous stresses in the fluid and displacements, stresses and strain in the solid are relevant state variables;
d) Move the mesh nodes to a new position in terms of the time increment size;

e) Generate a new mesh if needed. The mesh regeneration process can take place after a prescribed number of time steps or when the actual mesh has suffered severe distortions due to the Lagrangian motion;
f) Back to step 2 and repeat the solution process for the next time step.

3.4.2 Lagrangian Equations for an Incompressible Fluid.

Considering a viscous incompressible fluid, the standard infinitesimal equations can be written in a Lagrangian frame as

Momentum conservation

$$r_{m_i} - \frac{1}{2}\ h_j \frac{\partial r_{m_i}}{\partial x_j} = 0 \tag{3.25}$$

Mass balance

$$r_d - \frac{1}{2}\ h_j \frac{\partial r_d}{\partial x_j} = 0 \tag{3.26}$$

where

$$r_{m_i} = \rho \frac{\partial v_i}{\partial t} + \frac{\partial \sigma_{ij}}{\partial x_j} - b_i \quad , \quad \sigma_{ij} = \sigma_{ji} \tag{3.27}$$

$$r_d = \frac{\partial v_i}{\partial x_i} \quad , \quad i,j = 1, n_d \tag{3.28}$$

n_d is the number of space dimension, v_i is the velocity along the -ith global axis ($v_i = \frac{\partial u_i}{\partial t}$), where u_i is the -ith displacement, ρ is the (costant) density of the fluid, b_i are the body forces, σ_{ij} are the total stresses given by $\sigma_{ij} = s_{ij} - \delta_{ij} p$, p is the absolute pressure (defined positive in compression) and s_{ij} are

the viscous deviatoric stresses related to the viscosity μ through the standard expression:

$$s_{ij} = 2\mu\left(\dot{\varepsilon_{ij}} - \delta_{ij}\frac{1}{3}\frac{\partial v_k}{\partial x_k}\right) \tag{3.29}$$

where δ_{ij} is the Kronecker delta and the strain rates $\dot{\varepsilon_{ij}}$ are obtained as:

$$\dot{\varepsilon_{ij}} = \frac{1}{2}\left(\frac{\partial v_i}{\partial x_j} + \frac{\partial v_j}{\partial x_i}\right) \tag{3.30}$$

The problem definition is completed with the following boundary conditions

$$n_j\sigma_{ij} - t_i + h_j n_j r_{m_i} = 0 \quad on\ \Gamma_t \tag{3.31}$$

$$v_j - v_j^p = 0 \quad on\ \Gamma_v \tag{3.32}$$

and the initial condition is $v_j = v_j^0$ for $t = t_0$. In equations (3.31), (3.32) t_i and v_j^p are surface tractions and prescribed velocities on the boundaries Γ_t and Γ_v, respectively, n_j are the components of the unit normal vector to the boundary, h_j are characteristic lengths of the domain where balance of momentum and mass is enforced.

Equations (3.25-26) are the starting point for deriving stabilized finite element methods to solve incompressible Navier-Stokes equations in a Lagrangian frame by using equal order interpolation for the velocity and pressure variables.

The weighted residual expression of the final form of the momentum and mass balance equations can be written, respectively, as:

$$\int_{\Omega} \delta v_i r_{m_i} \, d\Omega + \int_{\Gamma_i} \delta v_i \left(n_j \sigma_{ij} - t_i \right) d\Gamma = 0 \tag{3.33}$$

$$\int_{\Omega} q \left[r_d - \sum_{i=1}^{n_d} \tau_i \frac{\partial r_{m_i}}{\partial x_j} \right] d\Omega = 0 \tag{3.34}$$

where δv_i and q are arbitrary weighting functions equivalent to virtual velocity and virtual pressure fields.

The term r_{m_i} in Eq.(3.34), the deviatoric stresses and the pressure terms within r_{m_i} in Eq. (3.30) are integrated by parts to give:

$$\int_{\Omega} \left[\delta v_i \rho \frac{\partial v_i}{\partial t} + \delta \dot{\varepsilon}_{ij} \left(s_{ij} - \delta_{ij} p \right) \right] d\Omega - \int_{\Omega} \delta v_i \, b_i d\Omega - \int_{\Gamma_t} \delta v_i t_i \, d\Gamma = 0 \tag{3.35}$$

$$\int_{\Omega} q \frac{\partial v_i}{\partial x_j} d\Omega + \int_{\Omega} \left[\sum_{i=1}^{n_d} \tau_i \frac{\partial q}{\partial x_i} r_{m_i} \right] d\Omega = 0 \tag{3.36}$$

Pressure gradient projection

The computation of the residual terms in Eq.(3.36) can be simplified by introducing the pressure gradient projection π_i, defined as

$$\pi_i = r_{m_i} - \frac{\partial p}{\partial x_i} \tag{3.37}$$

The final system governing equation is:

$$\int_\Omega \left[\delta v_i \rho \frac{\partial v_i}{\partial t} + \delta\dot{\varepsilon}_{ij}\left(s_{ij} - \delta_{ij} p\right)\right] d\Omega - \int_\Omega \delta v_i \, b_i d\Omega - \int_{\Gamma_t} \delta v_i t_i \, d\Gamma = 0 \tag{3.38}$$

$$\int_\Omega q \frac{\partial v_i}{\partial x_i} d\Omega + \int_\Omega \sum_{i=1}^{n_d} \tau_i \frac{\partial q}{\partial x_i}\left(\frac{\partial p}{\partial x_i} + \pi_i\right) d\Omega = 0 \tag{3.39}$$

$$\int_\Omega \delta\pi_i \tau_i \left(\frac{\partial p}{\partial x_i} + \pi_i\right) d\Omega = 0 \tag{3.40}$$

with $i, j, k = 1, n_d$. In (3.40) $\delta\pi_i$ are appropriate weighting functions and the weights τ_i are introduced for symmetry reasons.

3.4.3 Finite element discretization

In Particle Finite Element Methods there is a C^0 continuous interpolations of the velocities, the pressure and the pressure gradient projections π_i over each element with *n* nodes. The interpolations are written as:

$$v_i = \sum_{\mathrm{j}=1}^{\mathrm{n}} \mathrm{N_j} \, \bar{v}_i^j \,, \quad p = \sum_{\mathrm{j}=1}^{\mathrm{n}} \mathrm{N_j} \, \bar{p}^j \,, \quad \pi_i = \sum_{\mathrm{j}=1}^{\mathrm{n}} \mathrm{N_j} \, \bar{\pi}_i^j \tag{3.41}$$

where $(\bar{\cdot})^j$ denotes nodal variables and $\mathrm{N_j}$ are the common shape functions.

Substituting the approximations (3.38) into the equations (3.35-37) and choosing a Galerkin form with $\delta v_i = q = \delta \pi_i = \mathrm{N_i}$ leads to the following system of discretized equations

$$\mathrm{M}\dot{\bar{\mathbf{v}}} + \mathbf{g} - \mathbf{f} = 0 \tag{3.42}$$

$$\mathbf{G}^{\mathrm{T}}\bar{\mathbf{v}} + \mathbf{L}\bar{\mathrm{p}} + \mathrm{Q}\bar{\boldsymbol{\pi}} = 0 \tag{3.43}$$

$$\mathbf{Q}^{\mathrm{T}}\bar{\mathbf{p}} + \hat{\mathbf{M}}\bar{\boldsymbol{\pi}} = 0 \tag{3.44}$$

where

$$\bar{\mathbf{g}} = \int_{\Omega} \mathbf{B}^{T}[\mathbf{s} - \mathbf{m}p]d\Omega \tag{3.45}$$

$\bar{\mathbf{g}}$ is the internal nodal force vector derived from the momentum equations, $\mathbf{s}$ is the deviatoric stress vector, $\mathbf{B}$ is the strain rate matrix and $\mathbf{m} = [1,1,0]^{T}$ for 2D problems.

3.4.4 Fractional Step method for Fluid-Structure Interaction analysis

By splitting, the pressure from the momentum equations is possible to obtain a simple and effective iterative algorithm as follow:

$$\bar{\mathbf{v}}^{*} = \bar{\mathbf{v}}^{n} - \Delta t\mathbf{M}^{-1}\left[\mathbf{g}^{n+\theta,j} - \mathbf{f}^{n+1}\right] \tag{3.46a}$$

$$\bar{\mathbf{v}}^{n+1,j} = \bar{\mathbf{v}}^{*} + \Delta t\mathbf{M}^{-1}\mathbf{G}\delta\bar{\mathbf{p}} \tag{3.46b}$$

where in Eq. 3.46a

$$\mathbf{g}^{n+\theta_1,j} = \int_{\mathbf{\Omega}^{n+\theta,j}} \mathbf{B}^T \left[\mathrm{s}^{n+\theta_1,j} - \alpha \mathbf{m}^T p^n \right] d\Omega$$

and α is a variable taking values equal to zero or one. For $\alpha = 0$, $\delta p \equiv p^{n+1,j}$ and for $\alpha = 1$, $\delta p = \Delta p$. Note that in both cases the sum of Eqs. (3.46a) and (3.46b) gives the time discretization of the momentum equations with the pressures computed at t^{n+1}. In above equations and in the following, index j denotes an iteration number within each time step.

The value of $\bar{\mathbf{v}}^{n+1,j}$ from Eq. (3.46b) is substituted now into Eq. (3.43) to give

$$\mathbf{G}^{\mathrm{T}} \bar{\mathbf{v}}^* + \Delta t \mathbf{G}^{\mathrm{T}} \mathbf{M}^{-1} \mathbf{G} \delta \bar{\mathbf{p}} + \mathbf{L} \bar{\mathrm{p}}^{n+1,j} + \mathbf{Q} \bar{\boldsymbol{\pi}}^{n+\theta_{2,j}} = \mathbf{0} \tag{3.47}$$

The product $\mathbf{G}^{\mathrm{T}} \mathbf{M}^{-1} \mathbf{G}$ can be approximated by a laplacian matrix,

$$\mathbf{G}^{\mathrm{T}} \mathbf{M}^{-1} \mathbf{G} = \hat{\mathbf{L}} \quad \text{with} \quad \hat{L}_{ij} \simeq \int_{\mathbf{\Omega}^{\mathbf{e}}} \frac{1}{\rho} \boldsymbol{\nabla}^{\mathbf{T}} N_i \, \boldsymbol{\nabla} N_j d\Omega \tag{3.48}$$

In the above equations θ_1, θ_2 are algorithmic parameters ranging between zero and one.

A semi-implicit algorithm can be derived as follows. For each interation:

1) Compute $\mathbf{v}^*$ from Eq.(3.46a) with $\mathbf{M} = \mathbf{M}_d$ where subscript d denotes here onwards a diagonal matrix
2) Compute $\delta \bar{\mathbf{p}}$ and $\mathbf{p}^{n+1}$ from Eq.(3.47) as

$$\delta\bar{\mathbf{p}} = -\left(\mathbf{L} + \Delta t\hat{\mathbf{L}}\right)^{-\mathbf{1}}\left[\mathbf{G}^T\mathbf{v}^* + \mathbf{Q}\bar{\boldsymbol{\pi}}^{n+\theta_{2,j}} + \alpha\mathbf{L}\bar{\mathbf{p}}^n\right] \tag{3.49}$$

The pressure p^{n+1} is computed as follows

$$\text{For } \alpha = 0 \qquad \bar{\mathbf{p}}^{n+1,j} = \delta\bar{\mathbf{p}}$$

$$\text{For } \alpha = 1 \qquad \bar{\mathbf{p}}^{n+1,j} = \bar{\mathbf{p}}^n + \delta\bar{\mathbf{p}}$$

3) Compute $\bar{\mathbf{v}}^{n+1,j}$ from Eq. (3.46b) with $\mathbf{M} = \mathbf{M}_d$

4) Compute $\bar{\boldsymbol{\pi}}^{n+1}$ from Eq. (3.44) as

$$\bar{\boldsymbol{\pi}}^{n+1,j} = -\hat{\mathbf{M}}_d^{-\mathbf{1}}\mathbf{Q}^T\bar{\mathbf{p}}^{n+1,j} \tag{3.50}$$

5) Solve for the movement of the structure due to the fluid flow forces.

This implies solving the dynamic equations of motion for the structure written as

$$\mathbf{M}_s\ddot{\mathbf{d}} + \mathbf{K}_s\mathbf{d} = \mathbf{f}_{\mathbf{ext}} \tag{3.51}$$

where $\ddot{\mathbf{d}}$ and $\mathbf{d}$ are r the nodes acceleration and the displacement vectors of the discretized structure respectively, $\mathbf{M}_s$ and $\mathbf{K}_s$ are the mass and stiffness matrices of the structure and $\mathbf{f}_{\mathbf{ext}}$ is the vector of external nodal forces accounting for the fluid flow forces induced by the pressure and the viscous stresses. Solution of Eq. (3.51) in time can be performed using implicit or fully explicit time integration algorithms.

3.5 Particle dynamics simulation of fracture

Attaining a better understanding of the comminution of rocks, a phenomenon that commonly takes place in the mining industry, has been one of the targets of particle methods. Comminution involves complex crushing and fragmentation processes, which, from a basic engineering science perspective, are complex dynamic fractures of multi-phase materials. Thus, there is a need to simulate such processes from basic principles. The first tool that comes to mind is the continuum-type dynamic fracture mechanics. That approach, however, is best suited for analysis of well-defined boundary initial-value problems with simple geometries.

Structural materials need to retain their shape under mechanical loading. If the loading is too large, the material fails. During the fracture phenomenon the driving force, that breaks the bonds between atoms ahead of the crack, is concentrated at the crack tip; what ultimately controls the strength of the materials is the bonding between the atoms, so an understanding of the atomic scale processes at the crack tip permits to predict fracture development.

However, the range of length scales involved, from elastic strain fields to interatomic bonds, makes such simulations challenging. Many authors propose different types of coupling length scales approach that addresses some of these difficulties by combining different simulation methods in different parts of the system.

For example in [40] the author uses an implementation that combines two different atomistic simulations methods: a quantum-mechanical model of bonding near the crack tip, and an empirical interatomic potential far from the crack tip.

The particle modeling - also called *particle simulation*, *discrete modeling* or *quasi-molecular modeling* [45-47] - is a dynamic simulation method that typically uses a lattice of small (but not at the molecular level) particles, evolving according to laws of mechanics, as a discrete representation of fluids and/or solids.

The method is set up to maintain the conservation of mass and energy of the particle system and satisfies the interaction laws between all the particles. As demonstrated in the above-cited references, the PM can handle a wide range of complex material systems, problems with complicated boundary shapes and boundary conditions, dynamic evolving free surfaces, and fracture of solids.

Most recently, Abraham et al. [41] used large-scale molecular dynamics simulations to show that the elastic behavior of a solid by considering large strains (hyperelasticity), can play a governing role in the dynamics of fracture, and that linear elasticity theory is not capable of explaining all fracture phenomena. From their simulation results, they came to introduce the new concept of a characteristic length scale for the energy flux near the crack tip. Successively, they demonstrated that the local hyperelastic wave speed governs the crack velocity when the hyperelastic zone approaches this energy length scale [41].

The classical theory of dynamics fracture is no longer valid once the hyperelastic zone size becomes comparable to the energy characteristic length [41]. This characteristic length for local energy flux near the crack tip had never been discussed before. However, through their molecular dynamics simulations, it becomes now the central concept in understanding the effect of hyperelasticity.

Molecular dynamics fracture simulation has also contributed to the understanding of the limit of crack propagating speed [42–44]. Mechanisms of intersonic crack propagation along a weak interface under shear-dominated loading have been studied by molecular dynamics simulations, which also motivated extensive continuum studies of crack propagation at the speed over the sound barrier.

In addition to those introduced above, there have been numerous examples of MD simulations for fracture mechanism at the nanoscale [48].

3.6 Smoothed particle hydrodynamics

Smoothed Particle Hydrodynamics (SPH) is one of the earliest particle methods in computational mechanics [10]. SPH permits to obtain an approximate numerical solutions of the equations of fluid dynamics by replacing the fluid with a set of particles; the particles are interpolation points from which properties of the fluid can be calculated and can be treated like any other particle of the system. The collective movement of those particles is similar to the movement of a liquid, or gas flow, and it may be modeled by the governing equations of classical Newtonian hydrodynamics.

This method has some advantages, such as, pure advection is treated exactly. Another advantage is that with more than one material, each described by its own set of particles, interface problems are often trivial for SPH, but difficult for finite difference or FE schemes. The third advantage is that particle methods bridge the gap between the continuum and fragmentation in a natural way.

Because of the distinct advantages of the particle method, soon after its debut, the SPH method was widely adopted as one of the most efficient computational techniques to solve applied mechanics problems.

Therefore, the term *hydrodynamics* really should be interpreted as *mechanics* in general, if the methodology is applied to other branches of mechanics rather than classical hydrodynamics. To make distinction with the classical hydrodynamics, some authors called it *Smoothed Particle Applied Mechanics* [50-51].

This idea of the method is somewhat contrary to the concepts of the conventional discretization methods, which discretize a continuum system into a discrete algebraic system. In astrophysical applications, one of the first field of application of the method the real physical system is discrete; in order to avoid singularity, a local continuous field is generated by introducing a localized kernel function, which can serve as a smoothing interpolation field. If one wishes to interpret the physical meaning of the kernel function as the probability of a particle's position, he is dealing with a probabilistic method, otherwise. Otherwise it is only a smoothing technique. Thus, the essence of the method is to choose a smooth kernel, $W(\mathbf{x}, h)$ (h is the smoothing length), and to use it to localize *the strong form* of a partial differential equation through a convoluted integration. The interpolating kernel has to satisfy the following conditions:

$$\int W(\mathbf{x}-\mathbf{x}', h)\,\mathbf{dx}' = \mathbf{1} \tag{3.52}$$

$$\lim_{\mathrm{h}\to 0} W(\mathbf{x}-\mathbf{x}', h) = \delta(\mathbf{x}-\mathbf{x}') \tag{3.53}$$

$$W(\mathbf{x}, h) \geq 0 \tag{3.54}$$

where the limit is to be interpreted as the limit of the corresponding integral interpolants.

If the SPH averaging/localization operator is defined as

$$A_k(\mathbf{x}) = \int_{\mathbb{R}^n} W(\mathbf{x}-\mathbf{x}', h)A(\mathbf{x}')d\Omega_{\mathbf{x}'}$$
$$\approx \sum_{I=1}^{N} W(\mathbf{x}-\mathbf{x}_I, h)A(\mathbf{x}_I)\Delta V_I \tag{3.55}$$

it is possible to derive a SPH discrete equation of motion from its continuous counterpart [10]:

$$\langle \rho \frac{d\mathbf{v}}{dt} \rangle_I = -\langle \nabla \boldsymbol{\sigma} \rangle_I \Rightarrow \rho_I \frac{d\mathbf{v}_I}{dt}$$
$$\approx -\sum_{J=1}^{N} (\boldsymbol{\sigma_I} - \boldsymbol{\sigma_J}) \boldsymbol{\nabla} W(\mathbf{x_I} - \mathbf{x}_J, h)\, \Delta V_I \tag{3.56}$$

where $\boldsymbol{\sigma}$ is Cauchy stress, ρ is the density, $\mathbf{v}$ is the velocity, and ΔV_I is the volume element carried by the particle J.

Usually a positive function, such as the Gaussian function, is chosen as the kernel function:

$$W(\mathbf{x}, h) = \frac{1}{(\pi h^2)^{n/2}} \exp\left[-\frac{\mathbf{x}^2}{h^2}\right], \qquad 1 \le n \le 3 \tag{3.57}$$

The kernel representation is not only an instrument that can smoothly discretize a partial differential equation, but it also furnishes an interpolant scheme on a set of moving particles. By utilizing this property, SPH can serve as a Lagrangian type method to solve problems in continuum mechanics.

SPH technology has been employed to solve problems of both compressible and incompressible flow, multiple phase flow and surface tension, heat conduction, electro-magnetic (Maxwell equations), plasma/fluid motion, general relativistic hydrodynamics, heat conduction and nonlinear dynamics.

Various improvements of SPH have been developed through the years. Most of these improvement are aimed to fix the following shortcomings, or pathologies, in numerical computations: tensile instability [52], lack of interpolation consistency, or completeness [53], zero-energy mode [54], difficulty in enforcing essential boundary condition [55].

In solid mechanics the main advantage of SPH is the possibility of dealing with larger local distortion than grid-based methods. This feature has been exploited in many applications such as: metal forming, impact, crack growth, fracture, fragmentation, etc. Another important advantage of meshfree methods in general, and of SPH in particular, is that mesh dependence problems are naturally avoided given the meshfree nature of the method. In particular, mesh alignment is related to problems involving cracks and it is avoided in SPH due to the isotropic support of the kernel functions.

References

[1] Liu WK, Belytschko T, and Chang H (1986), An arbitrary Lagrangian-Eulerian finite element method for path-dependent materials. *Comput. Methods Appl. Mech. Eng.* **58**, 227–246.

[2] Liu WK, Chang H, Chen JS, and Belytschko T (1988), Arbitrary Lagrangian and Eulerian Petrov-Galerkin finite elements for nonlinear problems, *Comput. Methods Appl. Mech. Eng.* **68**, 259–310.

[3] Huerta A and Liu WK (1988), Viscous flow with large free surface motion, *Comput. Methods Appl. Mech. Eng.* **9**, 277–324.

[4] Liu WK, Chen JS, Belytschko T, and Zhang YF (1991), Adaptive ALE finite elements with particular reference to external work rate on frictional interface, *Comput. Methods Appl. Mech. Eng.* **93**, 189–216.

[5] Belyschko T, Liu WK, and Moran B (2000) *Nonlinear Finite Elements for Continua and Structures*, John Wiley and Sons, New York.

[6] Benz W (1990), Smooth particle hydrodynamics: a review. In: *Numerical Modeling of Non-linear Stellar Pulsation: Problems and Prospects*, Kluwer Academic, Boston.

[7] Gingold RA and Monaghan JJ (1977), Smoothed particle hydrodynamics: theory and application to non-spherical stars, *Mon. Not. R. Astron. Soc.* **181**, 375–389.

[8] Lucy LB (1977), A numerical approach to the testing of the fission hypothesis, *Astrophys. J.* **82**, 1013.

[9] Monaghan JJ (1982), Why particle methods work (Hydrodynamics), SIAM (Soc. Ind. Appl. Math.) J. Sci. Stat. Comput. 3, 422–433.

[10] Monaghan JJ (1985), Particle methods for hydrodynamics, *Comput.Phys. Rep.* **3**, 71–124.

[11] Bernard PS (1995), A deterministic vortex sheet method for boundarylayer flow, *J. Comput. Phys.* **117**, 132–145.

[12] Chorin AJ (1973), Numerical study of slightly viscous flow, *J. Fluid Mech.* **57**, 785–796.

[13] Chorin AJ (1973), Discretization of a vortex sheet, with an example of roll-up, *J. Comput. Phys.* **13**, 423–429.

[14] Chorin AJ (1978), Vortex sheet approximation of boundary layers, *J. Comput. Phys.* **27**, 428–442.

[15] Leonard A (1980), Vortex methods for flow simulation, *J. Comput. Phys.* **37**, 289–335.

[16] Leonard A (1985), Computing three-dimensional incompressible flows with vortex elements, *Annu. Rev. Fluid Mech.* **17**, 523–529

[17] Liszka T, and Orkisz J (1980), The finite difference method at arbitrary irregular grids and its application in applied mechanics, *Comput. Struct.* **11**, 83–95.

[18] Liszka T (1984), An interpolation method for an irregular net of nodes, *Int. J. Numer. Methods Eng.* **20**, 1599–1612

[19] Feldneier H and Schnack J (2000). Molecular dynamics for fermions. Technical report, Gesellschaft fur Schwerionenforschung mbH.

[20] Kobrak MN, and Bittner ER (2000), Quantum molecular dynamics study of polaron recombination in conjugated polymers, *Phys. Rev. B* **62**, 11473–11486.

[21] Rapaport DC (1995), The Art of Molecular Dynamics Simulation, Cambridge Univ Press, Cambridge, UK.

[22] Allen MP and Tildesley DJ (1987), *Computer Simulation of Liquids*, Oxford Univ Press, Oxford, UK.

[23] Bird GA (ed) (1994), Molecular Gas Dynamics and the Direct Simulation of Gas Flow, Oxford Univ Press, Oxford, UK.

[24] Oran ES, Oh CK, and Cybyk BZ (1998), Direct simulation Monte Carlo: Recent advances and applications, Annu. Rev. Fluid Mech. **30**, 403–441.

[25] Frisch U, Hasslacher B, and Pomeau Y (1986), Lattice gas cellular automata for the Navier-Stokes equations, *Phys. Rev. Lett.* **56**, 1505

[26] Kadanoff L (1986), On two levels, *Phys. Today* **39**, 7–9.

[27] Wang Y-H., Leung S-C. (2008), A particulate-scale investigation of cemented sand behavior, *Canadian Geotech J*;45:29–44,.

[28] Ergenzinger C, Seifried R, Eberhard P. (2010), A discrete element model to describe failure of strong rock in uniaxial compression, *Granul Matter*;13:1–24.

[29] Potyondy D, Cundall P. (2004), A bonded-particle model for rock, *Int J Rock Mech Min Sci*; 41:1329–64.

[30] Yu. A.Amenzade (1971), Theory of Elasticity, *Vysshaya Shkola*, Moscow.

[31] Wang Y, Alonso-Marroquin F. (2009), A finite deformation method for discrete modeling: particle rotation and parameter calibration, *Granul Matter*;11:331–43.

[32] Z.V. Nagoev, M.M. Oshkhunov (2008), Discrete-Dynamic Particle Method in Problems of Mechanics of Deformable Solids. ICSPRA, *Kabardino-Balkar Scientific Center*, Russian Academy of Sciences.

[33] Stephan Luding , Introduction to discrete element methods, Basics of Contact Force Models and hoe to perform the Micro-Macro Transition

to Continuum Theory. ICSPRA, *Multi Scale Mechanics, TS, CTW,* UTwente, Netherlands.

[34] E. Onate, S.R. Idelshon, F. Del Pin, R. Aubry (2004), The Particle Finite element Method. An Overview. *International Journal of Computational Methods*, Vol. 1 No. 2; 206-307.

[35] Zienkiewicz, O.C. and Taylor, R.L. (2000), *The finite element method*. 5th Edition, 3 Volumes, Butterworth–Heinemann.

[36] Donea, J. and Huerta, A. (2003), Finite element method for flow problems. *J.Wiley*.

[37] Tezduyar, T.E., Behr, M. and Liou, J. (1992), A New Strategy for Finite Element Computations Involving Moving Boundaries and Interfaces - The Deforming- Spatial-Domain/Space-Time Procedure: I. The Concept and the Preliminary Numerical Tests. *Computer Methods in Applied Mechanics and Engineering*, 94, 339–351.

[38] Tezduyar, T. (2001), Finite Element Interface-Tracking and Interface-Capturing Techniques for Flows with Moving Boundaries and Interfaces, ASME Paper IMECE2001/HTD-24206, *Proceedings of the ASME Symposium on Fluid- Physics and Heat Transfer for Macro- and Micro-Scale Gas-Liquid and Phase- Change Flows*, ASME, New York, New York, CD-ROM.

[39] Onate, E., Garcia, J. and Idelsohn, S.R. (2004), Ship hydrodynamics. In *Encyclopedia of Computational Mechanics*, E. Stein, R. de Borst and T.J.R. Hughes (Eds), J. Wiley.

[40] Bernstein, N., Atomisitc Multiscale Simulation of fracture. *Center of computational Materials Science*, Naval Research Laboratory, Washington, DC, USA.

[41] M. J. Buehler, F. F. Abraham and H. Gao (2003), Hyperelasticity governs dynamic fracture at a critical length scale, *Nature 426*, 141.

[42] H. Gao, Y. Huang and F. F. Abraham (2001), Continuum and atomistic studies of intersonic crack propagation,*J. Mech. Phys. Solids* 49, 2113, 2001.

[43] F. F. Abraham and H. Gao (2000), How fast can cracks propagate, *Phys. Rev. Lett*. 84, 3113.

[44] F. F. Abraham (2003), How fast can cracks move? A research adventure in materials failure using a million of atoms and big computers, *Adv. Phys*. 52:727.

[45] D. Greenspan (1981), Computer-Oriented Mathematical Physics, Pergamon press.

[46] D. Greenspan (1989), Supercomputer simulation of cracks and fractures by quasi-molecular dynamics, *J. Phys. Chem. Solids* 50 (10) 1245–1249.

[47] D. Greenspan (1997), Particle Modeling, Birkhauser Publishing.

[48] D. Greenspan (2002), New approaches and new applications for computer simulation of N-body problems, *Acta Appl. Math*. 71. 279–31.

[49] Shan Huang, Sulin Zhang, Ted Belytschko, Sachin S. Terdalkar, Ting Zhu (2009), Mechanics of nanocrack: Fracture, dislocation emission,and amorphization, *Journal of the Mechanics and Physics of Solids* 57. 840–850.

[50] Kum O, Hoover WG, and Posch HA (1995), Viscous conducting flows with smooth-particle applied mechanics, *Phys. Rev. E* **109**, 67–75.

[51] Posch HA, Hoover WG, and Kum O (1995), Steady-state shear flows via nonequilibrium molecular dynamics and smooth-particle applied mechanics, *Phys. Rev. E* **52**, 1711–1719.

[52] Swegle JW, Hicks DL, and Attaway SW (1995), Smoothed particlehydrodynamics stability analysis, *J. Comput. Phys.* **116**, 123–134.

[53] Liu WK, Jun S, and Zhang YF (1995), Reproducing kernel particle methods, *Int. J. Numer. Methods Eng.* **20**, 1081–1106.

[54] Vignjevic R, Campbell J, and Libersky L (2000), A treatment of zeroenergymodes in the smoothed particle hydrodynamics method, *Comput.Methods Appl. Mech. Eng.* **184**, 67–85.

[55] Randles PW and Libersky LD (1996), Smoothed particle hydrodynamics: Some recent improvements and applications, *Comput. Methods Appl. Mech. Eng.* **139**, 375–408

Chapter 4

CONTACT PROBLEMS ANALYSIS IN DEM

4.1 Introduction

Discrete Element Model (DEM) simulations rely on realistic contact force models; however too many details make both implementation and interpretation prohibitively difficult. A contact model must represent the physical properties of elastic-plastic repulsion, dissipation, adhesion, friction as well as rolling and torsion-resistance.

Research challenges involve not only the realistic quantitative and predictive simulation of many-particle systems and their experimental validation, but also the transition from the microscopic contact properties to the macroscopic flow behavior. The so-called micro-macro transition should allow understanding the collective flow behavior of many particles as function of their contact properties.

The main goal in DEM is to provide a minimal set of contact models as a compromise between a realistic and an easy to handle modeling approach. Naturally, the contact models needs to be over-simplified, since many details seem not to be important for the behavior on the mesoscopic or macroscopic level. As mentioned above, a single contact-model allows simulating various

systems and structures, and simpler contact models will facilitate a better and deeper understanding of the relation between micro- and macro-properties.

4.2 Configurations of colliding bodies

When a solid hits another solid, the surfaces of the two bodies come together with some relative velocity at an initial instant termed *incidence*.

At each instant during the impact period, a pressure arises in a small area of contact between the two bodies, leading to a local deformation and consequent indentation. During impact, the interface or contact pressure has a resultant force or reaction that acts in opposite directions on the two colliding bodies thereby resists interpenetration.

Initially during contact the force increases and produce a reduction of the speed at which the bodies are approaching each other. At some instant during the impact, the velocity is reduced to zero by the work done by the contact forces. Subsequently, the energy stored during compression drives the two bodies apart until finally they separate with some relative velocity.

Local deformations produce the contact force that acts during collision, these deformations vary according to the incident relative velocity at the point of initial contact as well as the hardness of the colliding bodies. Low speed collisions, for example, implies small deformations, that are significant solely in a small region adjacent to the contact area, at higher speeds there are large deformations (strains) near the contact area which results in plastic flows; these large localized deformations are easily recognizable, since they have gross manifestations such as cratering or penetration. In each case the deformations are consistent with the contact force that causes velocity changes of the colliding bodies.

Phenomena involved in bodies during the collision can be summarized as follow: there is an instant of time, time *t=0* termed *incidence* (the initial instant of impact) when a single contact point C on the surface of the first body B initially comes into contact with point C' on the surface of the second body B' (Fig.4.1). Usually is possible to determine a common tangent plane that passes through the coincident contact points C and C'; the orientation of this plane is defined by the direction of the unit normal vector **n**, which is perpendicular to the common tangent plane.

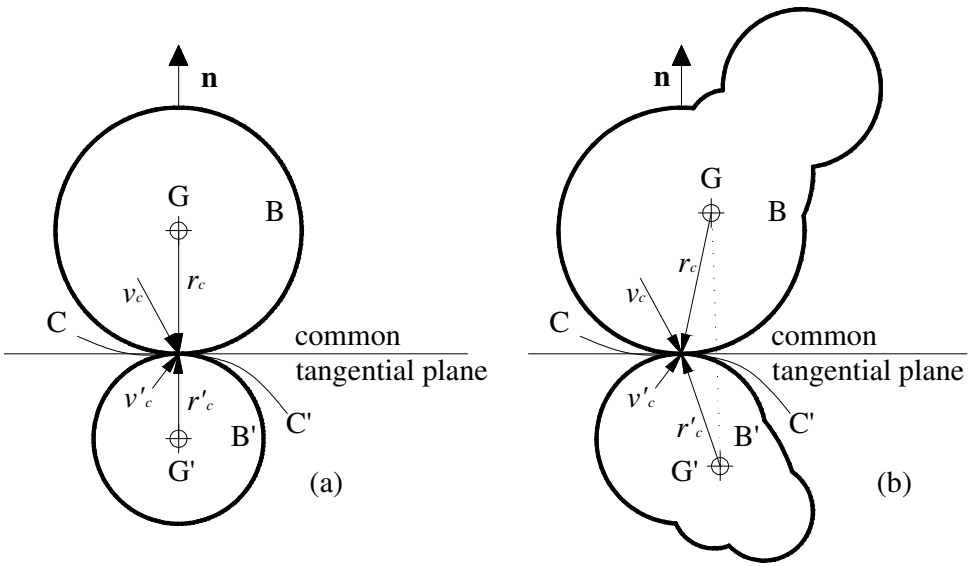

Fig.4.1 – Colliding bodies B and B' with (a) collinear and (b) non collinear impact configurations

Considering two bodies with centers of mass G and G' and colliding points C and C', it is possible to define different impact configurations; if the line that links G and G' passes through C the impact is termed *collinear*, or central (Fig.4.1a).

$$\mathbf{r}_C \times \mathbf{n} = \mathbf{r'}_C \times \mathbf{n} = 0 \tag{4.1}$$

In equations of motions collinear impact configurations can be decoupled in normal and tangential directions.

If the bodies are rough and the line that links G and G' does not pass through C, the configuration is *eccentric* and there is a tangential force of friction that oppose sliding; the equations of motions involve both normal and tangential forces and impulses (Fig4.1b).

$$\mathbf{r}_C \times \mathbf{n} \neq \mathbf{0} \qquad \text{or} \qquad \mathbf{r'}_C \times \mathbf{n} \neq 0 \tag{4.2}$$

4.2.1 Relative velocity at contact point

Initially at the instant when colliding bodies first interact, the coincident contact points C and C' have an initial or incident relative velocity $\mathbf{v}_0 \equiv \mathbf{v}(0) = \mathbf{v}_C(0) - \mathbf{v'}_C(0)$. The initial relative velocity at C has a component $\mathbf{v}_0 \cdot \mathbf{n}$ normal to the tangent plane and a component $(\mathbf{v}_0 \times \mathbf{n}) \times \mathbf{n}$ parallel to the tangent plane; the latter component is termed *sliding velocity.* The angle of obliquity at incidence, ψ_0, is the angle between the initial relative velocity vector $\mathbf{v}_0$ and the unit vector $\mathbf{n}$ normal to the common tangent plane, and can be obtained as:

$$\psi_0 \equiv tan^{-1}\left(\frac{|(\mathbf{v}_0 \times \mathbf{n}) \times \mathbf{n}|}{\mathbf{v}_0 \cdot \mathbf{n}}\right) \tag{4.3}$$

Direct impact occurs when in each body the velocity field is uniform and parallel to the normal direction. Direct impact requires that the angle of obliquity at incidence equals zero ($\psi_0 = 0$); on the other hand, oblique impact occurs when the angle of obliquity at incidence is nonzero ($\psi_0 \neq 0$).

4.2.2 Interaction force

Considering the common tangent plane of two colliding bodies, it is possible to divide the interaction force and the impulse, generated during the impact, into components normal and parallel to the plane. For particle impact, the impulse is considered to be normal to the contact surface. Contact forces for solid bodies arise from local deformation of the colliding bodies; compatibility of displacements in the contact areas are ensured by deformations associated to interactions forces that also prevent interpenetrations (overlap) of the bodies. If the bodies are rough and there is sliding in the contact area a tangential force called friction arises in such an area; it is usually negligible if the bodies are smooth.

The relative displacement of the interacting bodies governs the conservative part of the forces. In an elastic collision the forces associated with attraction or repulsion are conservative (reversible). In an inelastic collision the interaction forces (other than friction) are nonconservative, so there is a loss of kinetic energy as a result of the cycle of compression (loading) and restitution (unloading) that occurs in the contact region. The energy loss can be due to irreversible elastic-plastic material behavior, rate dependent material behavior, elastic waves trapped in the separated bodies, etc…

4.3 Classification of methods for analyzing impact

Deformations during collisions develop in different ways for different body types and they influence the period of contact; following this concept, in order to classify collisions into specific types, distinct methods of analysis are required.

Particle Impact, for example, is an analytical approximation that considers a normal component of interactions impulse only. Particles are smooth and spherical. The source of the interaction force is unspecified, but presumably it is strong and the force has a very short range, so that the period of interaction is a negligible small instant of time.

When the contact area remains small in comparison with all section dimensions of the compact bodies, the collision is called *Rigid Body Impact.* Increasing radial distance from the contact region, stresses generated in the contact area decrease rapidly and the internal energy is concentrated in a small region surrounding the interface, which acts like a short but very stiff spring separating the colliding bodies at the contact point. For bodies that are hard, only very small deformations are required to generate very large contact pressure; if the surfaces are initially nonconforming, the small deformations imply that the contact area remains small throughout the contact period. The contact force is large enough to rapidly change the normal component of the relative velocity across the small-deformed region that surround the contact path. From an analytical point of view, the most important consequence of the small compliance of hard bodies is that very little movement occurs during the very brief period of contact; despite large contact forces, there is insufficient time for bodies to displace significantly during impact. This observation leads to the fundamental hypothesis of *Rigid Body Impact Theory*

that, for hard bodies, assumes the period of contact as very small; consequently, any changes in velocity occur instantaneously in the initial or incident configuration.

Transverse Impact on Flexible Non-spherical Bodies occurs when at least one of the bodies suffers bending because of the interface pressures in the contact area; this bending reduces the interface pressure and prolongs the period of contact during collision and local deformation that arises near the contact, dissipates energy. Transverse impact on plates, shells or slender bars results in significant flexural deformations of the colliding members both during and following the contact period.

Another type of collision model is the *Axial Impact on Flexible Bodies* that generates longitudinal waves; these affect the dynamic analysis of the bodies only if there is a boundary at some distance from the impact point, which reflects the radiating wave back to the source. The time of contact for an impact in this case depends on the time required by a wave to travel between the impact surface and the center of the body.

There are many methods for analyzing changes in velocity and contact forces resulting from impact; the *stereomechanical theory* provides a relationship between incident and final conditions, leading to discontinuous changes in velocity at impact. Rigid bodies' theories are useful for analyzing body impact between compact bodies composed of stiff materials, but they have limited applicability for multibody impact problems because they can give accurate results only if the normal compliance of the point of external impact is very small or large in comparison with the compliance of any connections with adjacent bodies.

4.4 Elastic Particles Kinetics

Considering kinetics related to the dynamics of a particle is the basis for the fundamental form of most principles of dynamics. In DEM, a particle is a body of negligible or infinitesimal size, i.e. a point mass. If a particle with mass *M* is moving with velocity **V** it has momentum *M***V**. When a force **F** acts on the particle, this cause a change in momentum according to the Newton' s second law of motion

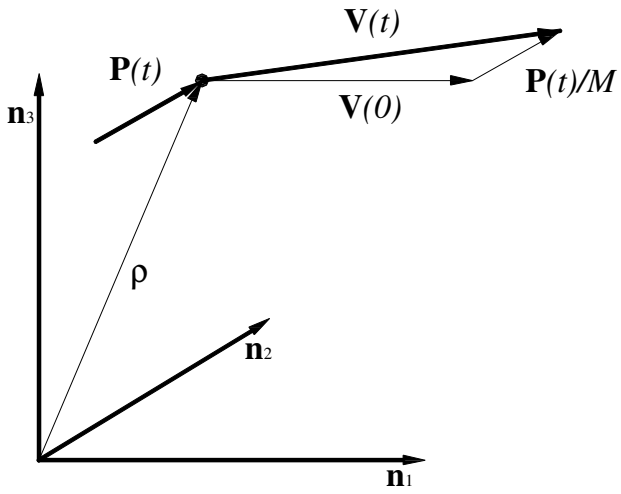

*Fig.4.2 – Change in velocity of particle with mass M resulting from impulse **P**(t)*

That reads "*The momentum MV of a particle has a rate of change with respect to time that is proportional to and in the direction of any resultant force **F**(t) acting on the particle"[1],*

$$\frac{d(M\mathbf{V})}{dt} = \mathbf{F} \tag{4.4}$$

Usually the particle mass is constant, so Eq. (4.4) can be integrated to obtain the changes in velocity as a continuous function of the impulse **P***(t)* :

$$\mathbf{V}(t) - \mathbf{V}(0) = M^{-1} \int_0^t \mathbf{F}(t')\, dt' \equiv M^{-1}\mathbf{P}(t) \tag{4.5}$$

This vector expression is illustrated in Fig 4.2.

Active forces $\mathbf{F}(t)$ and $\mathbf{F}'(t)$ acting on colliding particles B and B', during the interaction period t_f, prevent interpenetration. The particular nature of interaction forces depends on its origin: whether they are due to contact forces between solid bodies that cannot interpenetrate, or are interatomic forces acting between atomic particles. In any case, the force on each particle acts solely in the radial direction. These interaction forces are related by Newton's third law of motion. *"Two interacting bodies have forces of action and reaction that are equal in magnitude, opposite in direction and collinear"[1]:*

$$\mathbf{F}' = -\mathbf{F} \tag{4.6}$$

Second and third Newton's laws are the basis for impulse momentum methods for analyzing impact. Let particle B has mass M, and particle B' has mass M'. Integration of Eq.(4.5) gives equal but opposite impulses $-\mathbf{P}'(t) = \mathbf{P}(t)$, so that equation of motions for the relative velocity $\mathbf{v} \equiv \mathbf{V} - \mathbf{V}'$can be obtained as:

$$\mathbf{v}(t) = \mathbf{v}(0) + m^{-1}\mathbf{P}(t), \qquad m^{-1} = M^{-1} + M'^{-1} \tag{4.7}$$

where m is the effective mass. Eq. (4.7) is applicable only if the period of interaction $t_f \to 0$.

For a set of n particles where the i_{th} particle has mass M_i and velocity $\mathbf{V}_i$, the equations of translational motion can be expressed as

$$\frac{d}{dt}\sum_{i=1}^{n} M_i\mathbf{V}_i = \sum_{i=1}^{n} \mathbf{F}_i + \sum_{i=1}^{n} \mathbf{F'}_{ik}, \qquad i \neq k \tag{4.8}$$

where $\mathbf{F}_i$ is an external force acting on particle i and $\mathbf{F'}_{ik}$ is an internal interaction force of particle k on particle i. Since the internal forces are equal but opposite ($\mathbf{F'}_{ik} = -\mathbf{F'}_{ik}$), the sum of these forces over all particles vanishes; hence

$$\frac{d}{dt}\sum_{i=1}^{n} M_i\mathbf{V}_i = \sum_{i=1}^{n} \mathbf{F}_i \tag{4.9}$$

The moment of momentum $\mathbf{h}_O$ of particle i about point O is defined as $\mathbf{h}_O \equiv \rho_i \times M_i\mathbf{V}_i$, where ρ_i is the position vector of the particle and M_i is its mass.

Thus, a set of particles has a moment of momentum about O, equal to

$$\mathbf{h}_O \equiv \sum_{i=1}^{n} \rho_i \times M_i\mathbf{V}_i \tag{4.10}$$

For a set of n particles, the rate of change of moment of momentum about O is related to the moment about O of the external forces acting on the system:

$$\frac{d\mathbf{h}_O}{dt} = \frac{d}{dt}\sum_{i=1}^{n} \rho_i \times M_i\mathbf{V}_i = \sum_{i=1}^{n} \rho_i \times \mathbf{F}_i \tag{4.11}$$

If the configuration of the system does not change during the period of time *t,* integration of (4.11) with respect to time gives

$$\begin{aligned}\mathbf{h}_O(t) - \mathbf{h}_O(0) \equiv & \sum_{i=1}^{n} \rho_i \times \int_0^t \mathbf{F}_i(t')dt' \\ = & \sum_{i=1}^{n} \rho_i \times \mathbf{P}_i(t)\end{aligned} \tag{4.12}$$

4.4.1 Compression and restitution phases of collisions

After the colliding particles first touch, δ is defined as indentation or compression of the deformable particle, while $F(t)$ is the force that rises between the two bodies.

Only with detailed information about the compliance of the colliding bodies is possible to obtain δ directly. If the bodies have an elastic behavior, the maximum indentation and maximum force occur simultaneously when the normal component of relative velocity vanishes [2].

The Fig 4.3 shows the separation of the contact impulse into an initial phase of approach or *compression* and a subsequent phase of restitution. The contact force, during compression, transforms kinetic energy of relative motion into internal energy of deformation, the initial normal relative velocity is reduced by the contact force's work, while simultaneously the internal deformation energy of the deformable particle is increased by the work of an opposite contact force. When the normal relative velocity of the contact points vanishes, the compression phase terminates and restitution begins. During this last phase, the elastic part of internal energy is released. The bodies are driven by the force generated by elastic strain energy stored during

compression. In Fig.4.3 $v_0 \equiv v(0) = V(0) - V'(0)$, where $V(0)$ is the intial velocity of body B and $V'(0)$ is the initial velocity of the body B'; thus during the impact the normal component of relative velocity is a linear function of the normal impulse. Let the instant when indentation changes from compression to restitution be t_c. The colliding bodies have a relative velocity between contact points that vanishes at the end of compression: $v(t_c) = 0$; i.e. compression terminates when the contact points have the same speed V_c in the normal direction

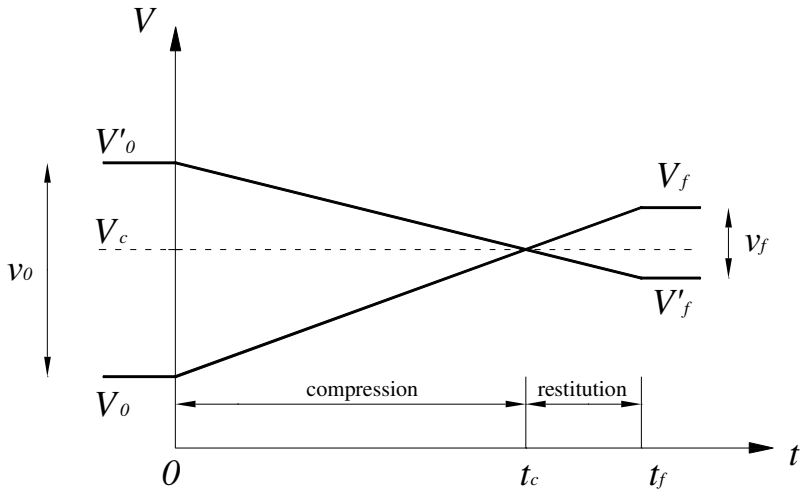

Fig.4.3 – Change of velocities of boies B and B'vs time at the contact point.

Fig.4.3 illustrates that the contact point of each body experiences a change in velocity that is directly proportional to the normal reaction impulse at the contact point C:

$$v = v_0 + m^{-1}p \ , \ \text{where} \ \ v_0<0 \tag{4.13}$$

During compression the increasing impulse slows the body B' and increases the speeds of B as illustrated in Fig.4.3. The reaction impulse is determinate by:

$$p_c = \int_0^{t_c} F(t)dt \tag{4.14}$$

termed the *normal impulse for compression,* which brings the two particles to a common speed; this impulse is a characteristic which is useful for analyzing collision processes.

The normal impulse for a compression is obtained from Eq. (4.13) and the condition that at the end of compression the normal component of relative velocity vanishes.

$$v(p_c) = 0 \tag{4.15}$$

Hence the normal impulse for compression is the product of the effective mass and the intial relative velocity v_0 at C

$$p_c = -mv_0 \ , \ \text{where} \ \ v_0<0 \tag{4.16}$$

4.4.2 Friction law for rough rigid bodies

In DEM typically the normal and tangential (frictional) contact forces are dealt with separately; the first realistic model for static friction was introduced by Cundall and Strack [3]: a virtual tangential spring is attached to each contact point and evolves while the contact partners are moving and rotating, relative to each other, due to the contact force and to the many forces from other particles.

Amontons-Coulomb law of sliding friction [4] can represent the dry friction between colliding bodies. This law relates the tangential component to the normal component of reaction force at the contact point by introducing a coefficient of limiting friction μ which acts if there is sliding; first define a common normal direction **n** that is perpendicular to the common tangent plane. Let $n_i, i = 1,2,3,$ be a set of mutually perpendicular unit vectors with n_1 and n_2 in the tangent plane while $n_3 = n$ is normal to this plane. v_1 and v_2 are the projection of the velocity on axis n_1 and n_2, i.e. $v_1^2 + v_2^2 > 0$. Denoting the magnitude of the normal component of a differential increment of impulse by $dp \equiv dP_n$, this law takes the form:

$$\sqrt{(dp_1)^2 + (dp_2)^2} < \mu dp \ , \qquad \text{if } \ v_1^2 + v_2^2 = 0 \tag{4.17a}$$

$$dp_1 = -\frac{\mu v_1}{\sqrt{v_1^2+v_2^2}}dp, \qquad dp_1 = -\frac{\mu v_2}{\sqrt{v_1^2+v_2^2}}dp \tag{4.17b}$$

$$\text{if } \ v_1^2 + v_2^2 > 0$$

Eq.(4.17a) expresses an upper bound on the ratio of tangential normal force for rolling impact; for ratios of tangential to normal contact force are less then μ the *sliding speed* $s \equiv \sqrt{v_1^2 + v_2^2}$ vanishes. When the sliding is present, $s > 0$, the tangential increment of impulse or friction force at any impulse, acts in a direction opposed to sliding and has a magnitude that is directly proportional to the normal force. The angle ϕ, measured in the tangential plane, defines the sliding direction, $\phi \equiv tan^{-1}\left(\frac{v_2}{v_1}\right)$, and the tangential velocity can be written as

$$v_1 = s\cos\phi, \quad v_2 = s\sin\phi \tag{4.18}$$

During the collision period, since the normal contact force must be of compressive type, the impulse of the normal component of reaction is a monotonically increasing scalar function. Consequently, rates of change for relative velocity at the contact point C can be expressed as a function of the rate of change of impulse for the normal component of reaction.

4.5 Direct impact of viscoelastic bodies

Typically, impact between bodies develops a contact force that is rate dependent or viscoelastic; this rate dependence has some consequences on force, strain and velocity of the collision.

The Maxwell-model (Fig. 4.4-a) is the simplest visco-elatic representation of the contact force [5] arising from mutual compression of colliding particles; an alternative representation is the Kelvin-Voigt model [6] (Fig.4.4-b). Both models have a linear spring and dashpot. For the Maxwell model, the compliance of the deforming region gives a normal relative motion that is restored during restitution through a coefficient in the range 0 to 1.

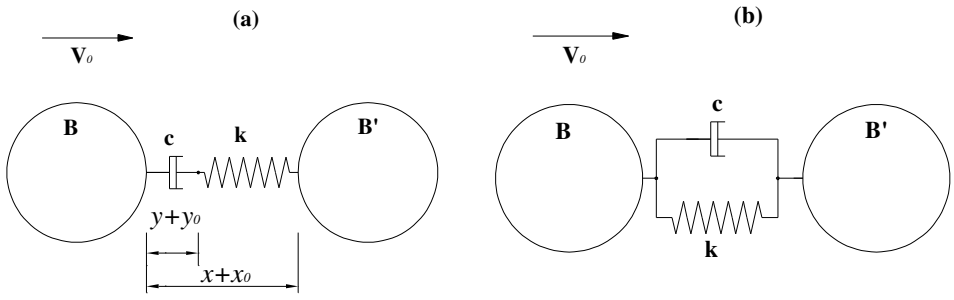

Fig. 4.4 Visco elastic Maxwell model (a) and visco- elastic Kelvin Voigt model

Let us consider two bodies B and B' separated by a Maxwell element: the spring is assumed to be characterized by a constant k and uncompressed length x_0, while the dashpot has a damping force constant c and uncompressed length y_0. Between the two particles the contact force rises: it depends by the relative displacement of the bodies x and by the fraction of this displacement that is due to the compression of the dashpot y; the same force acts in both the spring and dashpot,

$$F = -k(x - y) = -c\dot{y} \tag{4.19}$$

The Maxwell viscoelastic model results in a coefficient of restitution e_* that is independent of the incident of relative velocity:

$$e_* = e^{-\zeta\pi/\sqrt{1-\zeta^2}} \tag{4.20}$$

with the damping ratio

$$\zeta \equiv m\omega_0/2c \tag{4.21}$$

where the damped natural frequency is:

$$\omega_d \equiv \omega_0\sqrt{1-\zeta^2} \tag{4.22}$$

The normal force between the two particles, during collision, is given by the force in the spring or that in the dashpot, that are the same for equilibrium reason [2]:

$$F = -k(x-y) = (1-\zeta^2)^{-1/2} m\omega_0 v_0 e^{-\zeta\omega_0 t}\sin(\omega_d t), \quad \omega_d t \leq \pi \tag{4.23}$$

The Maxwell model gives an asymmetrical force with a contact period t_f that increases with the damping ratio ζ.

In a collision between viscoelastic bodies, the compliance relation is rate-dependent; consequently, the transition from the compression to the restitution phase of contact does not occur at the instant of maximum force when the spring compression is maximum; with the Maxwell model, the dashpot continues to compress throughout the entire contact period.

The transition from compression to restitution occurs when the normal impulse is equal in magnitude to the initial momentum of relative motion mv_0 and this impulse causes the normal velocity to vanish.

4.5 Impact of a spherical body with a flat surface

Let us consider a spherical body of mass *m* and radius *R* which is impacting a flat rigid surface with an initial velocity v_0; from the knowledge of the particle elastic modulus, E_1, and that of the rigid flat surface E_2, is possible to calculate the equivalent elastic modulus *E'*, considering the Poisson's ratios of the two materials, ν_1 , ν_2 the sought relation is[11]:

$$E' = \frac{1-\nu_1^2}{E_1} + \frac{1-\nu_2^2}{E_2} \tag{4.24}$$

If $E_1 = E_2 = E$ and $\nu_1 = \nu_2 = \nu$ then

$$E' = \frac{E}{2(1-\nu^2)} \tag{4.25}$$

The equivalent radius for two spheres in contact is given by [10]

$$\frac{1}{R} = \frac{1}{R_1} + \frac{1}{R_2} \tag{4.26}$$

When a spherical particle collides against a rigid flat surface $R_2 \to \infty$ and the equivalent radius is $R = R_1$.

An effective mass for two colliding bodies can be obtained from the definition

$$\frac{1}{m} = \frac{1}{m_1} + \frac{1}{m_2} \tag{4.27}$$

For the collision of the sphere with mass m_1 against the rigid flat surface with mass $m_2 \to \infty$, the effective mass is $m_1 = m$.

The interference, *x,* is the distance the sphere is displaced normally into the rigid flat plane. The Hertz solution assumes that the interference is small enough such that the geometry does not change significantly.

The motion of impact point during the collision can be of different nature.

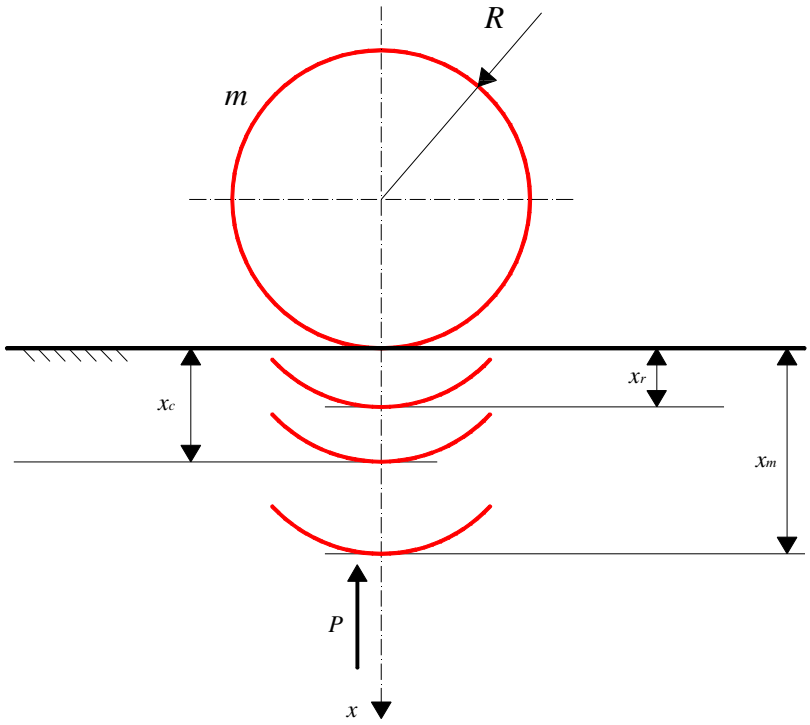

Fig.4.5 Different compression phases for a sphere colliding a flat surface.

4.5.1 Elastic compression phase

The first case occurs when an elastic compression phase starts with the intial impact instant, the contact force F is zero, $F = 0$, and ends when the contact force reaches the known value of the critical force, $F = F_C$. For the critical force the deformation is the critical deformation, $x = x_C$ (Fig.4.5). During this phase, there are only elastic deformations $x = x_e (x_e \leq x_c)$ and the Hertz law can be applied

$$F = k_1 x^{\frac{3}{2}} \tag{4.28}$$

where

$$k_1 = \frac{4}{3}E'\sqrt{R} = \frac{2E\sqrt{R}}{3(1-\nu^2)} \tag{4.29}$$

The equation of motion of the sphere is

$$m\ddot{x} = mg - F \quad \text{or} \quad m\ddot{x} = mg - k_1 x^{\frac{3}{2}} \tag{4.30}$$

The initial conditions at $t = 0$, are $x(0) = 0$, and $\dot{x}(0) = v_0$.

Stresses increase when the contact force F increase and these stresses could cause the material within the sphere to yield. x_c is the critical interference i.e. it is the distance at the initial point of yielding. This critical deformation has been obtained by Chang et al [7]:

$$x_c = \left(\frac{\pi KH}{2E'}\right)^2 R \tag{4.31}$$

where H characterizes the plastic property of the material and can be approximated with the Brinell hardness, K is a hardness factor and is given by $K = 0.454 + 0.41\nu$.

The critical value of the impact force can be expressed in terms of the critical deformation x_c,

$$F_C = k_1 x_c^{\frac{3}{2}} \tag{4.32}$$

Jackson and Green [8] derive this critical interference analytically using the von Mises yield criterion

$$x_c = \left(\frac{\pi C S_y}{2E'}\right)^2 R \tag{4.33}$$

where S_y is the yield strength and C is a critical yield stress coefficient given by

$$c = 1.295\, e^{0.736\nu} \tag{4.34}$$

The Poisson's ratio ν and the yield strength S_y to be used in Eq. (4.33) are that of the material which yields first between particle and surface.

Substituting the critical interference into Hertz theory one can calculate the critical force

$$F_C = \frac{4}{3}\left(\frac{R}{E'}\right)^2 \left(\frac{\pi C S_y}{2E'}\right)^3 \tag{4.35}$$

This model predicts the contact force between an elastic perfectly plastic hemisphere and a flat surface. For $0 \leq x/x_c \leq 1.9$ it effectively coincides with the Hertzian solution, even though the onset of plastic deformation occurs at $\frac{x}{x_c} = 1$

The equation of motion $m\ddot{x} = mg - k_1 x^{\frac{3}{2}}$ will be applied in the interval $0 \leq x \leq 1.9x_c$. At the end of this phase $x = 1.9x_c$ the time is t_I and the velocity is v_I . The time t_I and the velocity v_I are calculated numerically

from the equation of motion. The initial conditions for the next phase are the results of the elastic compression phase

$$t = t_I \text{ , } x(t_I) = 1.9x_c, \text{ and , } \dot{x}(t_I) = v_I. \tag{4.36}$$

4.5.2 Elastic-plastic compression phase

When the ratio (x/x_c) exceeds the value 1.9, the force at the contact point for modeling elastic-plastic impact is:

$$F_{EP} = F_C \left\{ \left[e^{-\frac{1}{4}\left(\frac{x}{x_c}\right)^{\frac{5}{12}}} \right] \left(\frac{x}{x_c}\right)^{\frac{3}{2}} + \frac{4}{C}\left(\frac{H_G}{S_y}\right) \left[1 - e^{-\frac{1}{25}\left(\frac{x}{x_c}\right)^{\frac{5}{9}}} \right] \frac{x}{x_c} \right\} \tag{4.37}$$

where $\frac{H_G}{S_y} = 2.84 - 0.92[1 - cos(\pi a/R)]$, H_G is the hardness geometric limit. The contact radius a, $0 < \frac{a}{R} < 1$, is calculated from

$$A = \pi a^2 = \pi R x \left(\frac{x_c}{1.9x_c}\right)^B \tag{4.38}$$

where B is the contact area material property coefficient, $B = 0.14e^{23\epsilon_y}$, and ϵ_y is the yield strength to elastic modulus ratio, $\epsilon_y = \frac{S_y}{E'}$

The equation of motion is very similar to the elastic case: the difference is only about the force

$$m\ddot{x} = mg - F_{EP} \tag{4.39}$$

with the initial condition at $t = t_I$, $x(t_I) = 1.9x_c$ and $\dot{x}(t_I) = v_I$. When compression is maximum and the velocity is zero this phase ends; for the

maximum compression the contact force F_m is maximum and the deformation is maximum x_m and during this phase the deformation is $1.9x_c \leq x \leq x_m$. Starting from the equation of motion, Eq.(4.36), the time t_m and the displacement x_m are numerically calculated, finally the initial conditions for the next phase are the final results of the elastic-plastic compression phase, i.e..

$$t = t_m \text{ , } x(t_m) = x_m, \text{ and , } \dot{x}(t_m) = 0. \tag{4.39}$$

4.5.3 Restitution phase

For both cases, elastic compression phase or elastic-plastic compression phase, the last phenomenon is the restitution phase, when the contact force decrease from its maximum value, F_m to zero. The elastic deformation decrease according to Hertz law and the eventual plastic deformation remains. Assuming that the sphere recovers in a completely elastic manner, the Hertz solution can be used to model the contact force as the sphere rebounds.

In the case of plastic deformations, the sphere will not fully recover to its original shape so the radius of curvature will change to R_r and the surface will be compressed permanently by a residual interference, x_r. There are two ways by which x_r and R_r can be obtained. According to Etsion et al.[10]

$$\frac{x_r}{x_m} = 1 - \frac{3F_m}{4E\prime a_m x_m} \text{ and } R_r = \frac{4E\prime a_m^3}{3P_m} \tag{4.40}$$

where a_m is the contact radius at the maximum interference, x_m

Another way to obtain x_r and R_r is by fitting an equation to finite element results [2] :

$$\frac{x_r}{x_m} = 1.02\left[1 - \left(\frac{\frac{x_m}{x_c}+5.9}{6.9}\right)^{-0.54}\right] \text{ and } R_r = \frac{1}{(x_m - x_r)^3}\left(\frac{3\,F_m}{4E'}\right)^2 \quad (4.41)$$

The rebound phase ends when the deformation x is equal to the maximum plastic deformation x_r.

The equation of motion of the sphere for the restitution phase is

$$m\ddot{x} = mg - \left(\frac{4}{3}E'\sqrt{R_r}\right)(x - x_r)^{3/2} \quad (4.42)$$

with the initial conditions at $x(t_m) = x_m$ and $\dot{x}(t_m) = 0$ $t = t_m$. This phase will end when $x = x_r$. At the end of the restitution, the rebound velocity v_f is obtained. The coefficient of restitution can be finally calculated as $e = v_f/v_0$.

4.6 Conclusions

The interaction of particles with boundaries can be studied by considering the contact mechanics concepts related to the case of particle-particle interaction as briefly discussed above; the contact stiffness, the equivalent Young modulus, and the equivalent radius are the quantities that permits to study and calculate the interaction during and after the impact.

In DEM the case of solid or granular materials, colliding with others elastic solids or boundaries can be treated exactly in the same way by simply using the proper force relations for both phenomena.

References

[1] Newton's Axioms or Laws of Motion, Starting on page 19 of volume 1 of the 1729 translation of the *Principia.*

[2] Stronge W.J., (2000) Impact Mechanics, *Cambridge University Press.*

[3] Cundall P., Strack O. (1979) A discrete numericalmodel for granular assemblies. *Geotechnique* 29(1):47–65.

[4] K.L. Johnson, (1985) Contact Mechanics, p. 306-311,*Cambridge Univ.Press.*

[5] Roylance D., (2001), Engineering Viscoelasticity. Cambridge, MA 02139: Massachusetts Institute of Technology. pp.8–11.

[6] Meyers and Chawla, (1999) Mechanical behavior of Materials, Section 13.10 pp. 570–580. Prentice Hall, Inc.

[7] Chang, W.R., Etsion, I., and Bogy, D.B., (1987), An Elastic-plastic Model for Contact of Rough Surfaces, *ASME Journal of Tribology*, Vol. 109, pp. 257-263.

[8] Jackson, R.L. and Green, I., (2005), A Finite Element Study of Elasto-Plastic hemispherical Contact, *ASME Journal of Tribology*, Vol. 127, pp. 343- 354.

[9] Green, I., (2005), Poisson ratio effects and critical values in spherical and cylindrical Hertzian contacts, *International Journal of Applied Mechanics and Engineering*, Vol. 10(3), pp. 451-462.

[10] Etsion, I., Kligerman, Y., and Kadin, Y., (2005) Unloading of an elastic-plastic loaded spherical contact, *Int. J. Solids and Structures*, Vol. 42(13) pp.3716-3729.

[11] H. Hertz, (1896) Über die berührung fester elastischer Körper, in Jones e Schott (cur.),Miscellaneous Papers, J. reine und angewandte

Mathematik, 92, Londra, Macmillan, , p. 156. Traduzione inglese: H. Hertz.

Chapter 5

THE PROPOSED POTENTIAL BASED INTERPARTICLE METHOD

5.1 Introduction

As discussed in the previous chapters the discrete nature of solids, despite typically modelled as continuous media, can be recognized by observing their structure at the microscale or at the molecular level [1-5]. On the other hand the simple continuous approach used in practical problems, normally adopted at the meso or macroscale, is based on the fundamental notion of a mesoscopic volume element, whose physical characteristics can be considered as averaged properties (evaluated over several discrete particles) obeying deterministic relationships.

Discrete Element Methods (DEM) or Particle Methods (PM), typically identified at the nano-scale as Molecular Dynamics methods (MD), are numerical procedures for the solution of a wide range of engineering and scientific problems. The main assumption for this class of methods is the idealization of the material through an assemblage of separate discrete elements, such as atoms, molecules, grains, particle solid elements, etc. [5, 6].

In these discrete approaches, complex non-linear interactions between bodies and within bodies (allowed to present different shapes and properties), are numerically obtained by solving in order to get the motion of particles non-linear differential equations.

It appears as such an approach is straightforward in modelling the mechanical behavior of solids from different scales levels (atomic, molecular, nano, micro, meso and mascroscopic), by properly adopting the interaction laws corresponding to the particle-particle interaction phenomenon. The approach can range from the very microscopic one, such as in the so-called ab initio approach (multi-body electronic structure theory, density functional theory, quantum chemistry, …) in which the force field arising between atoms, electrons and nuclei are considered [2], to the atomistic dynamics and statistics approaches (referred to as molecular dynamics, MD, or kinetic Monte Carlo models, suitable to describe kinetically dominated mechanisms) in which the effective bonds between molecules are properly described through potentials [3, 4], the mesoscale approaches based on the mean field rate theoretical methods (that typically mimic average dynamical properties [6]), up to the macroscopic scale such as the continuum-based thermodynamics or constitutive kinetic models, typically formulated by using variational methods. Multiscale analysis of solids has also been proposed in recent papers [7, 8].

On the other hand, such discrete nature is well evident for other class of materials such as the granular ones that are constituted by several deformable particles, usually interacting each other through elastic, contact, cohesive and friction forces [9-13]; among the different problems involving the simulation of materials, geomechanical and powders ones can be naturally studied by exploiting their noticeable granular nature [14-17].

At the macroscale the discrete methods have relevant applications in mineral processing, rock blasting, crushing, phenomena involving sand mechanics, powders technology, failure of compact or granular bodies [15, 17]; moreover materials like gases and liquids can be simulated with this class of methods [18, 19], i.e. through the simple scheme of interacting particles.

A generic solid can always be though to have a particle structure: the assumption of the average particles size and of the particular nature of the particles' interaction forces, allows to describe different materials; in such a way their behavior can be made to range from the very incoherent cases up to the compact materials ones, typical of granular (or powder) and of polycrystalline materials, respectively.

Particles can be viewed as objects carrying the physical characteristics of the system that can be therefore simulated through the study of the motion evolution of the properties carried by the particles (position, velocity, acceleration, forces, …); simulations of molecular phenomena or of continuum bodies can be formulated by following the motion of interacting particles enclosing the physical properties of the flow. In a continuum, these properties are typically macroscopically averaged, e.g. the fields of density, momentum, vorticity are of main interest, while for a discrete system at the atomic scale the mass, velocity and electric charge are normally sought.

The unavoidable particle nature of real materials suggests – in competition with classical continuum models – the possibility to use a different approach, namely a discrete one, to suitably describe their mechanical behavior, also at different scales.

In the light of the above considerations, at the macroscopic scale a material cannot be simply associated univocally to one of the two extreme classes (continuum or granular), but can be assumed to be characterized by an

intermediate behavior, since the nature of the forces between the discrete particles can be regarded to range from adhesion-like (such as in powders materials) up to strong covalent bond (as for compact materials).

Moreover, in heterogeneous materials the coexistence of different types of particles, interacting according to different bonding laws, requires to study the behavior of a generic multiphase solid.

The above observations suggest the possibility to adopt a discrete model for the simulation of different class of solids, by simply properly choosing the nature of the interaction forces existing between their discrete constituent elements, i.e. by modelling the material as an assemble of small discrete elements once the mechanical behavior and failure evolution at a local level are properly described.

By taking into account the particle-like nature of solids, such an approach can be suitably used for either continuum-like [20-22] or granular-like materials [23], by properly setting the law governing the mechanical and/or electrostatic interaction existing between particles. Such description allows us to get the overall response of the material at the macroscale, which is the main interest of materials science and mechanics of materials [24]. It should be also considered as the particle nature adopted for a solid matter naturally allows tackling the problem from a dynamic point of view, permitting the solution of high strain rate, impact, large displacements and large strains problems.

Solid mechanics problems involving history-dependent behavior, large deformation, large displacements, plasticity, etc. are expressed more naturally in a Lagrangian computational framework that is particularly suitable and useful when the material free surfaces or multiple materials interaction has to be followed.

When large deformations are present, a purely Lagrangian approach applied to continuum mesh-based computational techniques, can become not convenient due the requirement of complex mesh adjustment and smoothing, unreasonably small time steps, and so on. For the above reasons, particle methods for solid mechanics problems have gained an increasing popularity in the last decade [25-28].

The discrete approach applied at the meso- or macro-scale level is usually referred as the discrete-element method (DEM) or particle method (PM) [18].

In the present chapter, a computational discrete element method developed for continuum materials, granular-like or mixed cases – based on the concept of force potential interaction law for the quantification of the mutual forces exchanged by particles representing the solid – is presented in detail.

After illustrating the basic concepts related to the discrete nature of materials and their mechanical modelling, a simple particle-based approach for continuum solids or discrete incoherent aggregates is illustrated by taking into account for the dynamic nature and large strain characteristic of the problem.

5.2 Potential-based interparticle method

By considering the meso or macroscale level of observation, it can be assumed – analogously to the atomic description of solids – that the material is characterized by a potential energy functional $\Pi(\mathbf{x})$. Such an energy allows determining the pair-wise potential forces (Fig. 1) and can be written as follows:

$$E_{tot}(\mathbf{x}) = \Pi(\mathbf{x}) = \Phi_{tot}(\mathbf{x}) - \mathbf{P}_i \cdot \mathbf{x}_i \tag{5.1}$$

where $\Phi_{tot}(\mathbf{x})$ and $\mathbf{P}_i$ are the strain energy of the system and the force applied to the particle *i*, respectively. The configuration of minimum energy can be obtained by setting to zero all the derivatives of $E_{tot}(\mathbf{x})$ with respect to the position vectors $\mathbf{x}_i$,

$$\frac{\partial E_{tot}}{\partial \mathbf{x}_i} = \frac{\partial \Phi_{tot}(\mathbf{x})}{\partial \mathbf{x}_i} - \mathbf{P}_i = 0 \tag{5.2}$$

By writing the power series expansion of the total energy starting from the equilibrium state (identified by the position vectors synthetically indicated as $\mathbf{x}_0$), we get:

$$E_{tot}(\mathbf{x}) \cong \left\{ E_{tot}(\mathbf{x}_0) + \left.\frac{\partial E_{tot}}{\partial \mathbf{x}}\right|_{\mathbf{x}_0} (\mathbf{x}-\mathbf{x}_0) + \frac{1}{2}(\mathbf{x}-\mathbf{x}_0)^T \left.\frac{\partial^2 E_{tot}}{\partial \mathbf{x}^2}\right|_{\mathbf{x}_0} (\mathbf{x}-\mathbf{x}_0) + ... \right\} - \mathbf{P}_i \cdot \mathbf{x}_i \tag{5.3}$$

The stationary condition expressed by Eq. (5.2) can be rewritten in the following way:

$$\frac{\partial E_{tot}}{\partial \mathbf{x}} \cong \left.\frac{\partial E_{tot}}{\partial \mathbf{x}}\right|_{\mathbf{x}_0} + \left.\frac{\partial^2 E_{tot}}{\partial \mathbf{x}^2}\right|_{\mathbf{x}_0} (\mathbf{x}-\mathbf{x}_0) + ... - \mathbf{P} = \mathbf{0} \tag{5.4}$$

or

$$\left.\frac{\partial^2 E_{tot}}{\partial \mathbf{x}^2}\right|_{\mathbf{x}_0} (\mathbf{x}-\mathbf{x}_0) = \left.\frac{\partial^2 \Phi_{tot}}{\partial \mathbf{x}^2}\right|_{\mathbf{x}_0} (\mathbf{x}-\mathbf{x}_0) = \mathbf{P} - \left.\frac{\partial E_{tot}}{\partial \mathbf{x}}\right|_{\mathbf{x}_0} = \mathbf{K}\cdot(\mathbf{x}-\mathbf{x}_0) = \mathbf{P}$$

where the so-called tangential stiffness matrix can be identified through the second derivatives of the strain energy function as:

$$\mathbf{K}_{ij} = \frac{\partial^2 E_{tot}}{\partial \mathbf{x}_i \partial \mathbf{x}_j} = \frac{\partial^2 \Phi_{tot}}{\partial \mathbf{x}_i \partial \mathbf{x}_j} = \begin{bmatrix} \dfrac{\partial^2 \Phi_{tot}}{\partial x_i \partial x_i} & \dfrac{1}{2}\dfrac{\partial^2 \Phi_{tot}}{\partial x_{i-1} \partial x_1} & \dfrac{1}{2}\dfrac{\partial^2 \Phi_{tot}}{\partial x_{i-2} \partial x_1} & .... \\ \dfrac{1}{2}\dfrac{\partial^2 \Phi_{tot}}{\partial x_{i-1} \partial x_1} & 0 & 0 & .... \\ \dfrac{1}{2}\dfrac{\partial^2 \Phi_{tot}}{\partial x_{i-2} \partial x_1} & 0 & 0 & .... \\ .... & .... & .... & .... \end{bmatrix} \tag{5.5}$$

Several potentials have been proposed in the literature to represent the mechanical interactions between particles. Among them, we can mention here the Morse potential [29], the Lennard-Jones (LJ) potential [30], the classical strain energy potential (widely used in continuum mechanics), and so on.

In the following paragraphs are presented some potentials and their mechanical interpretation is given; they are introduced to study different kind of problems, everyone fitted for a particular situation.

5.2.1 Potential function for molecular-like forces

The above cited pair-wise Lennard-Jones (LJ) potential is usually employed to describe the forces between particles at the nanoscale (i.e. at the atomic or molecular level), but it has been also used for the description of continuum solids [20, 21]. Mathematically it can be written as follows:

$$\Phi_{LJ}(r = |\mathbf{x}_i - \mathbf{x}_j|) = D \cdot \left[\left(\frac{R}{r} \right)^{2n} - 2 \left(\frac{R}{r} \right)^{n} \right] \tag{5.6}$$

where R is the distance at which the potential reaches its minimum, D is the depth of the potential well, and r is the actual distance between the centres of the two considered particles; the typical assumption $n = 6$ leads to the so-called 12-6 Lennard-Jones potential used for the atomic simulation of matter.

It has been shown that it does not give adequate description of all the properties of metals; for example, the above recalled LJ potential imposes the Cauchy relationship $C_{12} = C_{44}$ (C_{12}, C_{44} are the elastic constants corresponding to the force-distance relation established by the potential) that has been demonstrated to be wrong for most of the known metals. Moreover, pair-wise potentials fail to estimate the structure relaxation and reconstruction around point defects (vacancies and self-interstitials) in metals. The vacancy formation energy obtained by means of pair-wise potentials is overestimated, and has been found to be equal to about the bulk cohesive energy; the more suitable potentials for simulations of metals are the so-called many-body potentials. A suitable interatomic potential for metals is thus a many-body

one which includes a pair-wise interaction only as a part of the full potential [31].

The above concept, related to the development of forces derived from interatomic potentials at the atomic scale, can be conveniently used – if properly tuned – also to tackle the problem of the mechanical description of solids at the macroscale [20] at which the matter can be assumed to be composed by particle elements.

By indicating with $d_i/2$ and $d_j/2$ the radii of the particles i and j (assumed for the sake of simplicity to have a spherical shape), respectively, the potential can be conveniently written through the distance s between the surfaces of the facing particles defined as $s' = r - (d_i/2 + d_j/2)$, where r is the distance between the centres of the particles (Fig. 5.1).

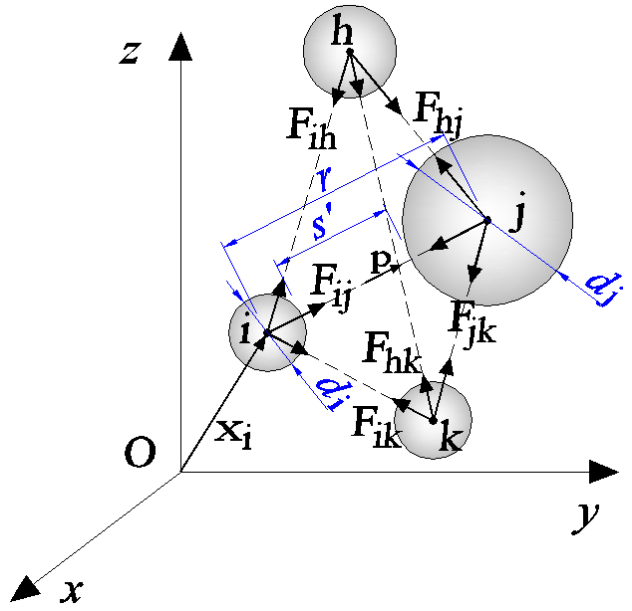

Fig. 5.1. Scheme of pair-wise interparticle forces.

In order to have a realistic description of the interaction forces, a very high (theoretically infinite) repulsive force value can be reasonably assumed to appear when the two elements co-penetrate by a given amount $\delta = \alpha \cdot (d_i + d_j)/4 = \alpha \cdot \bar{r}$ (where α is a proper coefficient, and $\bar{r} = (d_i + d_j)/4$ is the average particles radius) (Fig. 5.2).

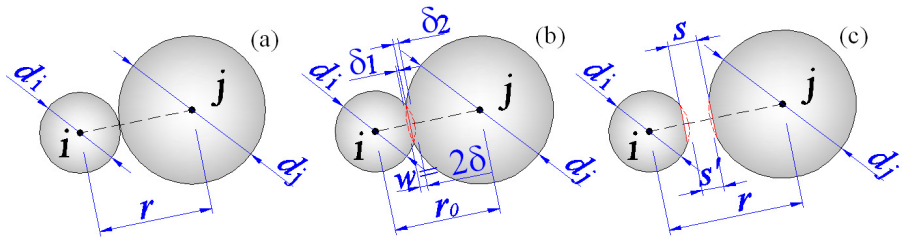

Fig. 5.2. A pair of particle at the equilibrium distance. (a) Maximum co-penetration corresponding to $F(r = r_0) \to -\infty$ (b) and generic particles relative position with geometrical parameters (c).

The effective surface distance ($s > 0$) can be expressed as follows:

$$s = s' + \delta_1 + \delta_2 \cong s' + 2\delta = r - r_0 = r - (2 - 2\alpha)\frac{(d_i + d_j)}{4} \tag{5.7}$$

with $r_0 = -2\delta + (d_i + d_j)/2 = (2 - 2\alpha)\dfrac{(d_i + d_j)}{4}$

where, for not too different particles radii, it has been assumed that $\delta_1 \cong \delta_2 = \delta$, where r_0 is the distance between the centres of the particles at which $F(r = r_0) \to -\infty$.

The co-penetration distance w of the particles is finally expressed as:

$$w = \left(\frac{d_i}{2} + \frac{d_j}{2} - r \right) = -s' = 2\delta - s, \; w \geq 0 \tag{5.8}$$

By assuming, as in the previous case, that an infinite repulsive force takes place when the two elements co-penetrate by the amount δ (or when $s = 0, \text{i.e.} s' = -2\delta$, Fig. 5.2b, c), the Lennard-Jones- potential can be rewritten as (Fig. 5.3a):

$$\Phi_{LJ}(s = r - r_0 = \left| \mathbf{x}_i - \mathbf{x}_j \right| - r_0) = D \cdot \left[\left(\frac{R}{s} \right)^{2n} - 2 \left(\frac{R}{s} \right)^{n} \right] \tag{5.9}$$

where the case $s = R$ corresponds to the value of s for which the potential attains its minimum or, equivalently, the interaction force becomes equal to zero, $F(s = R) = 0$.

As can be observed in Fig. 5.3b, the $F(s)$ relationship corresponds to the force-displacement behaviour of a softening-like material, since – once the force attains its maximum for $s = s_d$ – $F(s)$ - decreases by increasing the distance s, tending to zero for high values of s. In the present formulation a repulsive force is assumed always to be negative while an attracting force is taken as positive.

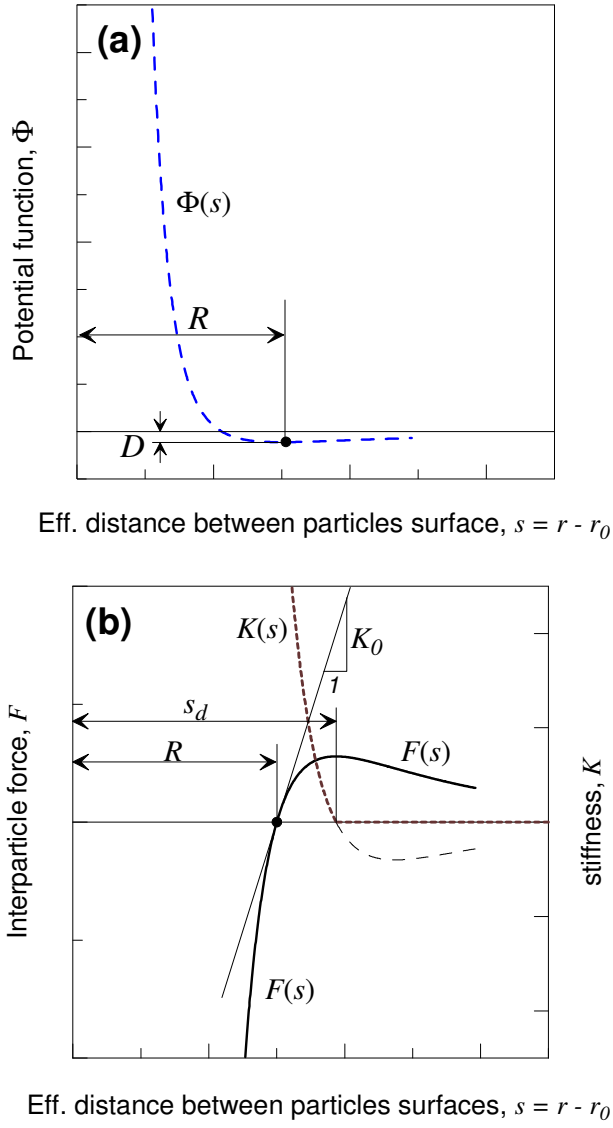

Fig. 5.3. (a) A graphical schematic representation of the Lennard-Jones potential for $n = 2$ *; (b) the related force and stiffness.*

The corresponding stiffness $K(s)$ is also depicted in Fig. 5.3b; it presents unlimited values when $s \to 0$, afterwards it decreases by increasing s up to

the value $s = s_d$ at which it becomes equal to zero. Subsequently it attains negative values giving rise to the above mentioned softening behaviour. For computational purposes, the $K(s)$ relationship can be assumed as plotted in Fig. 5.3b (thick dashed line), i.e. by only considering values greater or equal to zero (i.e. for $s > s_d$ $K(s)$ is assumed to be zero).

The last assumption corresponds to case of non-interacting particles, situation that occurs when they are located at a distance, measured between their centers, greater than $r_0 + s_d$.

By setting the stiffness $K(s)$ to be equal to K_0 when $F(s) = 0$, i.e. when $s = R$, the constant D in Eq. (5.7) can be explicitly evaluated:

$$D = K_0 \frac{R^2}{2n^2} \tag{5.10}$$

Moreover, the distance at which the force $F(s)$ reaches its maximum can also be determined by setting $K(s) = dF(s)/ds = 0$. This condition leads to the following particular value of the effective distance s_d between the particle surfaces (Fig. 5.3b):

$$s = s_d = \frac{R \cdot (2n+1)^{1/n}}{(n+1)^{1/n}} \tag{5.11}$$

It can reasonably be assumed that such an interaction completely vanishes for a sufficiently large distance. In other words, it can be assumed the existence of a cut-off distance s_c for which the force becomes equal to zero

(as well as for greater distances). From the above discussion, such a non-interacting distance can be conveniently assumed as $s_c = s_d$ (Fig. 5.3b), i.e. the interparticle force is set to zero in the softening branch of the $F(s)$ relationship.

It must be emphasised as in the present model the rotational inertia, and consequently the angular coordinates, have not been considered for sake of simplicity, since the particles are assumed to be spherical and with very small dimensions with respect to the structural size.

5.2.2 Potential function for granular-like solid materials

In the case of granular materials, for which the simple scheme of multi-interacting bodies is straightforward, a suitable force-particle distance description could be as that shown in Fig.5.4a where the corresponding potential is also displayed. As can be noted, a quadratic potential $\Phi(s')$ implies a linear force-distance relationship when the particles are in contact ($-w = s' < 0$), whereas the force becomes equal to zero when the contact disappears ($s' \geq 0$). The stiffness K_0 of such an interaction force corresponds to the slope of the F - s' relationship when $s' < 0$ (Fig. 5.4a).

A regularised (smooth) version of the above cited potential – suitable for such a class of materials (see Fig. 5.4a) – and the corresponding force-distance relation, can be introduced in order to avoid possible problems in computational analyses. Such a regularised (smooth) potential can mathematically be described through the following equation (Fig. 5.4b):

$$\Phi(s = r - r_0 = \left|\mathbf{x}_i - \mathbf{x}_j\right| - r_0) = \frac{c}{n-1} \cdot \frac{1}{s^{n-1}} = \frac{c}{n-1} \cdot \frac{1}{(2\delta + s')^{n-1}} \qquad (5.12)$$

where c , n are constants ($n > 2$), while the corresponding particle pair forces relationship can be expressed as follows:

$$\mathbf{F}(s = r - r_0 = \left|\mathbf{x}_i - \mathbf{x}_j\right| - r_0) = -\frac{\partial \Phi(s)}{\partial s}\mathbf{p} = F \cdot \mathbf{p} = -\frac{c}{s^n} \cdot \mathbf{p} \qquad (5.13)$$

where $\mathbf{p}$ is the unit vector identifying the direction connecting the two particles centres (Fig. 5.1).

The use of the effective surface distance s in Eq. (5.11), instead of the real distance s' between the particle surfaces, allows to get an unbounded repulsive force when the two particles have co-penetrated each other by the amount $\delta = \alpha \cdot \bar{r}$.

The coefficient c in Eqs (5.12, 5.13) can be determined, for example, by setting the value of the stiffness when the two spheres are at incipient contact ($s' = 0$), i.e. $K(s'=0, s=2\delta) = \partial F / \partial s\big|_{s=2\delta} = K_0$.

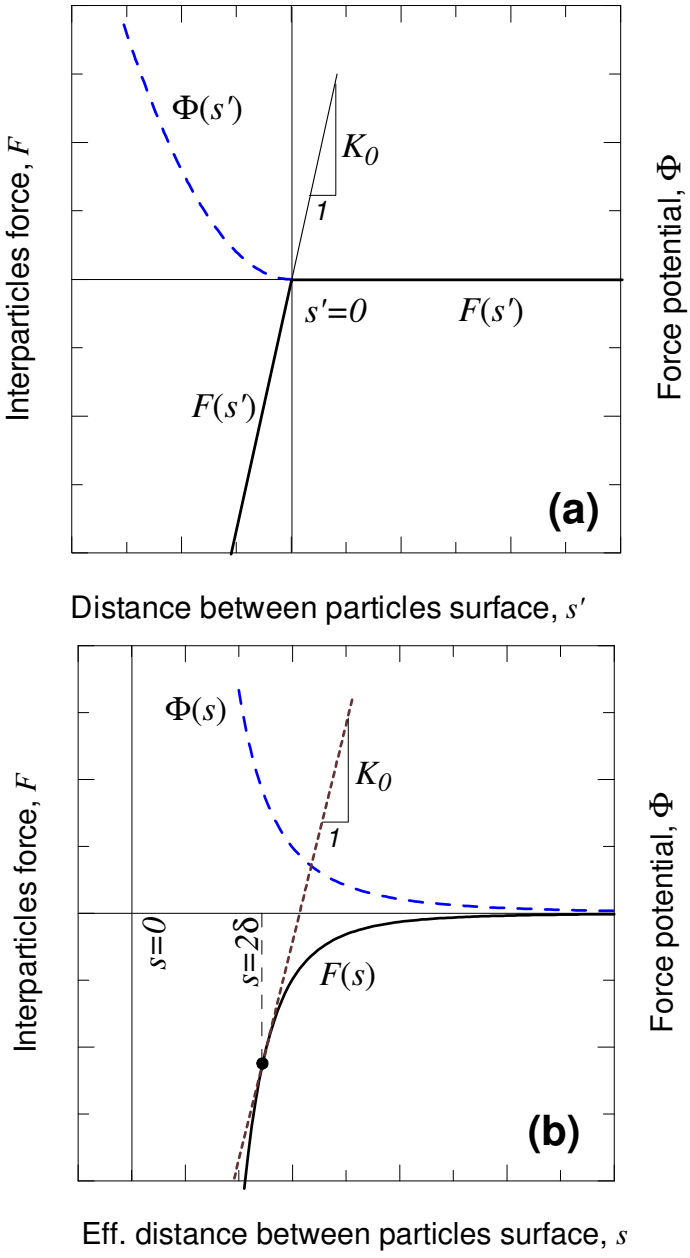

Fig. 5.4. (a) Interparticles potential and corresponding forces for an ideal granular material without cohesion; (b) corresponding regularised counterpart .

The force $F(s)$ given by Eq. (5.13) is never equal to zero, irrespectively of the particles distance, but such interaction becomes smaller and smaller as the effective distance s increases as shown in Fig. 5.4b.

Finally, when the two particles are at a distance corresponding to the first contact ($r=\overline{d}=(d_i+d_j)/2$), by assuming an elastic interaction, the value of the tangent stiffness can be assessed through the relation:

$$K(s=r-r_0=\left|\mathbf{x}_i-\mathbf{x}_j\right|-r_0)=K_0=\left.\frac{\partial^2\Phi(s)}{\partial s^2}\right|_{r=\overline{d},(s=2\delta)}=\frac{c\cdot n}{s^{n+1}} \tag{5.14a}$$

that allows to determine the value of the constant c:

$$c=K_0\cdot\frac{s^{n+1}}{n}=K_0\cdot\frac{(2\delta)^{n+1}}{n} \tag{5.14b}$$

The contact force arising when two particles i and j are in contact, can be also evaluated through the well-known Hertz law; according to this approach the normal force-co-penetration relationship and the contact stiffness can be expressed as follows [32, 33]:

$$F(w)=\overline{K}w^{3/2},\quad K(w)=\frac{3}{2}\overline{K}\sqrt{w} \tag{5.15a}$$

$$\text{where } \overline{K}=\frac{4}{3}\overline{E}\sqrt{\frac{d^*}{2}} \text{ with } \overline{E}=\left(\frac{1-\nu_i^2}{E_i}+\frac{1-\nu_j^2}{E_j}\right)^{-1} \tag{5.15b}$$

$$d^*=\left(\frac{1}{d_i}+\frac{1}{d_j}\right)^{-1} \text{ or}$$

$$\overline{K} = \frac{2}{3}\frac{E}{1-\nu^2}\sqrt{\frac{d^*}{2}} \quad \text{when} \quad E = E_i = E_j,\ \nu = \nu_i = \nu_j \tag{5.15c}$$

where E_i, ν_i, d_i (E_j, ν_j, d_j) are the elastic modulus, the Poisson ratio and the diameter of the particle i,j, respectively. The potential corresponding to the above Hertzian-like contact force can be finally expressed as (Fig. 5.5):

$$\Phi(s) = \frac{2}{5}\overline{K}\cdot w^{5/2} = \frac{2}{5}\overline{K}\cdot(2\delta - s)^{5/2}, \quad 0 \le s \le 2\delta \tag{5.16}$$

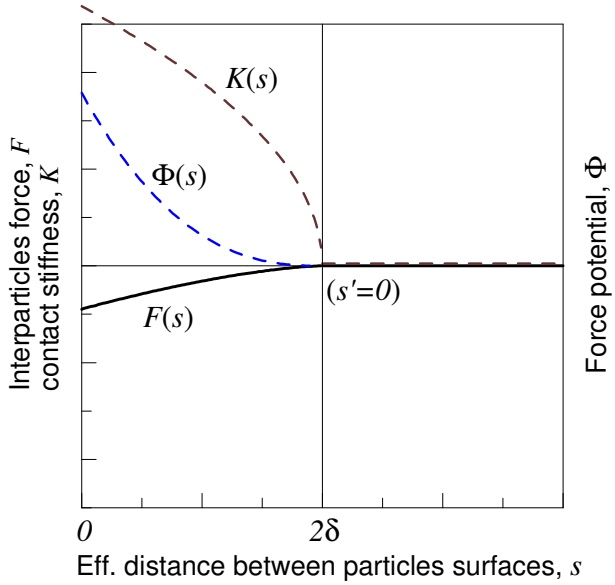

Fig. 5.5. Interparticles potential and corresponding forces and stiffness according to the Hertzian contact law Eq. (5.15a) for a granular-like material.

In the framework of the Hertzian theory of contact between elastic bodies, in case of dynamic problems the viscoelastic effects during collision can also

be taken into account; in such cases the normal force acting between two particles in reciprocal contact can be expressed by updating Eq. (5.15a) as follows [34]:

$$F(w) = \frac{2}{3}\frac{E}{1-\nu^2}\sqrt{\frac{d^*}{2}}\left(w^{3/2} + H\sqrt{w}\frac{dw}{dt}\right) \tag{5.17}$$

where H is a constant and dw/dt is the particles co-penetration velocity.

Furthermore during contact it can be also assumed the existence of a tangential force $T(w)$; it acts parallel to the relative tangential velocity between particles and can be expressed through the relation:

$$T(w) = -\text{sign}(\mathbf{u}_{t,rel}) \cdot \min\left(\eta \cdot \left\|\mathbf{u}_{t,rel}\right\|, \mu_{md} \cdot \left|F(w)\right|\right) \tag{5.18}$$

where η is the viscosity coefficient and μ_{md} is the dynamic friction coefficient of the materials, while $\mathbf{u}_{t,rel}$ is the relative tangential velocity between the two particles surfaces under contact; in practice Eq. (5.18) quantifies such tangential force as the minimum value between the dynamic friction and the viscosity action.

5.2.3 A simple potential function for linear-elastic solids

As is well known the simplest mechanical model describing the behavior of a continuum solid can be represented by the generalized Hooke's law; according to such relationship the force between two infinitely closed

material points is proportional, through proper coefficients, to the strain value occurring in such a small region. Let us assume that two particles are representative of two material points of the solid (Fig. 5.6a); it can be argued that in the reference state at the equilibrium distance r_e between the two considered particles in the reference state, the reciprocal force is equal to zero. Since the problem under study is not restricted to the small strain assumption, the large strain corresponding to a generic distance $r \neq r_e$ between the particle centers, can be written as (Fig. 5.6b):

$$\varepsilon = \frac{r - r_e}{r_e} + \frac{1}{2}\left(\frac{r - r_e}{r_e}\right)^2 = \frac{s - s_e}{s_e} + \frac{1}{2}\left(\frac{s - s_e}{s_e}\right)^2 \tag{5.19}$$

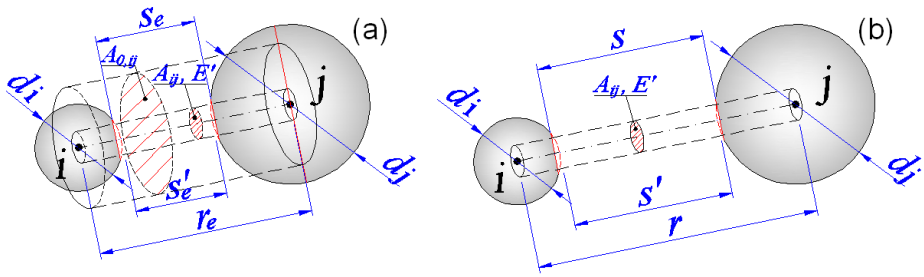

Fig. 5.6. A pair of particles at the equilibrium distance (a). Configuration corresponding to a generic positive stretch (b).

The force corresponding to such simple linear elastic behaviour, acts along the line joining the particle centres and can be expressed as:

$$F(s)=\begin{cases} A_{ij}\cdot E'\cdot\left[\dfrac{s-s_e}{s_e}+\dfrac{1}{2}\left(\dfrac{s-s_e}{s_e}\right)^2\right] & \text{if} \quad s<r_{\text{infl}}+\dfrac{d_i+d_j}{2}+2\delta \\ 0 & \text{if} \quad s\geq r_{\text{infl}}+\dfrac{d_i+d_j}{2}+2\delta \end{cases} \tag{5.20}$$

where A,E are the cross-section and the elastic modulus of a suitable truss element that can be assumed to join between the two particles (Fig. 5.6). In the above equation, the influence distance r_{infl} represents the maximum interacting distance between the couple of particles, i.e. the distance over which two particles are not interacting or, in other words, no bonding force exists between them. Note that according to such model the interaction between particles can exist also for elements that are not in direct contact each other.

The potential and the stiffness function in this case are given by:

$$\begin{aligned} \Phi(s)&=A_{ij}\cdot E'\cdot\left[\frac{1}{s_e}\left(\frac{s^2}{2}-s\cdot s_e\right)+\frac{1}{6}\frac{(s-s_e)^3}{s_e^2}\right], \\ K(s)&=A_{ij}\cdot E'\cdot\left[\frac{1}{s_e}+\frac{(s-s_e)}{s_e^2}\right] \end{aligned} \tag{5.21}$$

In order to represent the real problem of the elastic contact between particles, the condition of non co-penetration should be considered: the distance between the particle centres cannot become lower than a limit value r_0 (Fig. 5.2) corresponding to the maximum allowable co-penetration depth,

$w = 2\delta$. This aspect can be taken into account – under the assumption of an unlimited compressive strength of the particle's material by assuming that the stiffness of the truss element increases as $s \to 0$ (or equivalently $w \to 2\delta$); this can be obtained by adopting the elastic modulus E' not to be constant but dependent on the effective distance s . A suitable expression for the elastic modulus-relative distance relationship can be written as:

$$E' = c(s) \cdot E_0 \tag{5.22}$$

where $$c(s) \begin{cases} \to \infty & \text{if } s \to 0 \\ \cong 1 & \text{if } s > 0 \end{cases}$$

As an example the function $c(s)$ can be assumed in the form:

$$c(s) = \left[1 + (s+1)^{-m}\right] / \left[1 - (s+1)^{-m}\right] \tag{5.23a}$$

where the exponent m allows to set the elastic modulus gradient when $s \to 0$ The stiffness term can therefore be written as:

$$\begin{aligned} K(s) &= A_{ij} \cdot E_0 \cdot c(s) \cdot \left[\frac{1}{s_e} + \frac{(s - s_e)}{s_e^2}\right] = \\ &= A_{ij} \cdot E_0 \cdot \frac{\left[1 + (s+1)^{-m}\right]}{\left[1 - (s+1)^{-m}\right]} \cdot \left[\frac{1}{s_e} + \frac{(s - s_e)}{s_e^2}\right] \end{aligned} \tag{5.23b}$$

In Fig. 5.7 dependence of the potential, of the force and of the stiffness, on the distance is displayed for the linear elastic particles interaction for two different equilibrium distances ($\frac{s_e}{d} = 1$, Fig. 5.7a; $\frac{s_e}{d} = 2$, Fig. 5.7b); the same quantities are illustrated for the case of no co-penetration according to Eqs (5.22, 5.23b) (Fig. 5.7c).

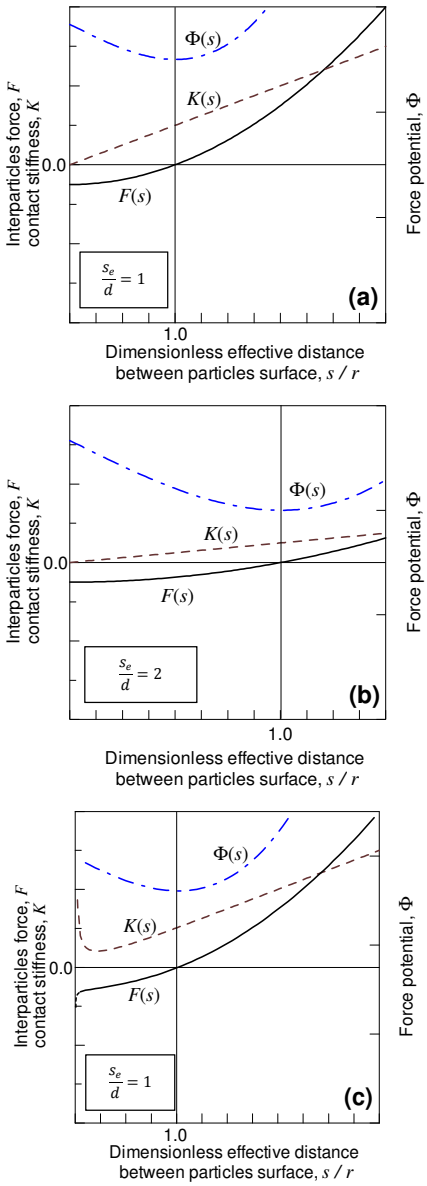

Fig. 5.7. Interparticles potential and corresponding forces and stiffness according to the linear elastic behaviour law Eqs (5.18, 5.19) for different equilibrium distance ((a) $\frac{s_e}{d} = 1$; (b) $\frac{s_e}{d} = 2$). Corresponding functions for the corrected stiffness (Eq. (5.21)) enabling to consider the interparticles non co-penetration condition (c).

In order to correctly represent the elastic behaviour of continuous bodies discretized through particle elements, the trusses connecting each couple of particles (Fig.5.6) must be characterized by a suitable choice of their cross-section area; since the number and layout of the resulting truss lattice structure depends on the particle arrangements in the space (Fig.5.1) and on their influence distance r_{infl}, the above relation (5.20) must consider a corrected cross-section area, $A_{ij} = a(r_{\text{infl}}) \cdot A_{0,ij}$, in order to correctly represent the elastic body. In the previous equation $A_{0,ij} = \frac{\pi}{4} \cdot (d_i + d_j)^2$ is the area of the assumed circular cross-section truss, having radius equal to the average radius of the two connected particles *i* and *j* (Fig. 5.6a). The pattern of the function $a(r_{\text{infl}})$, determined through numerical analyses, is reported in Fig. 5.8a, b for the cubic and tetrahedric particle arrangements.

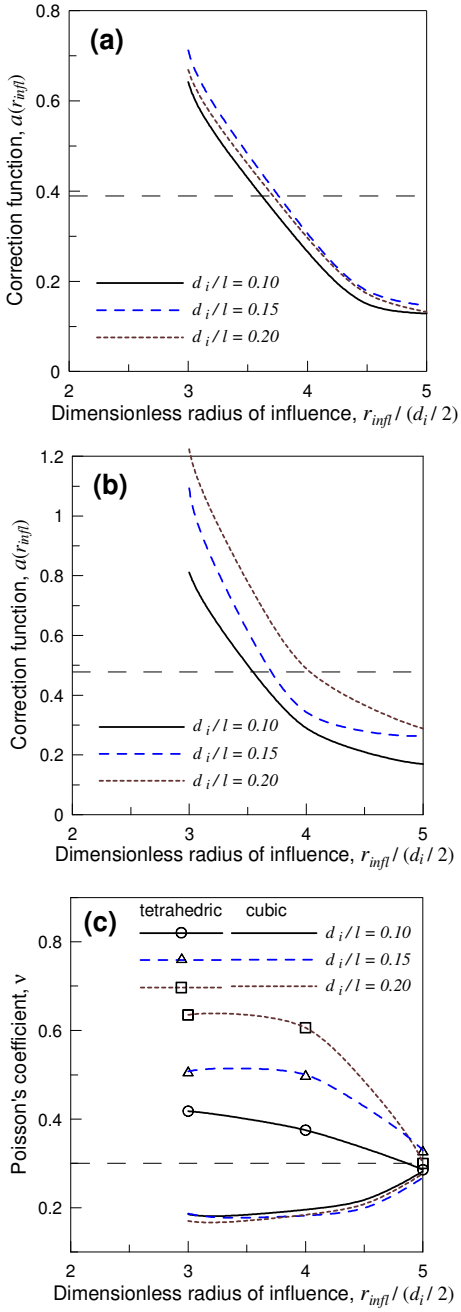

Fig. 5.8. Cross-section corrections function $a(r_{\mathrm{infl}})$ for cubic and tetrahedric particle arrangements (a), (b) and Poisson's coefficient vs the dimensionless influence radius for different relative particle sizes (the assumption $d_i = d_j$ has been made for sake of simplicity).

The function $a(r_{\text{infl}})$ has been evaluated by discretizing through spherical particles (in reciprocal contact) having diameter d_i, an elastic cube with edge length l under uniform tension, by changing the influence radius in the range $3 \le r_{\text{infl}} \le 5$. As can be noted the correction function $a(r_{\text{infl}})$ is almost independent by the relative particle size d_i / l for a specific particles arrangement (Fig. 5.8a, b) while the Poisson's coefficient tends to the value 1/3 as the influence radius is increased (Fig. 5.8c). As a matter of fact, the Poisson's coefficient cannot be modified once the arrangement and the particle size have been assumed: however, for sufficiently high value of the influence radius $r_{\text{infl}} \ge 4$, the obtained Poisson's value 1/3 can be considered to be suitable for a wide class of materials.

From the above results it appears as a suitable choice of the correction function $a(r_{\text{infl}})$ for an influence radius values equal to about $r_{\text{infl}} /(d_i / 2) \cong 4$ – the value assumed in the following examples, Chapter 6 – is approximately equal to $a(r_{\text{infl}}) \cong 0.4$ for both cubic or tetrahedric arrangements. The case of granular materials can be also tackled in the same way by adopting $r_{\text{infl}} /(d_i / 2) \le 2$, i.e. by assuming the interaction of particles only when they are in reciprocal contact, while no forces exist when $s' > 0$; the tangential force eventually present between the colliding particles when the distance between their surfaces is $s' \le 0$, can be evaluated exactly as in Eq. (5.18) by considering the actual force $F(s)$ – instead of $F(w)$ – acting along the particles' centres.

5.2.4 Material Failure

The lattice scheme of a continuum solid easily allows to model internal failure of the material; in fact the force exerted by a truss representing the bonding between two interacting particles can be set to zero when its tensile (or compressive) strength is reached; this corresponds to the failure condition of the connecting element; from then on, the two originally connected particles can interact in successive time instants only if a compressive contact takes place. This simple criterion enables to manage brittle failure and compressive contact between the failed particles, such that occurring in the crack closure phenomenon in fracture mechanics.

5.2.5 Strains calculation

The strain field in the solid can be recovered once the strains in the trusses are known; Eq. (5.19) allows to obtain the strains in a given point of the body measured along given directions (coincident with the truss directions connecting the particles). The strain tensor $\boldsymbol{\varepsilon}(\mathbf{x}_i)$ in the equivalent continuum body represented through particles identified by the position vector $\mathbf{x}_i$ can be approximately evaluated by using the relation

$$\varepsilon_{ij}(\mathbf{x}_i) = \mathbf{n}_{ij}^T \boldsymbol{\varepsilon}(\mathbf{x}_i)\mathbf{n}_{ij} \tag{5.24}$$

where $\varepsilon_{ij}(\mathbf{x}_i)$ is the strain in the truss element connecting the particle *i* with *j* and $\mathbf{n}_{ij}$ is the unit vector identifying the *i-j* direction. Once the strains $\varepsilon_{ij}(\mathbf{x}_i), \quad j = 1,2,..p$ are known (*p* indicates the number of particles that are within the region of influence of the particle *i*), the above relations can be

arranged in a (rectangular) system of equations where the unknown is the strain tensor $\boldsymbol{\varepsilon}(\mathbf{x}_i)$. If $p \geq 6$ the system is overdetermined and such a strain tensor can be obtained through the least square-like algorithm or equivalent approaches.

By performing such approximate solution for all the particles constituting the solid under study, the strain tensor field can be reconstructed throughout the region occupied by the body.

5.3 Particles-Boundary Contact simulation

The interaction of particles with boundaries can be studied by considering the contact mechanics concepts as briefly discussed at the end of par. §5.2.2, related to the case of particle-particle interaction; the contact stiffness, the equivalent Young modulus, and the equivalent radius related to the case of an elastic sphere impacting an elastic plane can be assessed as [33]:

$$K_n(w) = 2\overline{E}\sqrt{r_i}\cdot w^{1/2} = 2\overline{E}\sqrt{r^*}\cdot w^{1/2}$$
$$\text{with } \overline{E} = \left(\frac{1-\nu_i^2}{E_i} + \frac{1-\nu_j^2}{E_j}\right)^{-1}, \quad r^* = r_i \tag{5.25}$$

where E_i, ν_i, r_i are the elastic modulus, the Poisson's ratio and the diameter of the particle, while E_j, ν_j are the elastic modulus and the Poisson's ratio of the elastic surface (assumed to be flat, i.e. with local radius of curvature of the contact area tending to infinity, $r_j \to \infty$) representing the boundary constraint. The above equation is analogous to the relation (5.17) related to the contact between two colliding particles.

The force acting normal to the tangent plane at the particle-surface contact point can be assessed as

$$\mathbf{T}_n(w) = K_n \cdot w^{3/2} \cdot \mathbf{n} \tag{5.26}$$

where $\mathbf{n}$ is the unit normal to the boundary surface in the contact point, while the tangential force belonging to such a tangent plane is assumed to be expressed by the following friction-like relation

$$\mathbf{T}_t = -\mu_d \cdot T_n \cdot \frac{\dot{\mathbf{x}}_{i,t}}{\left|\dot{\mathbf{x}}_{i,t}\right|} = -(\mu_d \cdot K_n \cdot w^{3/2}) \cdot \mathbf{t} \tag{5.27}$$

where μ_d is the coefficient of dynamic friction and $-\mathbf{t} = -\dot{\mathbf{x}}_{i,t} / \left|\dot{\mathbf{x}}_{i,t}\right|$ represents the unit vector opposite to the direction of the tangential velocity of particle *i* with respect to the boundary surface (Fig. 5.9).

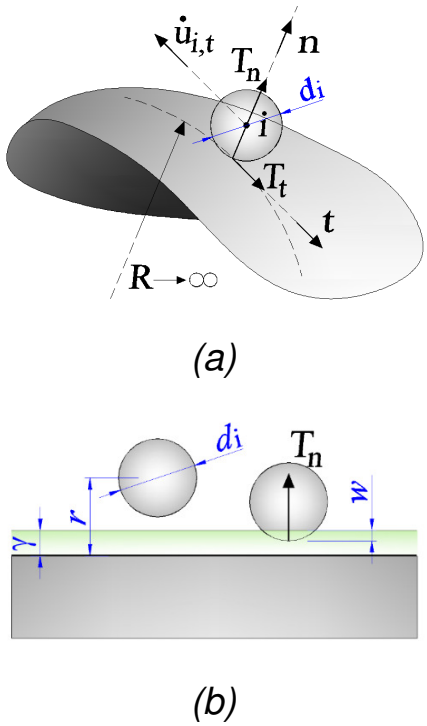

Fig. 5.9. Scheme of the forces transmitted to a particle in contact with an external boundary surface (a). Scheme of the approach used to attenuate the forces produced by the impact of the particle with an elastic boundary (b).

In order to avoid possible numerical instabilities due to the high value of the contact force given by Eqs (5.26, 5.27) when a very stiff plane is considered, the contact force co-penetration w relation can be attenuated by introducing a smoothing function $\chi(w)$ for the contact stiffness:

$$K_n(w) = \chi(w) \cdot K_n \ , \quad 0 \le \chi(w) = (w/\gamma)^{1/m} \le 1, \quad m > 1 \tag{5.28}$$

The above relation corresponds to assume that the interaction with the boundary takes place when the particle touches a layer having a small

thickness γ superposed to the surface; the contact force increases progressively up to the final co-penetration depth *w* (Fig.5.9b).

It can be observed that the potential function concept adopted for the particles interaction, can be used also to describe the particle-boundary phenomenon, i.e. the forces acting on a particle due to the contact with an elastic boundary can be described through a suitable potential with an influence radius for the impacting particle *i* equal to $r_{\text{infl}} = r_i + \gamma$ (see Eq. (5.20)).

The case of solid or granular materials colliding with others elastic solids or boundaries can be treated exactly in the same way, by simply using the proper force potential.

Generally, in the examples presented in Chapter 6, a soft layer with relative thickness equal to $\gamma / r_i = 0.1$ and $m = 2$ are adopted for the numerical simulations.

5.4 Model implementation

5.4.1 Equation of motion and time integration algorithm

The governing equations of the discretized problem under dynamic conditions can be written as:

$$-\mathbf{M}\,\ddot{\mathbf{x}} + \mathbf{F}_i + \mathbf{F}_d + \mathbf{F}_e + \mathbf{F}_b = \mathbf{0} \quad \text{or} \quad \mathbf{M}\ddot{\mathbf{x}} = \mathbf{F}_T \tag{5.29}$$

where $\mathbf{M}$ is the mass matrix, $\ddot{\mathbf{x}}$ is the vector of the particles center acceleration (the rotation degrees of freedom are herein neglected), while

$\mathbf{F}_i, \mathbf{F}_d, \mathbf{F}_e$ are the internal force vector evaluated through the adopted potential force, the damping force vector and the external force vector, respectively. Finally, the force vector $\mathbf{F}_b$ represents the eventual actions transmitted by the collision of the particle with the elastic boundaries.

5.4.2 Damping of particles interaction

The numerical simulation of the dynamic interaction of particles can benefit by the presence of damping effects that helps in maintaining a stable evolution of the phenomenon; since most of the constitutive laws do not contain any velocity-related damping, it is convenient to introduce a so-called numerical damping [11]. The main feature of the numerical damping is the introduction of forces leading to a reduction of the particle velocity, i.e. the particle is subjected to a force responsible for an acceleration opposite to its current velocity.

In this context, Cundall [9] proposed the following expression for the numerical damping force $\mathbf{F}_d$:

$$\mathbf{F}_d = -\lambda_d \cdot \mathbf{F} \cdot \mathrm{sgn}\left(\mathbf{F} \cdot \dot{\mathbf{x}}\right) \tag{5.30}$$

where $\lambda_d, \mathbf{F}, \dot{\mathbf{x}}$ are the damping coefficient, the actual force acting on the particle and the particle velocity, respectively.

5.4.3 Numerical integration in the time domain

In the above paragraphs it has been explained as each particle is subjected to generalized forces deriving from the interactions with other bonded

particles, contact with boundaries, colliding particles, damping effects, etc.. The knowledge of the force vector enables to integrate the equations of motion for each particle separately, without the need to solve a huge system of equations, as typically required when the stiffness matrix (in the context of implicit methods) is adopted; explicit methods, despite being conditionally stable with respect to the adopted time step value, are normally preferred with respect to implicit ones in particles simulations due to their memory saving properties.

Among explicit methods, the so-called leapfrog method or Verlet integration scheme [35], is frequently adopted for numerical problems in which the trajectories of particles (such as in molecular dynamics simulations and computer graphics) is required. Such integration method provides a satisfactory numerical stability property, provides time-reversibility and preservation of the symplectic form on phase space. Its name derives from the fact that even derivatives of position are known at on-step points, whereas odd derivatives are known at mid-step points.

The procedure determines the particle acceleration at the current time step k as:

$$\ddot{\mathbf{x}}_{i,k} = \mathbf{F}_{T,i,k} / m_i \tag{5.31}$$

Using the second order finite difference method to approximate $\ddot{\mathbf{x}}_{i,k}$, the mean velocity vector during the time step interval $k \div k+1$ can be written as:

$$\dot{\mathbf{x}}_{i,k+1/2} = \dot{\mathbf{x}}_{i,k-1/2} + \Delta t \cdot \ddot{\mathbf{x}}_{i,k}\,, \quad \text{where} \quad \dot{\mathbf{x}}_{i,k-1/2} = \frac{\dot{\mathbf{x}}_{i,k} - \dot{\mathbf{x}}_{i,k-1}}{\Delta t} \tag{5.32}$$

is the mean velocity during the previous time interval $k-1 \div k$.

The position vector of particle i at time step $k+1$ can be finally written as:

$$\begin{aligned} \mathbf{x}_{i,k+1} &= \mathbf{x}_{i,k} + \Delta t \left(\dot{\mathbf{x}}_{i,k-1/2} + \Delta t \cdot \ddot{\mathbf{x}}_{i,k} \right) \quad \text{or} \\ \mathbf{x}_{i,k+1} &= \mathbf{x}_{i,k} + \Delta t \cdot \dot{\mathbf{x}}_{i,k+1/2} \end{aligned} \tag{5.33}$$

Positions of particles are thus known at time instants $t_k = k \cdot \Delta t$, while velocities are known at time instants $t_{k\pm1/2} = (k \pm 1/2) \cdot \Delta t$.

The leapfrog integration scheme can be used, with some proper adjustments, also for the evaluation at discrete intervals of the rotation position, velocity and acceleration of non-spherical particles.

5.4.4 Stability in explicit integration

A numerical model consisting of *N* degrees of freedom contains *N* natural frequencies and corresponding mode shapes. Mathematically, natural frequencies and mode shapes are eigenvalues and eigenvectors, respectively. Since explicit integration is conditionally stable, the theory of spectral stability shows that the time step Δt should satisfy

$$\Delta t < \frac{2}{\omega_{\max}} \left(\sqrt{1-\xi^2} - \xi \right) \tag{5.34}$$

for linear viscous damping, where ξ is the fraction of critical damping at ω_{max}, which is the highest natural frequency of the mesh. Mass proportional damping can be implemented implicitly if the mass matrix is diagonal, although this improves the time step only marginally since mass proportional damping decreases at higher frequencies. Nonetheless, if mass proportional damping is used and is treated implicitly, then Eq. 5.34 applies where ξ is the fraction of critical damping at ω_{max} due to stiffness proportional damping only.

The leapfrog integration scheme can be used, with some proper adjustments, also for the evaluation at discrete intervals of the rotation position, velocity and acceleration of non-spherical particles. Typically, admissible timestep size Δt in DEM simulation is obtained from the eigenfrequency of a couple of particles, $\Delta t = \alpha \cdot \sqrt{m / K}$, where the minimum ratio m / K among all the particles constituting the discretized body must be considered and $\alpha < 1$ is a proper constant [36].

References

[1] W.A. Curtin, R.E. Miller, (2003) Atomistic/continuum coupling in computational materials science, *Modelling Simul. Mater. Sci. Eng*. 11 R33–R68.

[2] K. Ohno, K. Esfarjani, Y. Kawazoe (2000), Ab Initio to Monte Carlo Methods, *Computational Materials Science*, Springer Series in Solid-State Sciences.

[3] B. Liu, Y. Huang, H. Jiang, S. Qu, K.C. Hwang, (2004), The atomic-scale finite element method, *Comput. Methods Appl. Mech. Engng*. 193 1849–1864.

[4] B. Liu, H. Jiang, Y. Huang, S. Qu, M.-F. Yu, (2005), Atomic-scale finite element method in multiscale computation with applications to carbon nanotubes, *Physical Rev*. B 72 035435.

[5] W.G. Hoover, (2007), Computational physics with particles – nonequilibrium molecular dynamics and smooth particle applied mechanics, *Comput. Meth. Sci. Tech.* 13 83–93.

[6] V. Yamakov, E. Saether, E.H. Glaessgen, (2008) A New Concurrent Multiscale Methodology for Coupling Molecular Dynamics and Finite Element Analyses, NASA/TM-2008-215328.

[7] X. Zeng,· X. Wang,· J.D. Lee,· Y. Lei, (2010), Multiscale modeling of nano/micro systems by a multiscale continuum field theory, *Comput Mech* 47 205–216.

[8] V.R. Coffman, J.P. Sethna, G. Heber, M. Liu, A. Ingraffea, N.P. Bailey, E.I. Barker, (2008), A comparison of finite element and atomistic modelling of fracture, *Modelling Simul. Mater. Sci. Eng.* 16 065008.

[9] P.A. Cundall, O.D.L. Strack, (1979), A discrete numerical model for granular assemblies, *Geotechnique* 29 47–65.

[10] P.G. De Gennes, (1999), Granular matter: a tentative view, *Reviews of Modern Physics* 71 S374–S382.

[11] G.A. D'Addetta, F. Kun, E. Ramm, (2002), On the application of a discrete model to the fracture process of cohesive granular materials, *Granular Matter* 4 77–90.

[12] C.H. Rycroft, K. Kamrin, M.Z. Bazant, (2009), Assessing continuum postulates in simulations of granular flow, *J. Mech. Phys. Sol*. 57 828–839.

[13] M. Wojtkowski, J. Pecen, J. Horabik, M. Molenda. (2010), Rapeseed impact against a flat surface: Physical testing and DEM simulation with two contact models, *Powder Technology* 198 61–68.

[14] M. Obermayr, K. Dressler, C. Vrettos, P. Eberhard, (2011), Prediction of draft forces in cohesionless soil with the Discrete Element Method, *J. Terramechanics* 48 347–358.

[15] M. Obermayr, K. Dressler, C. Vrettos, P. Eberhard, (2013), A bonded-particle model for cemented sand, *Comp. and Geotechnics* 49 299–313.

[16] J. Kleinert, B. Simeon, M. Obermayr, (2014), An inexact interior point method for the large-scale simulation of granular material, *Comp. Meth. App. Mech. Engng* 278 567–598.

[17] A. Tasora, M. Anitescu, (2010), A convex complementarity approach for simulating large granular flows, *J. Comp. Nonl. Dyn*. 5 1–10.

[18] E. Oñate, (2011), Particle-Based Methods: Fundamentals and Applications, Springer Science & Business Media.

[19] R. Aubry, S.R. Idelsohn, E. Oñate, (2005), Particle finite element method in fluid mechanics including thermal convection-diffusion, *Comput. & Struct*. 83 1459–1475.

[20] A. Krivtsov, (2003), Molecular dynamics simulation of impact fracture in polycrystalline materials. *Meccanica* 38 61–70.

[21] F.A. Gilabert, A.M. Krivtsov, A. Castellanos, (2006), A Molecular Dynamics Model for Single Adhesive Contact, *Meccanica* 41 341–349.

[22] G. Wang, M. Ostoja-Starzewski, (2005), Particle modelling of dynamic fragmentation-I: theoretical considerations, *Comput. Mat. Sci*. 33 429–442.

[23] E. Onate, S.R. Idelson, F. Del Pin, R. Aubry, (2004), The particle finite element method. An overview, *Int. J. Comput. Meth.* 1 267–307.

[24] V.R. Coffman, J.P. Sethna, G. Heber, M. Liu, A. Ingraffea, N.P. Bailey, E.I. Barker, (2008), A comparison of finite element and atomistic modelling of fracture, *Modelling Simul. Mater. Sci. Eng*. 16 1–15.

[25] S. W. Attaway, B. A. Hendrickson, S. J. Plimpton, D. R. Gardner, C. T. Vaughan, K. H. Brown, M. W. Heinstein, (1998), A parallel contact detection algorithm for transient solid dynamics simulations using PRONTO3D, *Comput. Mech.* 22 143–159.

[26] T. Belytschko, Y.Y. Lu, L. Gu, (1994), Element-free Galerkin methods, *Int. J. Numer. Methods Eng*. 37 229–256.

[27] L.D. Libersky, A.G. Petschek, A.G. Carney, T.C. Hipp, F.A. Allahdadi, (1993), High strain Lagrangian hydrodynamics - A threedimensional SPH code for dynamic material response, *J. Comput. Phys*. 109 67–75.

[28] W.K. Liu, S. Jun, Y.F. Zhang, (1995),Reproducing kernel particle methods, *Int. J. Numer. Meths. Fluids* 20, 1081-1106.

[29] P.M. Morse, (1930), Diatomic molecules according to the wave mechanics. II. Vibrational levels*, Phys. Rev.* 34 57–64.

[30] W.K. Liu, S. Jun, D. Qian, (2005), Computational Nanomechanics of Materials. in Handbook of Theoretical and Computational Nanotechnology, in M. Rieth and W. Schommers (Eds.), American Scientific Publishers, Stevenson Ranch, CA.

[31] M.S. Daw, S.M. Foiles, M.I. Baskes, (1993), The embedded-atom method: a review of theory and applications, *Mat. Sci. Rep. 9* 251–310.

[32] K.L. Johnson, K. Kendall, A. D. Roberts, (1971), Surface energy and the contact of elastic solids, *Proc. R. Soc. London A* 324 301–313.

[33] K.L. Johnson, (1985), Contact mechanics, Cambridge University Press.

[34] N. Brilliantov, F. Spahn, J. Hertzsch, T. Pöshel, (1996), Model for collision in granular gases, *Phys. Rev. E* 53 5382–5392.

[35] L. Verlet, (1967), Computer Experiments on Classical Fluids. I. Thermodynamical Properties of Lennard–Jones Molecules, *Phys. Rev.* 159 98–103.

[36] O'Sullivan C., Bray J.D, (2004), Selecting a suitable time step for discrete element simulations that use the central difference time integration scheme, *Engineering Computations* 21 278–303.

Chapter 6

NUMERICAL APPLICATIONS

6.1 Introduction

The numerical analysis, illustrated in the following paragraphs, simulate different cases of compact and granular solids. In some cases, the use of the real elastic parameters of brittle solids (such as concrete…) in the constitutive equation would result in extremely small time steps in the integration of the dynamic equations determining very high computational cost. In order to prevent this, in some case where the main interest is to study the large deformations, brittle fragmentation, granular flows etc.., from a qualitative point of view an artificial smaller elastic modulus is used.

6.2 Elastic cantilever beam under impulsive load

In order to verify the accuracy of the developed particle method in modelling elastic solids, the simple problem of the dynamic response of a cantilever beam subjected to an impulsive load applied to its free end is herein considered (Fig. 1a). The beam is supposed to have an elastic modulus equal to $E = 5 \cdot 10^9 Pa$, Poisson's ratio $\nu = 0.1$ and mass density equal to 2400

kgm^{-3}. The beam dimensions are assumed as those employed for the beam considered in paragraph 6.2, while the concentrated load F is assumed to vary according to the relation $F(t) = F_0 \cdot f_i(t)$, where $F_0 = 1000N$ and the impulsive functions $f_i(t)(i = 1,2)$ are represented in Fig. 6.1b; a negligible damping of the system has been considered.

The force potential described in Chapter 5 has been used to describe the interaction forces inside the beam's particles by adopting an influence distance of the discrete elements particles equal to $r_{infl} = 2d$.

2D plane stress FE analyses have been used for comparison with the particle method approach; in Fig. 6.1c the time histories of the vertical displacement of point A, located at the free edge of the beam, are represented for both the FE (250 quadrilateral quadratic elements have been used to discretized the beam) as well as for the 3D PM model (that considers the beam discretized through about 1200 particles, arranged in cubic fashion, Fig. 6.1a) under the two assumed impulsive loads.

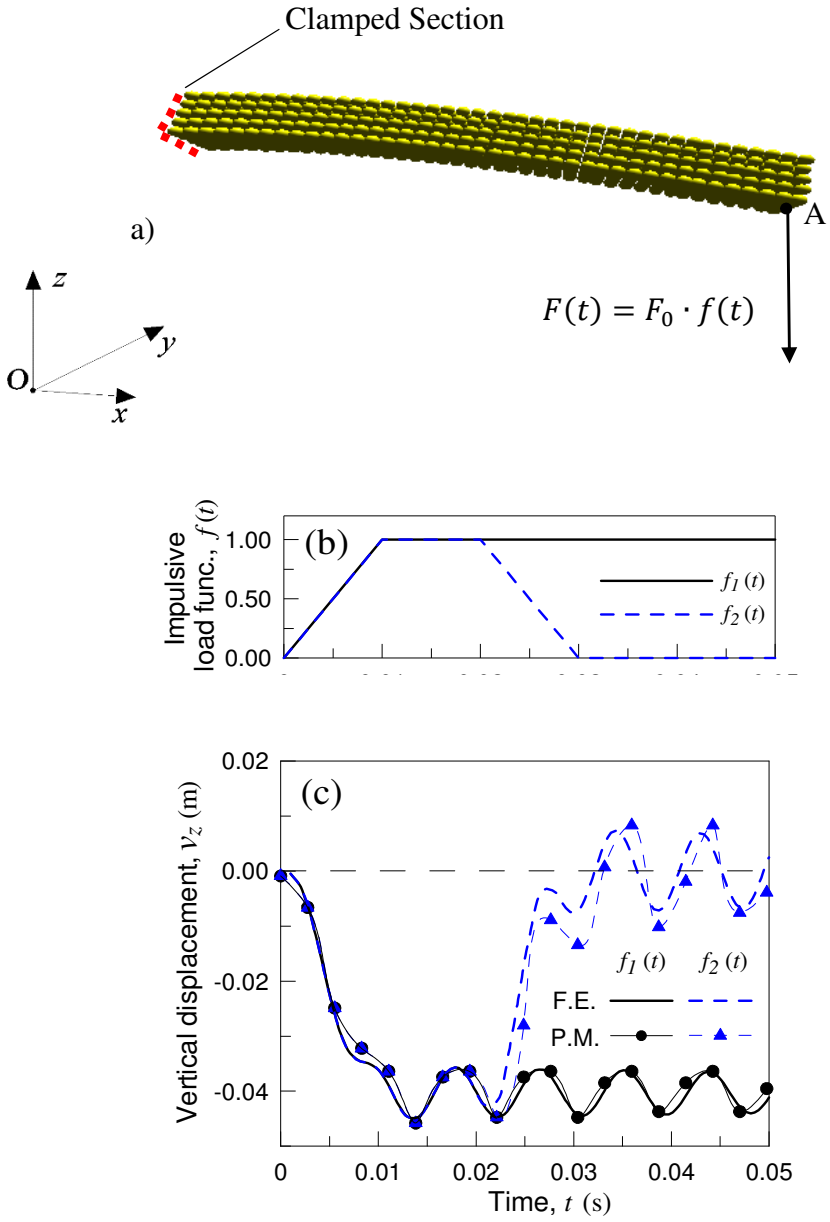

Fig. 6.1 - Cantilever beam under impulsive load (a); load functions (b) and time histories of the free edge vertical displacement at point A (c) .

As can be observed the discrete approach provides results that are in satisfactory agreement with the FE results, in term of magnitude of displacements as well as of period of oscillation, confirming the good capability of the developed PM approach to correctly represent the dynamic behavior of an elastic body.

6.3 Impact of an elastic body on a cantilever beam

In the present example the impact of a cubic elastic body on a cantilever beam is considered; the falling cube has an initial velocity equal to v_0 and is located above an elastic cantilever beam at a distance H, while its horizontal position with respect to the beam is given by the distances c and d. Both bodies are assumed to be in the gravitational field acting in the vertical direction, $-z$. The material of the beam is supposed to be brittle with an elastic modulus equal to $E = 3 \cdot 10^6 Pa$ and a tensile strength equal to $f_t = 2 \cdot 10^5 Pa$, while the force potential described in Chapter 5 has been used to quantify the interaction forces inside the two solids and between the different bodies, by adopting an influence distance of the particles equal to $r_{infl} = 2d$ and $r_{infl} = d$ for the beam and the falling body, respectively. In some cases the tensile strength of the cantilever beam is considered to have higher values to prevent its failure and to study the different responses of the impact between the beam and the falling body.

Below the described mechanical system, an elastic ($E = 3 \cdot 10^{10} Pa$) flat horizontal boundary plane surface π – lying on the x-y plane – is assumed to be placed at a distance h from the bottom of the beam (Fig. 6.2). In the numerical particle approach the beam is modelled through 1200 spheres (arranged in a cubic lattice with diameters assumed to be normally distributed

with a mean value equal to 5mm and variance 0.1mm) while the falling body is supposed to have an elastic modulus equal to $E = 3 \cdot 10^7 Pa$ and a very high tensile strength to avoid failure. The geometry of the system is characterised by $L = 10a$, $H = a$ and $h = 5a/2$, while the falling body is assumed to be initially located in a position identified by: i) $c = a, d = 0$; ii) $c = a/2, d = 5a$; iii) $c = a/2, d = 0$. The initial velocity of the falling body has been assumed equal to $v_0 = 3m/s$ and $5m/s$.

It must be emphasised as the elastic constants of the bodies have been assumed very small, with respect to real materials, to get large displacements in the structure in order to underline the geometrical nonlinear feature of the computational algorithm. The mass density of the beam has been assumed equal to 2400 kgm^{-3}, while the falling block density has been assumed equal to 7800 kgm^{-3}. The time integration procedure has been conducted by using a time step amplitude $\Delta t = 5\mu s$ (the analysis duration has been extended up to 0.4s).

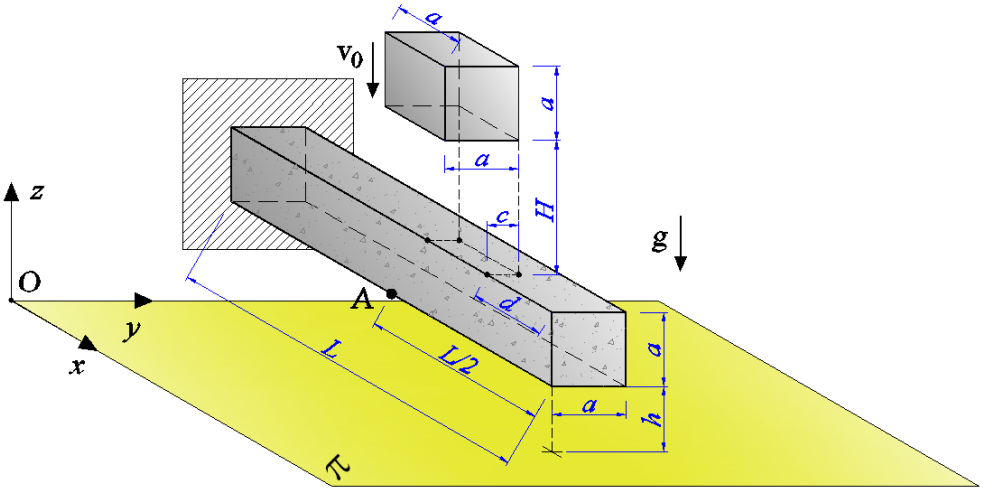

Fig. 6.2. Cubic elastic body falling on a cantilever beam: geometry of the system.

Case *i*) Impact at the beam extremity with failure

In Fig. 6.3 and Fig. 6.4 the configuration for the falling case i) at three time instants is shown for the two cases $v_0 = 3m/s$ (Fig. 6.3a, b, c) and $v_0 = 5\ m/s$ (Fig. 6.4a, b, c). It can be noted as the initially slower falling block causes a local rupture of the beam in the impacted zone and the failure of the restrained cross section of the beam while only the local failure takes place for the case $v_0 = 5\ m/s$, since the shock elastic wave produced in the beam is lower in the second case because of the suddenly failure of the impacted part of the beam.

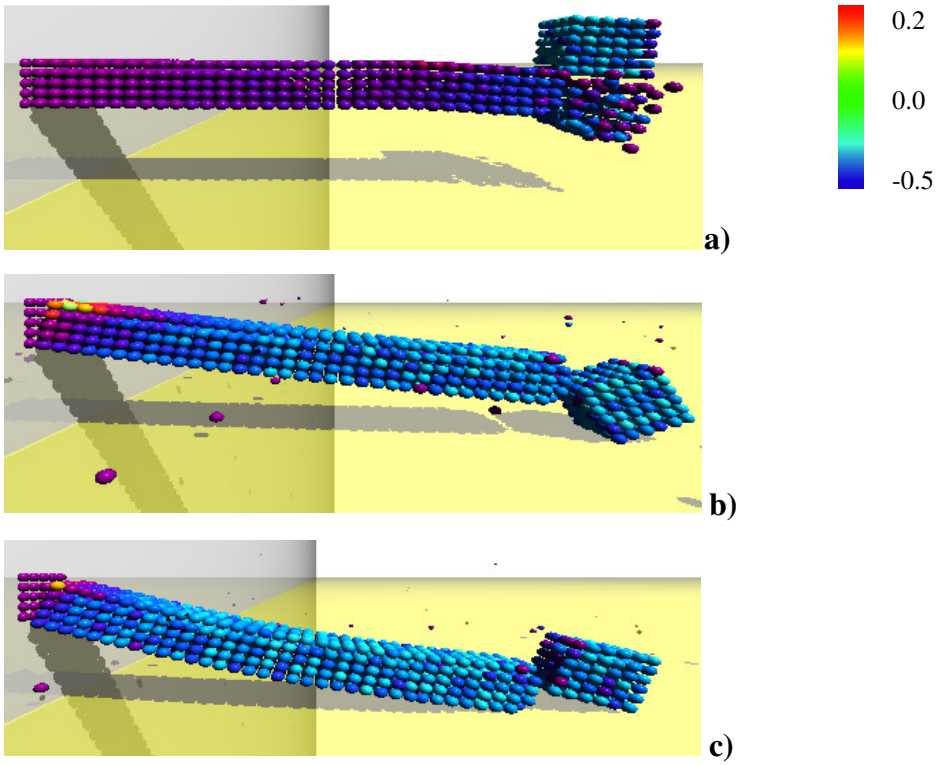

Fig. 6.3. Beam configuration at different time steps, falling body $v_0 = 3m/s$ a) t = 0.016s, b) t = 0.200s, c) t = 0.400s. Color scale indicates the strain values in the beam axis direction

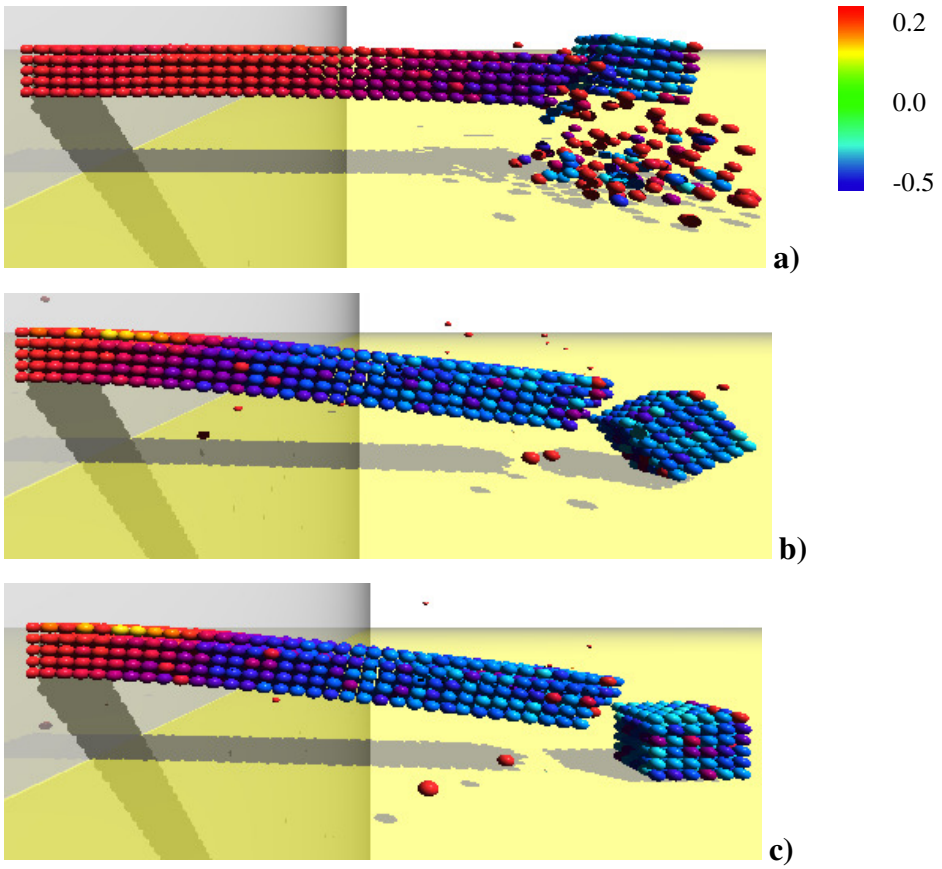

Fig. 6.4. Beam configuration at different time steps, falling body $v_0 = 5m/s$ a) t = 0.016s, b) t = 0.200s, c) t = 0.400s.Color scale indicates the strain values in the beam axis direction

Case *ii*) Impact along the beam span with failure

In Fig. 6.5 and Fig. 6.6 the bumped beam for the case ii) is shown; it can be noted as the falling block produces a local failure of the beam leading to two separated parts. As in the previous case, for $v_0 = 3m/s$ the restrained cross section failure occurs (Fig. 6.5 c), while this is not the case when $v_0 = 5m/s$ (Fig. 6.6 b), i.e. the slower falling block causes a local rupture of the

beam in the impacted zone and the failure of the restrained section, while only the local failure takes place for the case $v_0 = 5m/s$.

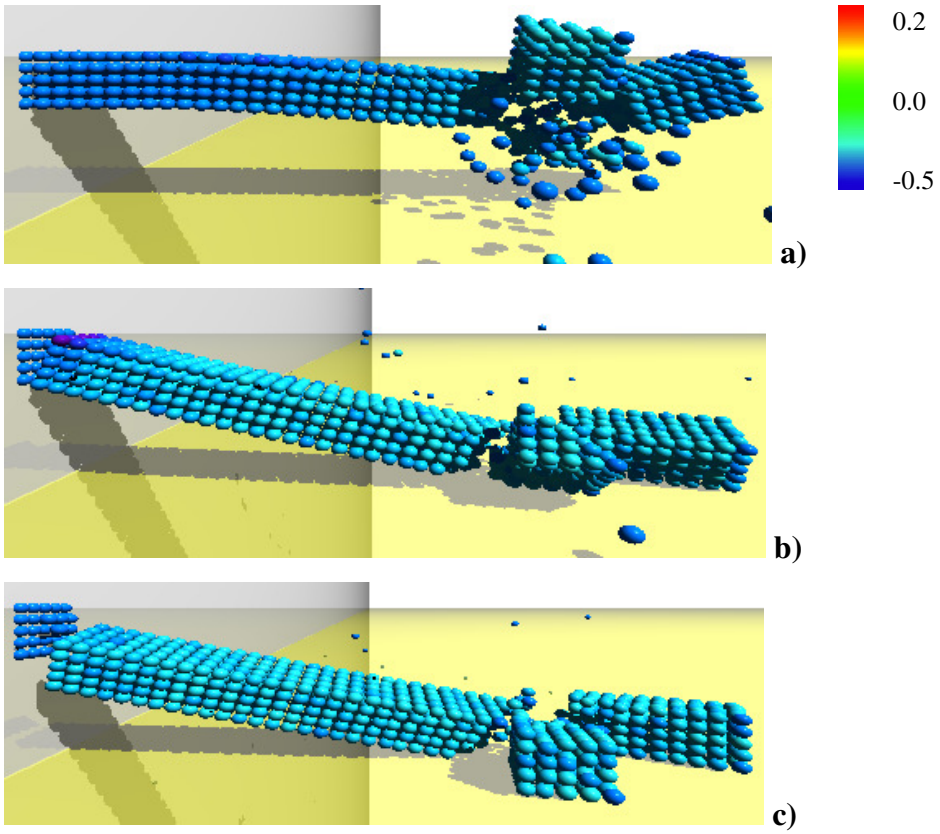

Fig. 6.5. Beam configuration at different time steps, falling body $v_0 = 3m/s$ a) t = 0.016s, b) t = 0.200s, c) t = 0.400s. Color scale indicates the strain values in the beam axis direction

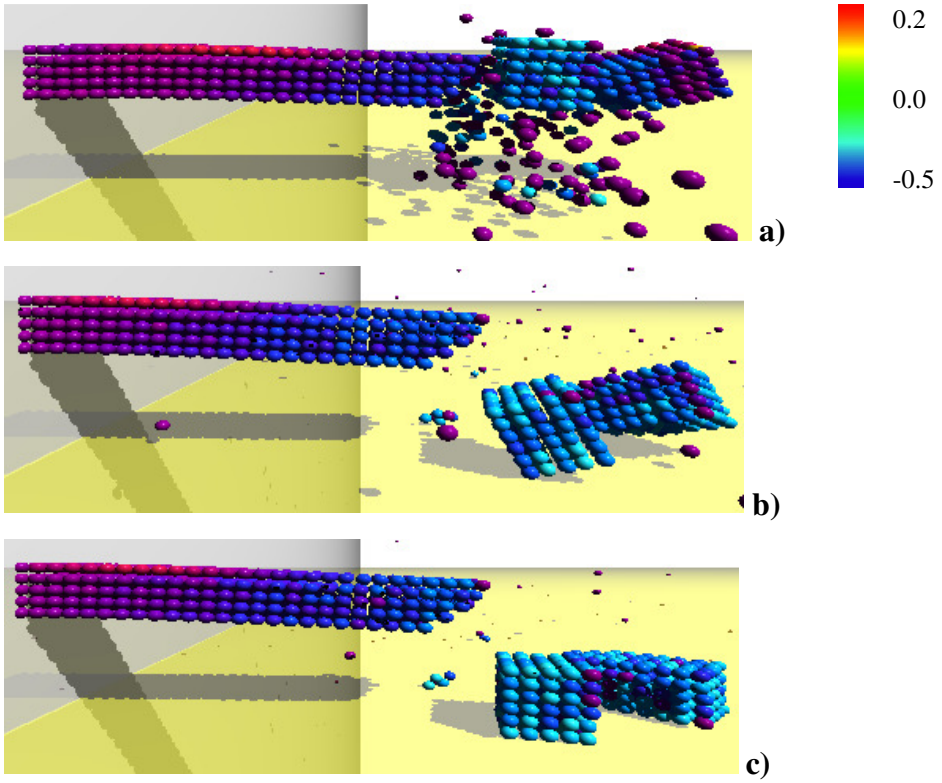

Fig. 6.6. Beam configuration at different time steps, falling body $v_0 = 5m/s$ a) t = 0.016s, b) t = 0.200s, c) t = 0.400s. Color scale indicates the strain values in the beam axis direction

Case *i*) Impact at the beam extremity without failure

In Fig. 6.7 and Fig. 6.8 the configuration for the falling case i) without failure of the beam, at three time instants is shown for the two cases $v_0 = 3m/s$ (Fig. 6.7a, b, c) and $v_0 = 5m/s$ (Fig. 6.8a, b, c). It can be noted as the slower falling block, $v_0 = 3m/s$, causes a dynamic response to the impact different from the faster falling block, $v_0 = 5m/s$.

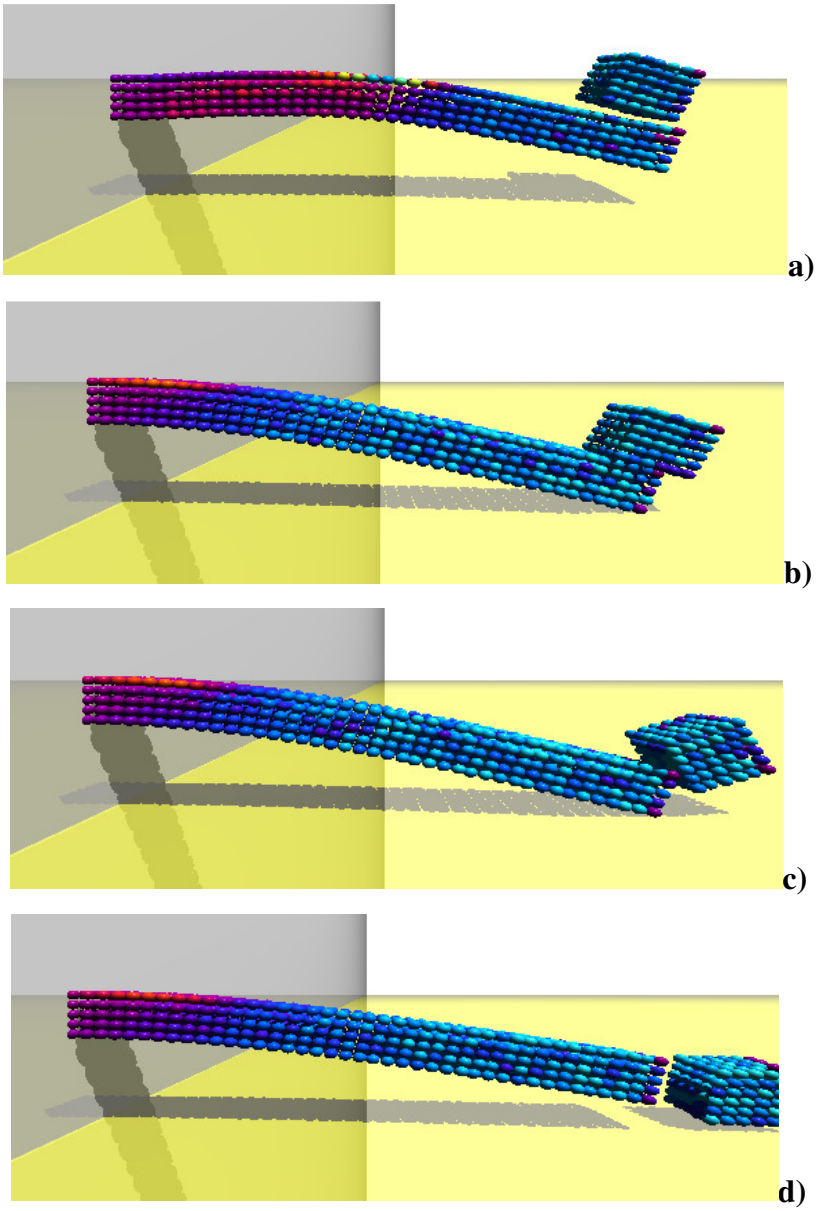

Fig. 6.7. Beam configuration at different time steps, falling body $v_0 = 3m/s$ *a) t = 0.024s, b) t = 0.240s, c) t = 0.420s, d) t = 0.600s*

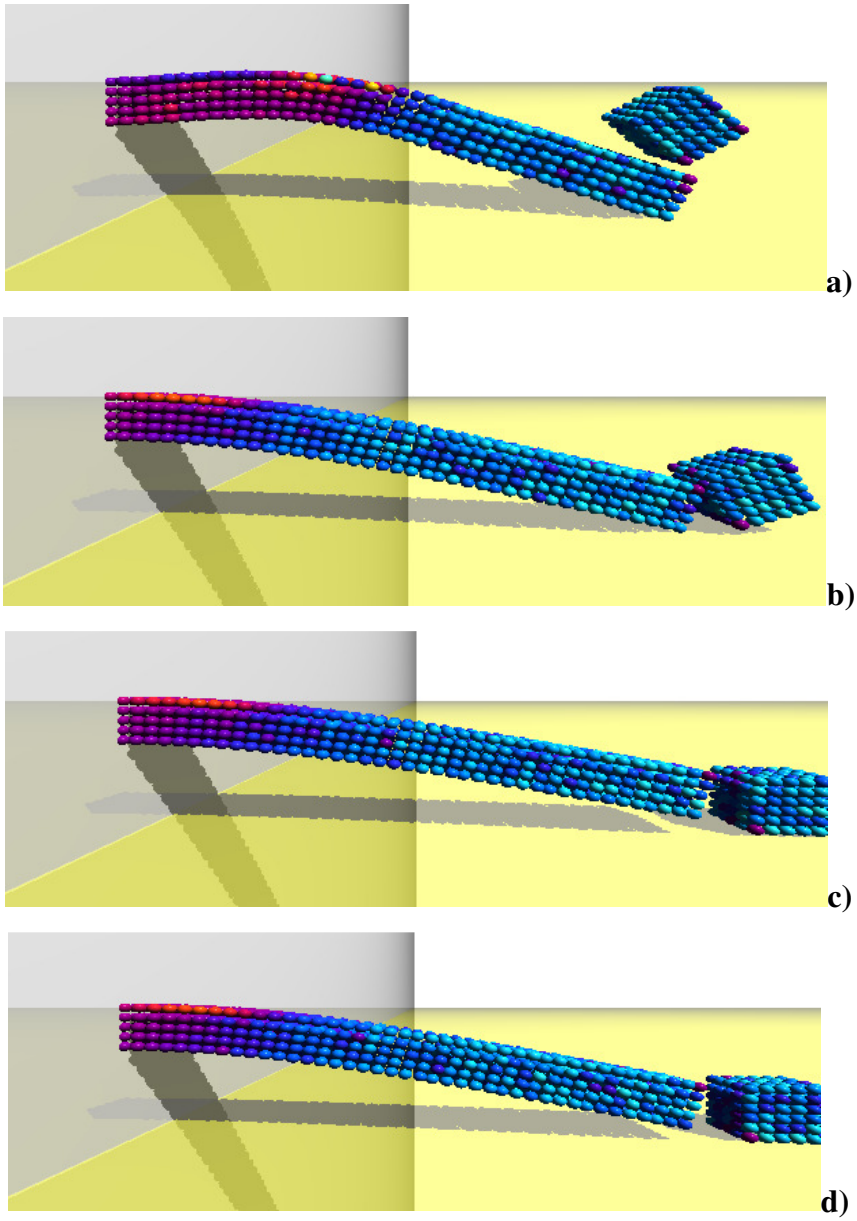

Fig. 6.8. Beam configuration at different time steps, falling body $v_0 = 3m/s$ *a) t = 0.024s, b) t = 0.240s, c) t = 0.420s, d) t = 0.600s*

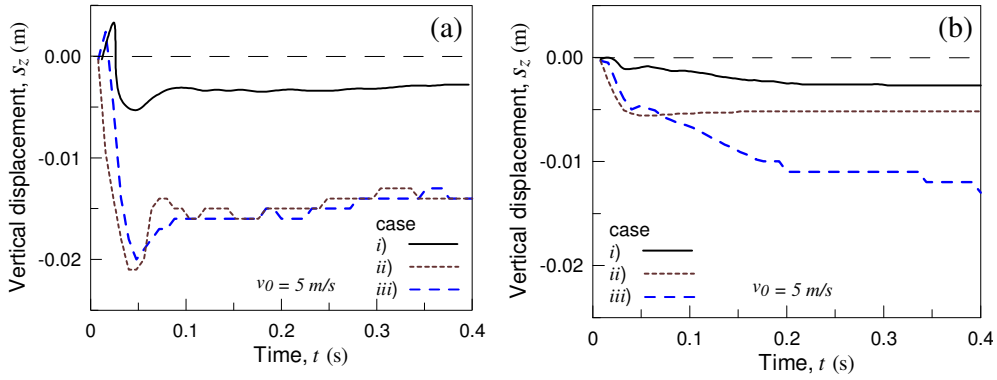

Fig. 6. 8₁. Time history of the vertical displacement of point A (Fig. 6.2): elastic beam without failure (a), elastic beam with failure (b) for three different initial positions of the falling block (i), ii) and iii)) and $v_0 = 5m/s$.

In Fig. 6.8₁ the time history of the vertical displacement of point A, placed on the middle beam section (Fig. 6.2), is shown for three different initial positions of the falling block for both the cases of beam without failure (Fig. 6.8₁a) and with failure (Fig. 6.8₁b); it can be noted as the displacement is lower in the case of beam allowed to fail while it is more pronounced for elastic beam without break.

Impact along the span of a cracked beam

In Fig. 6.9 the bumped beam is assumed to contain a crack placed in L/10 along the beam span having a depth equal to L/20, while the case i) with falling bodies velocity $v_0 = 5m/s$ is considered.

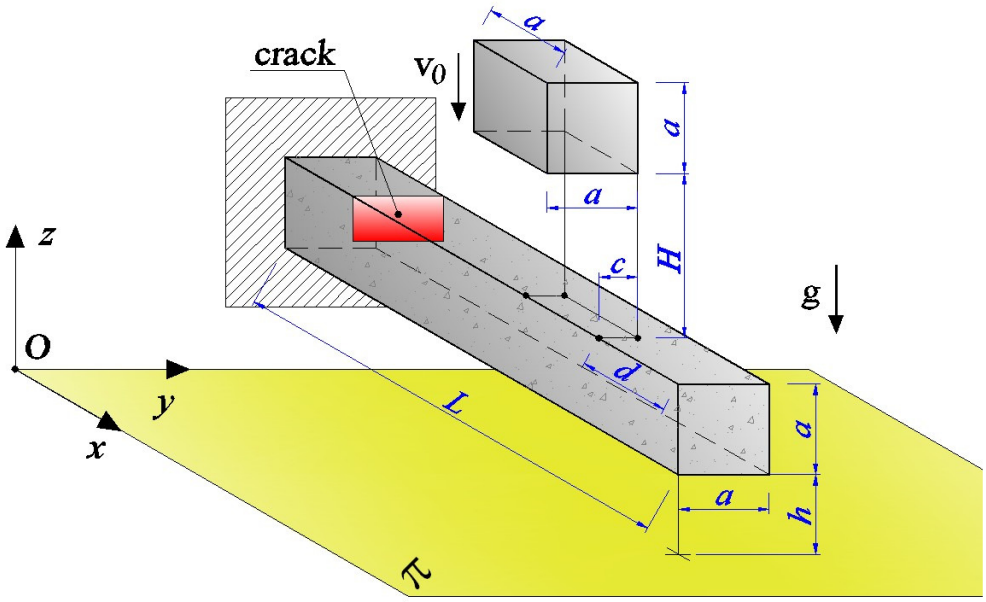

Fig. 6.9. Cubic elastic body falling on a cantilever cracked beam: geometry of the system

In Fig.6.10 are reported some instants of the impact phenomenon, it can be noted as the falling block produces a local failure of the beam leading into two separated parts; such behavior is different from that of then the cantilever beam without crack considered above (§6.3).

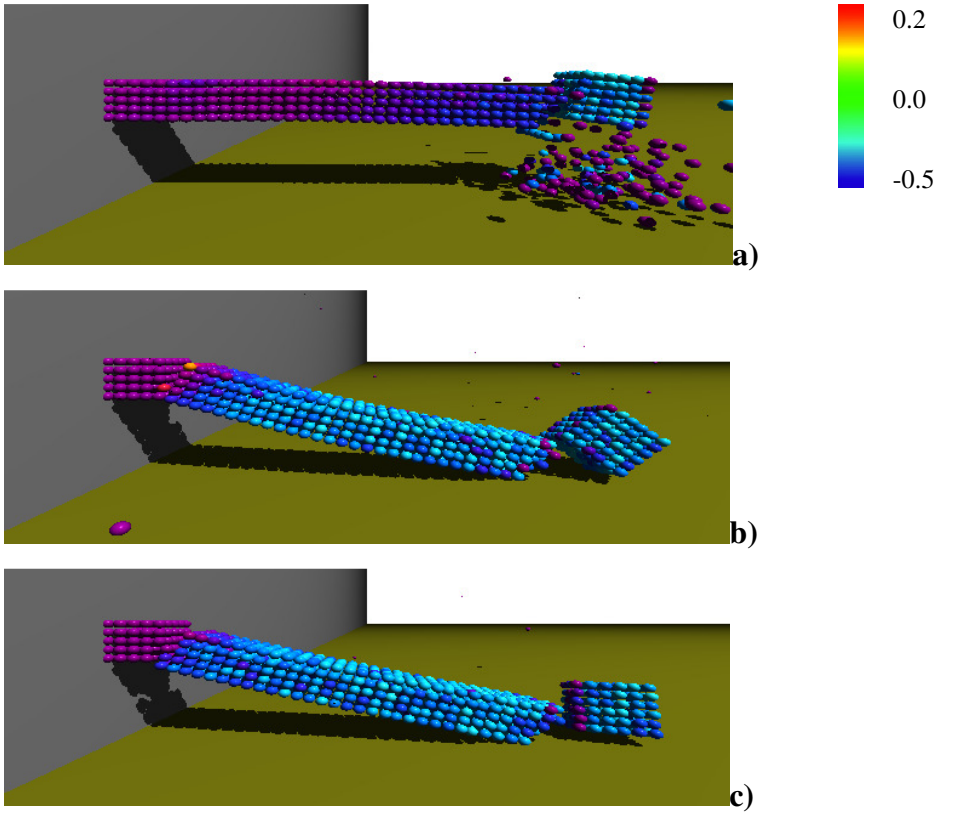

Fig. 6.10. Beam configuration at different time steps, falling body $v_0 = 5m/s$ a) t = 0.016s, b) t = 0.200s, c) t = 0.400s. Color scale indicates the strain values in the beam axis direction

6.4 Plain concrete beam under impact load

In the present example, the case of a simply supported plain concrete beam (body labelled 1 in Fig. 6.11) under impact load presented in [1]. The system is characterised by the reference size $b = 0.3m$, while the mechanical properties of the materials are as follows: elastic modulus $E = 3 \cdot 10^{10} Pa$, Poisson's ratio $\nu = 0.18$, tensile strength $f_t = 2.7 \cdot 10^6 Pa$ and mass density

equal to 2300 kgm^{-3} for the concrete material, while the falling hammer (body labelled 2 in Fig. 6.11) is supposed to be made of steel (with elastic modulus $E = 2 \cdot 10^{11} Pa$, mass density equal to 8000 kgm^{-3}). The system is modelled with about 2200 particles with cubic arrangement and radius equal to 35mm.

The impact velocity of the steel mass has been assumed to be equal to $v_0 =$ 2,4,6 and $8 m/s$. The force potential has been used to quantify the particles interaction by adopting an influence distance of the particles equal to $r_{infl} = 2d$ and a time step increment for the dynamic analysis equal to $\Delta t = 6 \mu s$.

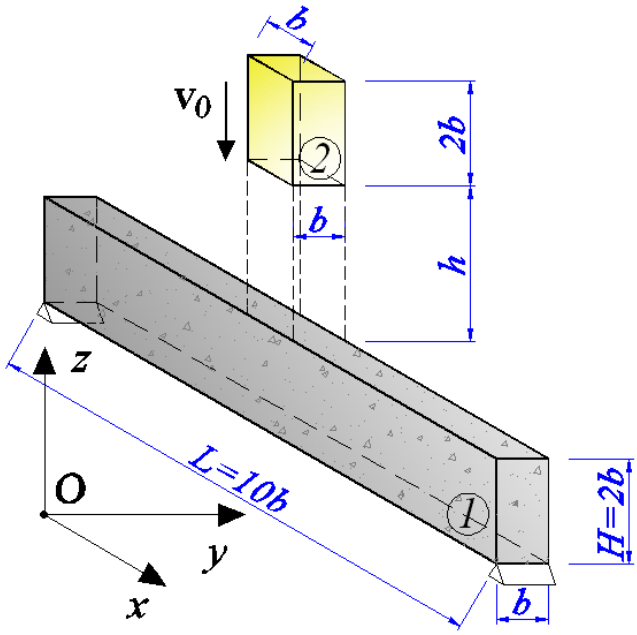

Fig. 6.11. Simply supported plain concrete beam under impact load [1].

In Fig. 6.12 the configuration of the system at different time instants is reported; in particular the initial development of the elastic wave propagating inside the beam is shown in Fig. 6.12a, while the failure pattern at t=0.125 s after the first impact is represented in Fig. 6.12b. As can be observed a wedge-

like failure mechanism takes place, responsible for the detachment of a wide bottom portion of the beam. A diffused separation of the bottom part of the beam can be also acknowledged. In Fig.6.12c the time history of the reaction force is displayed and compared with the FE results, provided in [1], obtained through a FE smeared crack band method where the contact is simulated through a Lagrangian multiplier algorithm.

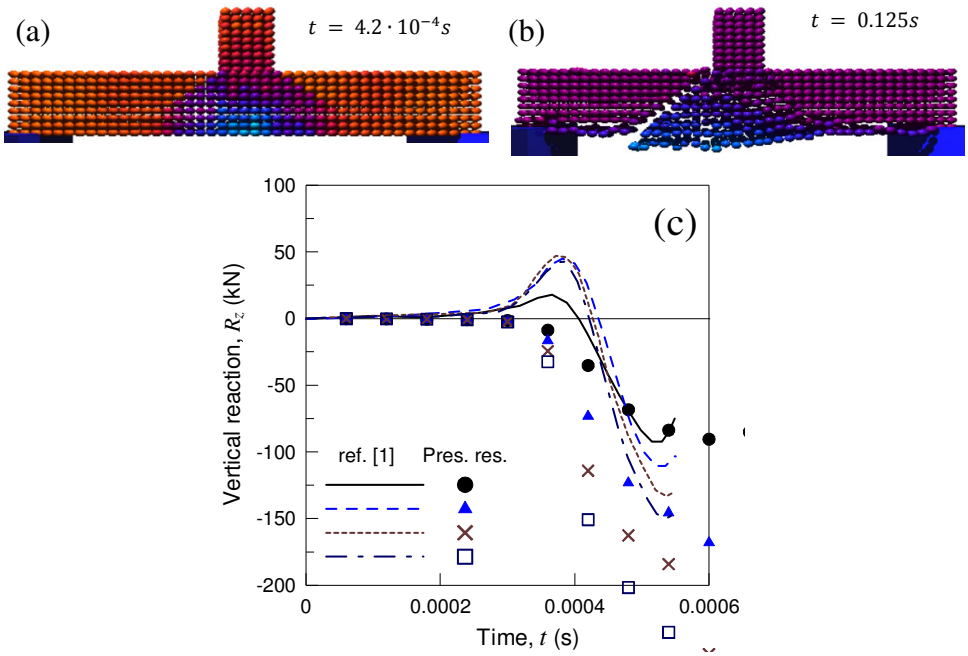

Fig. 6.12. Elastic wave propagation (a), failure pattern (b) for the case $v_0 = 2 \cdot m/s$ and time history of the reaction force at the beginning of the impact phenomenon (c) for $v_0 = 2,4,6,8 \cdot m/s$.

As can be noted the reactions obtained by using the particle method approach are fairly close to the FE results, despite these two approaches are very different and the time interval of observation so short; after a first time interval equal to about $30ms$, where the reaction is practically zero due to the

time required by the elastic wave to propagate from the hit zone to the support, such boundary force raises very quickly. Higher impact speed correspond to higher reaction force value.

In the following images some configurations at different instants after the impact between the two bodies are reported, for two cases: a) impact velocity $v_0 = 2\ m/s$ falling height $h_0 = 204mm$, b) velocity $v_0 = 4\ m/s$ falling height $h_0 = 805mm$.

In the present case an impact velocity equal to $v_0 = 2\ m/s$ and falling height $h_0 = 204mm$ is considered.

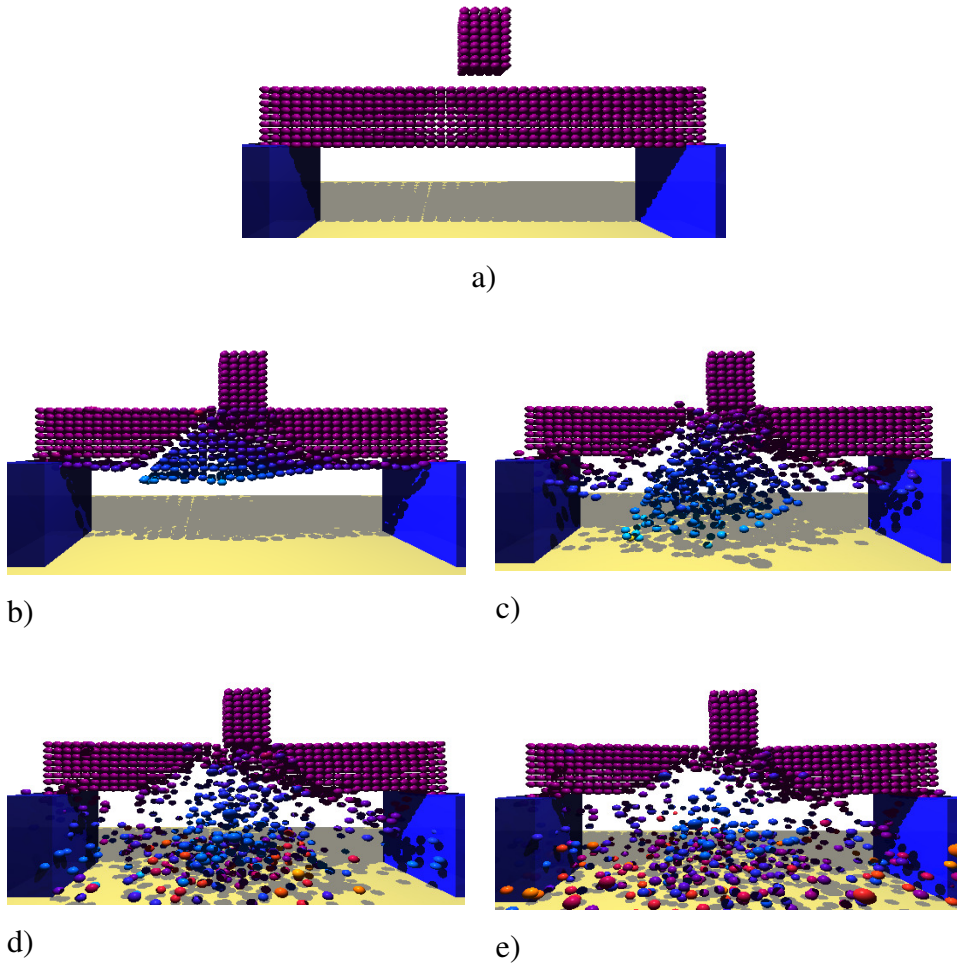

Fig. 6.13 - Simply supported plain concrete beam under impact load Case a) t = 0, different configurations after the first impact, b) t = 0.125s, c) t = 0.25s, d) t = 0.375s, e) t = 0.5s

In the following case the assumed impact velocity is equal to $v_0 = 4\ m/s$ while the falling height is $h_0 = 805mm$.

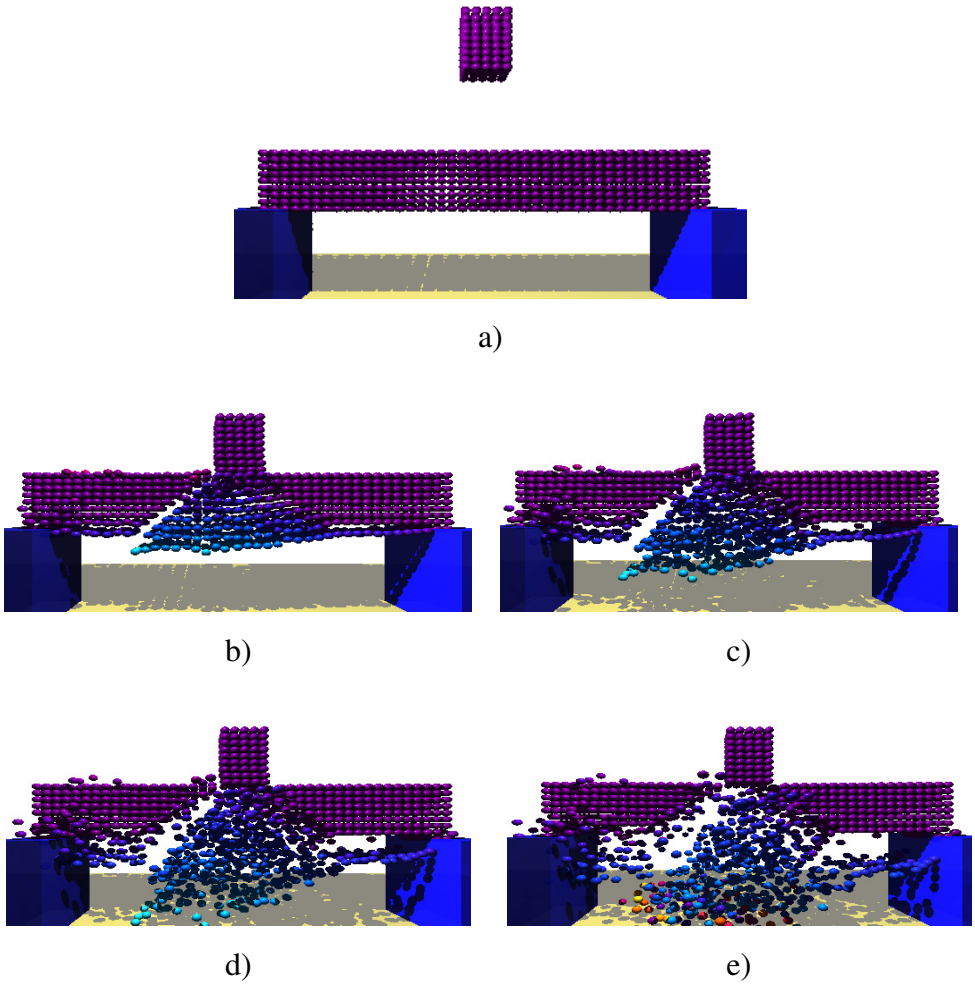

Fig. 6.14 - Simply supported plain concrete beam under impact load Case a) t = 0; different configurations after the first impact, a) t = 0.45s, b) t = 0.495s, c) t = 0.54s, d) t = 0.6s

In both cases beam fragmentation presents a triangular shape; since the falling body do not hit the beam exactly at the centerline, the developed failure pattern is not perfectly symmetric with respect the two supports.

In [1] this problem is analyzed with a continuous FE model by determining the stress and damage state in the beam; however, with the discrete model it is also possible to calculate great displacements and dislocations that produce beam fragmentation.

These two cases underline a different impact behavior: in the first case (lower velocity), the breakage marginally involves the beam zones over the supports, while this is not the case with impact velocity equal to $v_0 = 4\ m/s$

6.5 Granular flow in a hopper

This example considers the flow of a granular material in a hopper with elastic walls. An initial cubic volume of particles (Fig. 6.15) under the gravity action is assumed to be placed inside the upper left hand side of the hopper. A horizontal plane, placed at the position z_0, is assumed to exist below the particles; the simulation consists in removing instantaneously the above plane, causing the material inside the hopper to fall down. The performed dynamic analysis is aimed at determine the particles configuration at different time instants.

The material of the particles (with a mass density equal to 2000 kgm^{-3}) is supposed to have an elastic modulus equal to $E = 3 \cdot 10^6 Pa$ and a negligible tensile strength (or equivalently no cohesion for a granular matter); the force potential has been used to describe the particles interaction by adopting an influence distance of the particles equal $r_{infl} = d$.

The particles volume, occupying the initial volume V_p, is modelled through about 1400 spheres (with diameter value assumed to be normally distributed with a mean value equal to 9 mm and variance of 0.1 mm), initially arranged in a tetrahedrical fashion, while the hopper walls are supposed to have an

elastic modulus equal to $E = 3 \cdot 10^8 Pa$. The geometry of the system is depicted in Fig. 6.15.

The elastic constants of the particles have been assumed very small in order to allow a reasonable wide integration time step that has been taken equal to $\Delta t = 50\mu s \cdot 10^6 Pa$ (the analysis duration has been extended up to 2.0s); however the results, without loss of generality, provides useful qualitative information on the considered phenomenon despite these unrealistic mechanical constants. The damping coefficient for the dynamic analyses has been assumed equal to $\lambda_d = 0.20$ and the coefficients of dynamic friction μ_d, μ_{md}, (between the particles and the boundaries and between the particles, respectively) has been assumed equal to 0.0 or 0.3.

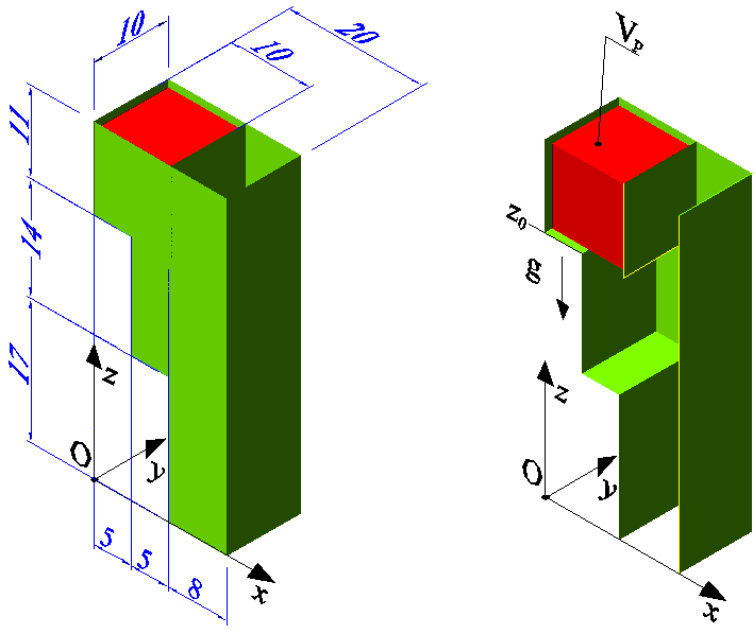

Fig.6.15. Granular material flowing down in a hopper (green: hopper walls; red: initial volume position of the granular material, V_p). Dimensions are expressed in cm.

In Fig. 6.16-17 the system configuration at three time instants (t=0.12, 0.36 and 0.8s after removing of the horizontal plane) is shown: as can be noted, initially the right hand part of the volume V_p tends to move downward approximately as a rigid block and subsequently hit the lower horizontal surface; some particles remain on this plane while others continue their motion along the hopper. Others particles bouncy on the right hand side of the hopper and, due to the presence of the left wall, proceed moving down with an increasing vertical velocity to the hopper exit. Some particles finally remain at a rest on the two horizontal planes of the hopper; the number of these particles depends on the dynamic friction value assumed for walls and particles.

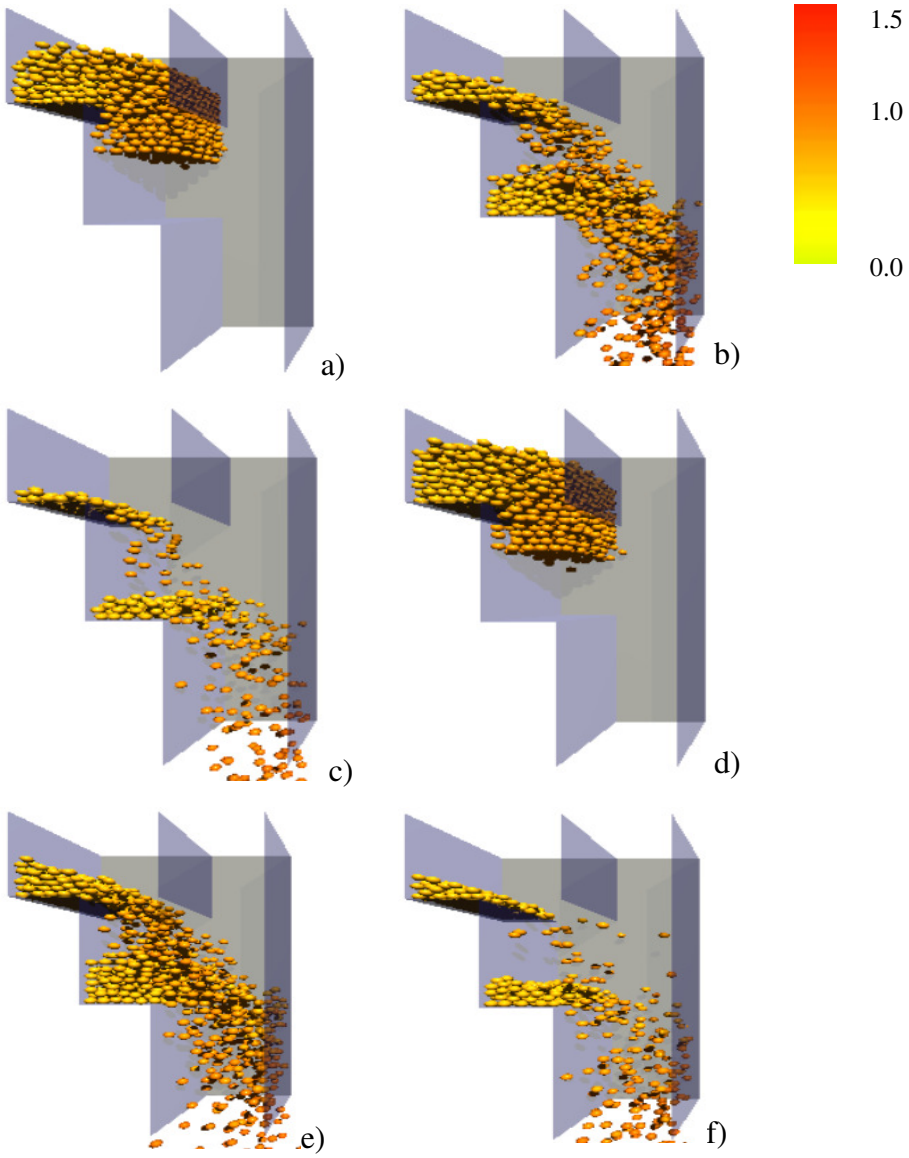

Fig.6.16. Particles configuration in the hopper at three different time steps: situation without any friction forces (a-c), for $\mu_d = 0.3$, $\mu_{md} = 0.0$ *(d-f). Colour scale indicates the downward vertical velocity of the particles in m/s.*

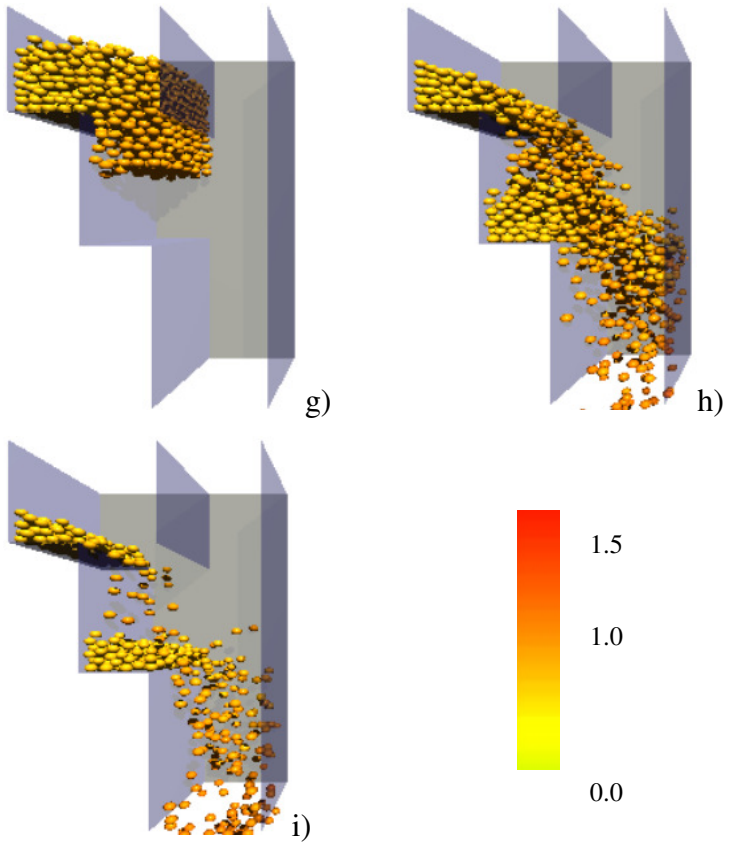

Fig.6.17. Particles configuration in the hopper at three different time steps for $\mu_d = \mu_{md} = 0.3$ *(g-i). Colour scale indicates the downward vertical velocity of the particles in m/s.*

6.6 Impact of a cylinder on a rigid plane

The present example considers the problem of an elastic cylinder (with $a = 3d, a = 6m$) falling down on a rigid plane. The cylinder is supposed to have an initial velocity $v_0 = 10m/s$ in the $-z$ direction and is subjected only to its own weight due to the gravity field acting downward (Fig.6.18). The material of the cylinder is assumed to have an elastic modulus equal to $E = 3 \cdot 10^6 Pa$, while both cases of brittle (tensile strength equal to $f_{t1} = 1 \cdot$

$10^6 Pa$, $f_{t2} = 2 \cdot 10^5 Pa$) and indefinitely elastic material (obtained by adopting a high value of the material tensile strength, $f_{t3} = 2 \cdot 10^8 Pa$) are considered.

In the numerical particle approach the cylinder is modelled through 2261 spheres (having diameter assumed to be normally distributed with a mean value equal to 0.1m and variance equal to 0.002, arranged in cubic fashion.

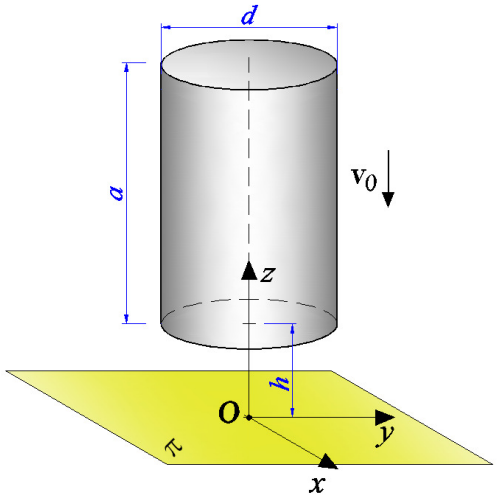

Fig.6.18 Cylindrical elastic body falling on a rigid plane.

In the first case (Fig.6.19) the material of the cylinder is assumed to have an elastic modulus equal to $E = 3 \cdot 10^6 Pa$, tensile strength equal to $f_{t1} = 1 \cdot 10^6 Pa$.

It can be notice that the brittle behavior of the cylinder produces fragmentation of the material; in particular, at the first impact, when the kinetic energy is relevant, the fragmentation of the cylinder is similar to those of a granular material. During the final phases of impact, when the kinetic

energy has decreased, fragmentation produces large blocks (or clusters) of particles of materials.

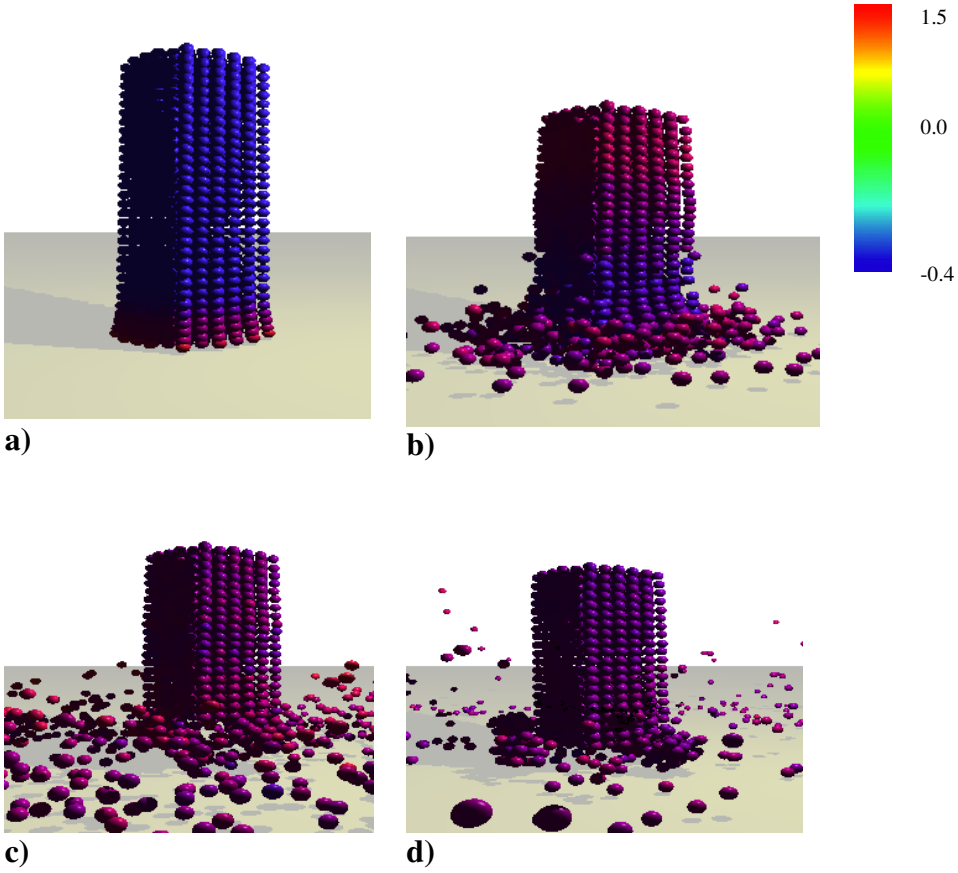

Fig. 6.19.Configuration at different time steps for failure case. a) t = 0.04, b) t = 0.20, c) t = 0.40 d) t = 0.80. Color scale indicates the vertical velocity of the particles ($v_0 = 10 m/s$).

In the second case (Fig.6.20) the material of the cylinder is assumed to have an elastic modulus equal to $E = 3 \cdot 10^6 Pa$, tensile strength equal to $f_{t2} = 2 \cdot 10^5 Pa$.

It can be notice that with such a low tensile strength, the cylinder shows a granular-like behavior.

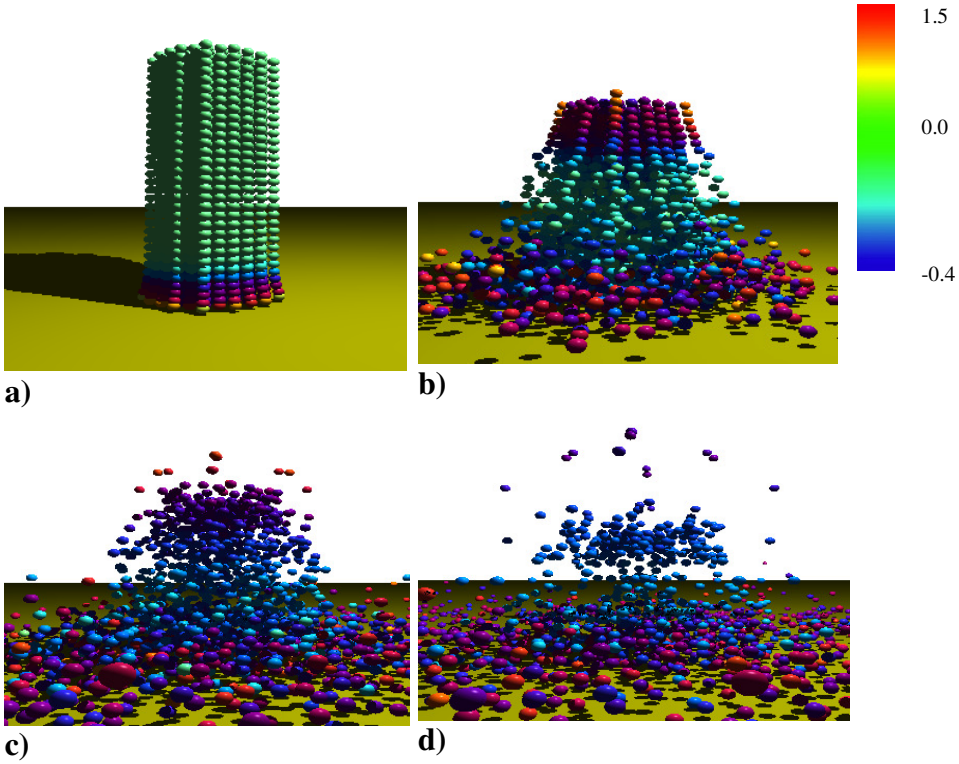

Fig. 6.20. Configuration at different time steps for failure quasi-granular case. a) t = 0.04, b) t = 0.20, c) t = 0.40 d) t = 0.80. Color scale indicates the vertical velocity of the particles

In the third case (Fig. 6.21) the material of the cylinder is assumed to have an elastic modulus equal to $E = 3 \cdot 10^6 Pa$, and a high tensile strength equal to $f_{t3} = 2 \cdot 10^8 Pa$. The choice of very high tensile strength produces an elastic behavior of the cylinder without failure or fragmentation, and the rebound of the body on the rigid plane can be noticed.

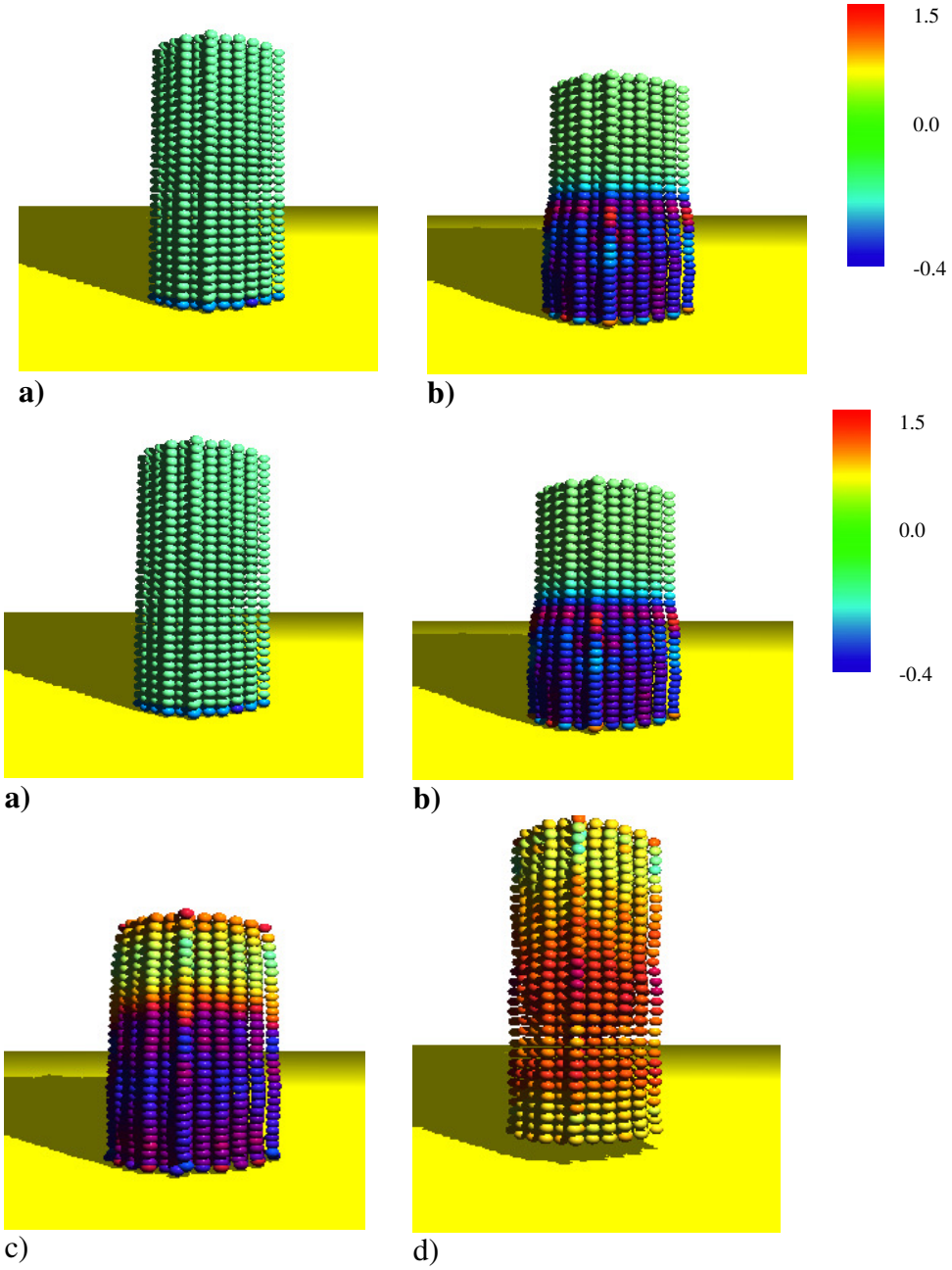

Fig. 6.21. Configuration at different time steps for failure quasi-granular case. a) t = 0.02, b) t = 0.10, c) t = 0.20 d) t = 0.40. Color scale indicates the vertical velocity of the particles

6.7 Granular material cutting simulations

This example considers a vertical flat blade between and normal to two glass panels, the blade has a constant horizontal velocity $v = 10mms^{-1}$ [2]. Particles of the model represent seed grains, because they closely resemble natural granular flow into dragline buckets. The seed grains are suitable for an easy discrete simulations because the stiffness of the grains is less than the stiffness of sand or gravel; the smaller stiffness results in a larger time step and decreases the total computing time. An initial cubic volume of particles (Fig. 6.22) under the gravity action is assumed to be placed inside a box. The vertical blade is placed at the position x_0, with vertical dimension smaller than the box vertical planes; the simulation consists in moving the blade, causing the material inside the box redistribute. The performed dynamic analysis is aimed at determining the particles configuration at different time instants.

The material of the particles (with a mass density equal to 855 kgm^{-3}) is supposed to have an elastic modulus equal to $E = 2.76 \cdot 10^6 Pa$ and a negligible tensile strength (or equivalently no cohesion); the force potential has been used to describe the particles interaction by adopting an influence distance of the particles equal to $r_{\text{infl}} = d$.

The particles volume, occupying the initial volume V_p, is modelled through about 1162 spheres with diameter with size equal to 20mm, initially arranged in a cubic fashion, while the box and the blade are supposed to have an elastic modulus equal to $E = 3 \cdot 10^8 Pa$. The geometry of the system is depicted in Fig. 6.22.

The integration time step has been taken equal to $\Delta t = 2 \cdot 10^{-1} ms$. The final blade displacement is equal to *200mm,* with an analysis duration equal

to 2.0s. The damping coefficient for the dynamic analyses has been assumed equal to $\lambda_d = 0.20$ and the coefficients of dynamic friction particle – particle and particle planes are supposed $\mu = 0.10$.

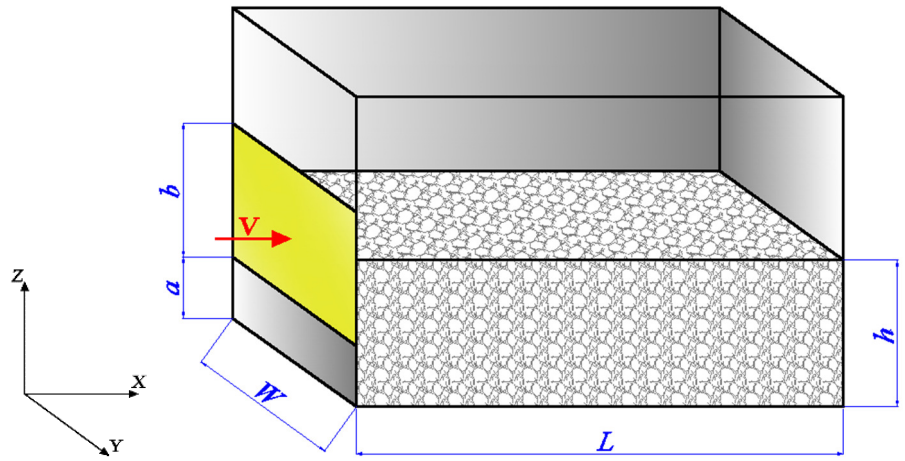

Fig.6.22. Granular material cutting [2].

The configurations of the granular material for the blade displacement equal to $10cm$ and $20cm$, are shown in Fig. 6.23; the obtained arrangement of the particles show a behavior similar to soil cutting problem analyzed in [2],

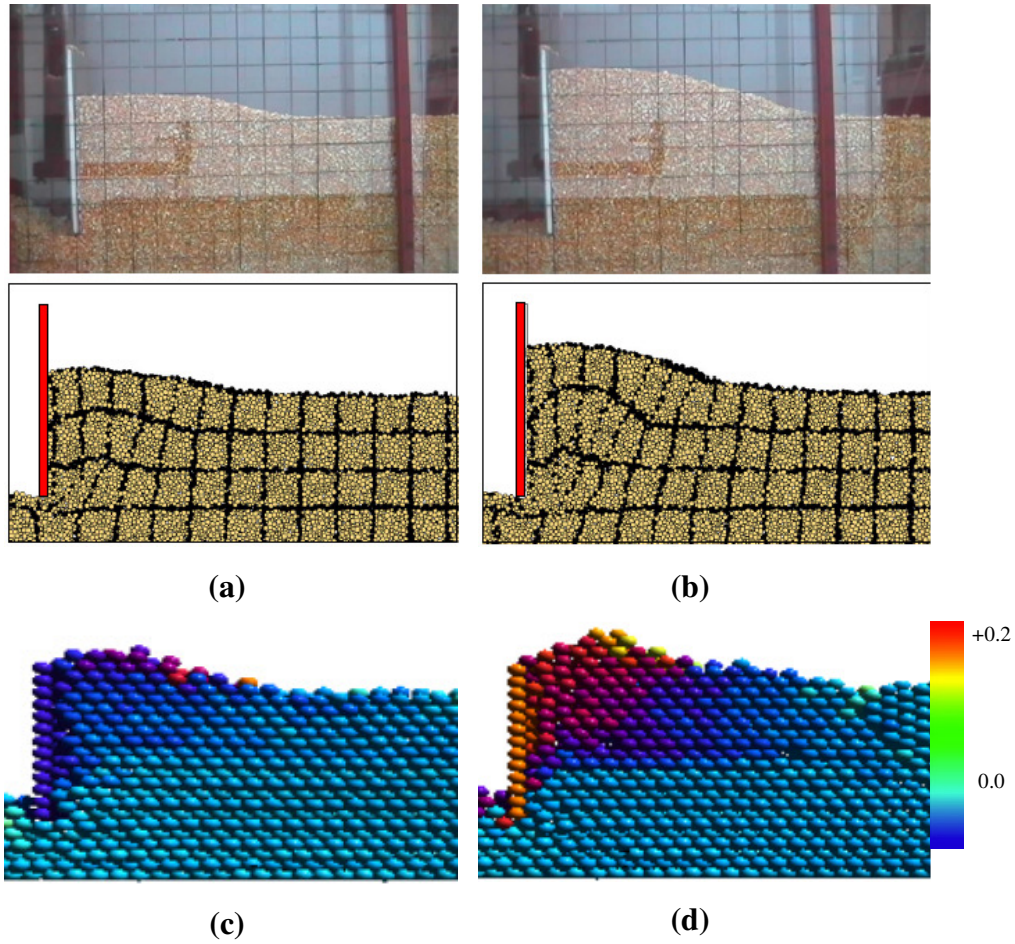

Fig. 6.23. Final configuration in Ref.[2] for: a) displacement 10cm, b) 20cm;configuration of the present particle model for c) displacement 10cm and d) displacement 20cm. Color scale indicates the horizontal displacement of the particles expressed in [m].

It is possible to note that in the present study the blade is shorter than in [2], this cause a little difference in the disposition of the particles near the blade (Fig. 6.23 c-d). Neglecting this last aspect, the shape assumed by the particles representing the granular material obtained in the present study, reflects the configuration presented in [2].

6.8 Column drop test

In this example, a column with an initial height-radius ratio of h_0/r_0 of approximately *1.51* is considered (Fig. 6.25a-c). The column is prepared by dropping particles into a box and letting them settle under gravity [3]; particles are assumed with a diameter value obeying normal distribution with a mean value equal to 18 mm and variance of 5 mm, initially arranged in a tetrahedral fashion. The number of particles is 1440, while the material of the particles has a mass density equal to 2000 kgm^{-3} and it is supposed to have an elastic modulus equal to $E = 3 \cdot 10^6 Pa$ and a negligible tensile strength (or equivalently no cohesion). The friction coefficient of the base supporting the column is $\mu = 0.5$ while smooth vertical walls, are placed beside the column. The drop test is conducted by removing the left hand side wall of the box and letting the column spread under gravity.

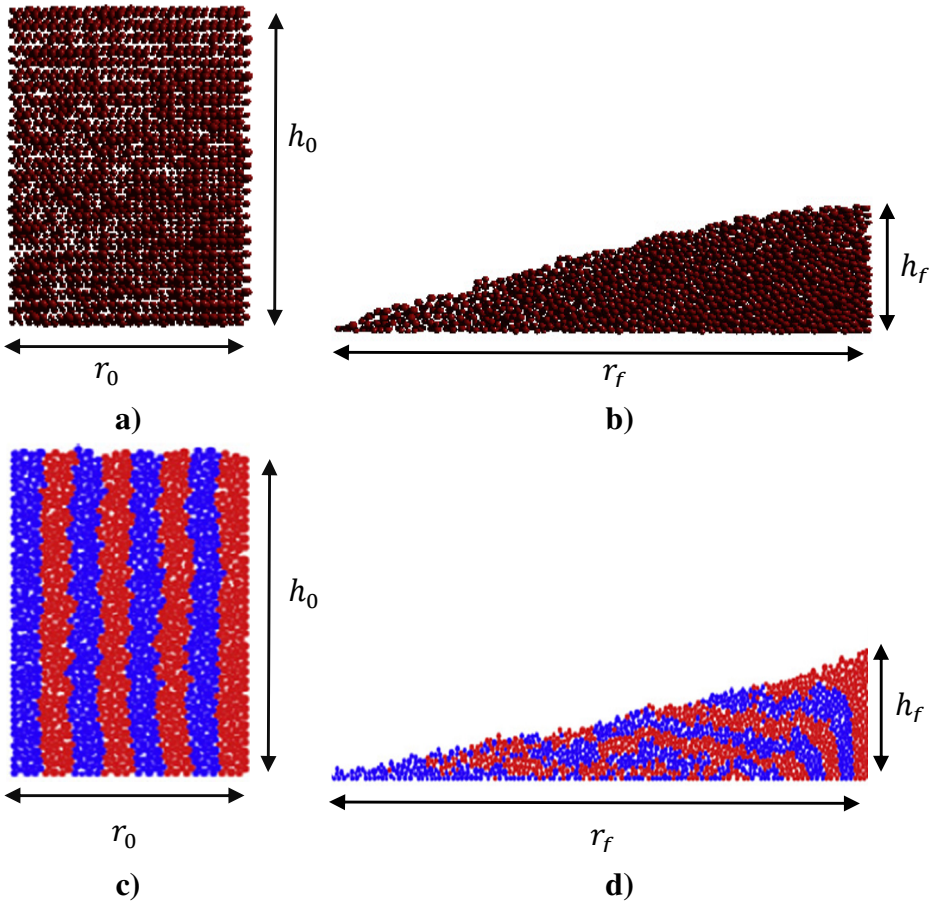

Fig. 6.25. Configuration at initial and final time instants obtained with the present study (a-b) and according to Ref.[3](c-d)

It is possible to notice a good quality agreement provided by the particle model; moreover the final configuration in [3] is characterized by the height/width ratio equal to $\frac{h_f}{r_f} = 0.2185$, while the present model provides the value $\frac{h_f}{r_f} = 0.2230$ (Fig. 6.25b).

6.9 Elastic disc falling in a bed of particles

The present example considers the problem of an elastic disc (with radius $r = 0.4m$) falling down on a bed of particles contained in a box (1.45x0.65x0.20m). The center of the disc is supposed falling from the height $h_0 = 0.95m$, with respect the bottom horizontal plane of the box and the initial velocity of the falling body is $v_0 = 5m/s$ in the $-z$ direction. It is subjected to only its own weight due to the gravity field acting downward (Fig.6.26). The material of the disc is assumed to have an elastic modulus equal to $E = 3 \cdot 10^{10} Pa$, Poisson's ratio $\nu = 0.18$, tensile strength $f_t = 2.7 \cdot 10^6 Pa$ and mass density equal to 2300 kgm^{-3}, the granular material is assumed to have an elastic modulus equal to $E = 3 \cdot 10^{10} Pa$, a negligible tensile strength and mass density equal to 1900 kgm^{-3}, particles are assumed to be initially arranged in a tetrahedral fashion.

In the numerical particle approach, the disc is modelled through 1254 spheres having diameter $d = 6cm$, the bed of particles is modelled through 1581 spheres having diameter $d = 6cm$. The integration time step has been taken equal to $\Delta t = 50\mu s$, while the analysis duration has been extended up to 1.5s.

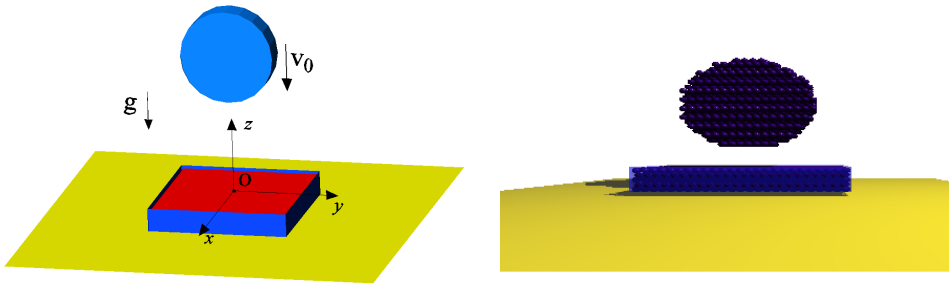

Fig.6.26 Elastic disc falling on a bed of particles. a) geometric configuration, b) discrete model.

In Fig. 6.27 the system configuration at four time instants (t=0.03, 0.12, 0.66 and 1.47s) is shown.

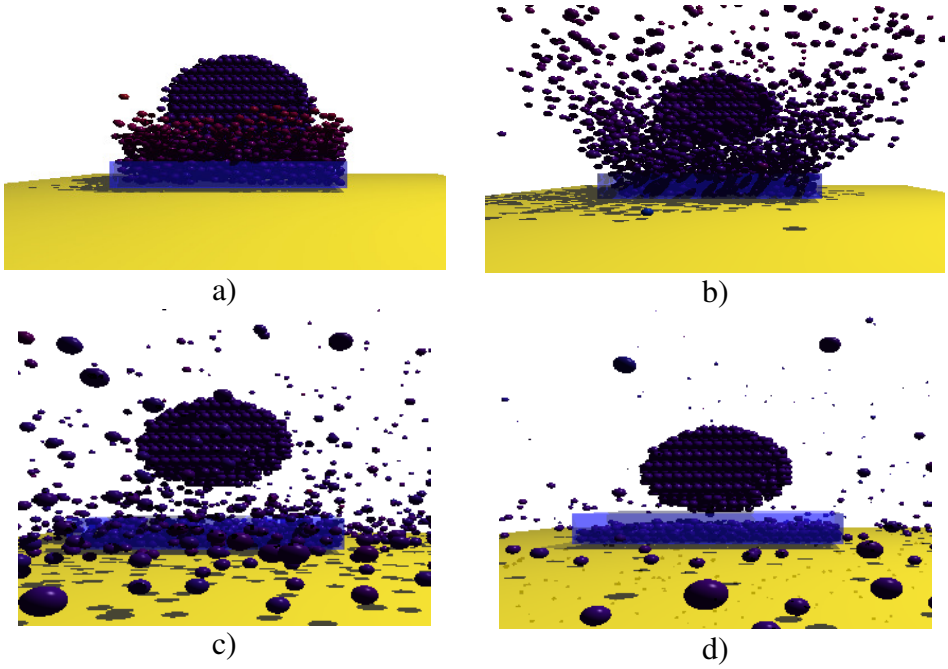

Fig. 6.27. Configuration at different time; a) t = 0.03, b) t = 0.12, c) t = 0.66 d) t = 1.47.

As can be noted granular particles contact with disc causes rebound and fracture in the disc and great displacements of the granular material, this behavior is compatible with a falling disc of concrete falling in a box of gravel. This example underlined the possibility to use the proposed method in some situations like demolitions or material delivering.

6.10 Conclusions

The case studies shown in the previous sections, demonstrate the versatility of the proposed particle method; indeed the method has been used indifferently for solid or granular materials by only setting the appropriate influence distances and mechanical properties.

Numerical results have demonstrated also a good capability to deal with large deformations problems. This aspect is fundamental to understand the versatility and superior mechanical prediction of the discrete method in opposite to continuous ones such as the finite elements method; it does not require the use of any remeshing technique or complex and computationally expensive operations to study fragmentation, clustering or large strains and deformations even under dynamic conditions.

Some examples have shown as it is possible to exploit the developed particle method also for granular-solid interaction and fragmentation problems. However it is evident as one limitation of the developed discrete method resides is the necessity to use small time steps increments leading to high computational costs.

References

[1] V. Travaš, J. Ožbolt, I. Kožar (2009), Failure of plain concrete beam at impact load: 3D finite element analysis, *Int. J. Fract. 160*, 31–41.

[2] C.J.Coetzee (2014), Discrete and continuum modelling of soil cutting, *Comp. Part. Mech.*

[3] Keng-Wit Lim, Kristian Krabbenhoft, Josè E. Andrade (2014), A contact dynamics approach to the Granular Element Method, Comput. *Method Appl. Mech. Engng* 268, 557-573

Chapter 7

CONCLUSIONS

7.1 Introduction

Although empirical equations for local damage give a reasonable prediction of quantities such as depth of penetration, they do not describe the behavior of the solids structure at different scales. In order to understand the behavior of solid or granular materials subjected to dynamic loadings or severe damages, a combination of experiments and numerical methods are needed for a complete analysis.

In this work, a discrete element method was developed as a general computer technique for unified modeling of the mechanical behavior of solid and granular materials, including the transition from solid phase to particulate phase. As a result of this research, the following contributions in the field of mechanical structure were made:

- A unified potential-based particle approach suitable for taking into account the dynamic nature and large strain characteristic of the problem;

- Failure and Fracture of brittle solids under dynamic conditions can be predicted, model not use complex remeshing procedures, stress field enrichment, discontinuous elements as in continuous approaches;
- Same formulation for both continuum-like, granular-like or mixed interaction by simply setting the nature of the forces exchanged between particles;
- Capability of the method to capture very different and complex mechanical phenomena in dynamic problems.

7.2 Convergence studies

The proposed method used a particle model based on force potentials to calculate stiffness and failure. The simulations showed very good correlation (for both the elastic behavior and fracture) with theoretical results. However, the convergence rate was not clear from the simulations performed, and it appears to have a little change depending on element arrangement (i.e. simple cubic or tetrahedral arrangement). Nevertheless, the use of potential functions to determine forces between elements of the discretized domain was very beneficial because it avoided the procedure of model calibration for a given mesh refinement, saving computational time.

7.3 Recommendation for Future Work

This work represent a first step in study of dynamic and fracture problems involving both solid and granular materials, recommendations for future research are summarized below.

In this work, only one force potential was used to study solids and granular dynamic problems, other potentials are developed inside the software but not improved with study cases; the next step will be to fit them, for instance in liquid-solid or liquid granular interactions.

It would be useful to determine the degree of variability in the results for penetration depth, scabbing thickness, and perforation thickness for similar models where the only difference is the element distribution (randomness) in the medium.

Another target in the development of the model would be to use elements of different shape to better simulate granular materials like soils and sands or for instance, in a material such as concrete, large elements would represent the aggregates and a larger number of small elements would represent the concrete matrix.

It would be beneficial to perform simulations where macroscopic mixed mode fracture is involved and compared with the numerical results along with theoretical and experimental studies to test the validity of the present approach to treat different crack orientations and modes of fracture.

The failure criteria developed in this work utilizes the material's ultimate tensile strength and the force potential used was dependent on the material's elastic modulus and distance between particles.

Each of these parameters has an important influence on the overall behavior of the model. Future research should include a parametric study to

examine the influence of each of these parameters in the penetration depth, scabbing, and overall cracking and fragmentation of the medium.

It is important to mention that thermodynamic effects were disregarded in this work. Even though it was concluded that such effects would not cause a considerable change in the numerical results, by including these effects, a better understanding of the thermo-mechanical coupling and energy released in the form of heat due to friction can be gained.

A possible continuation of this work would be to study interactions between brittle and ductile materials, as reinforced concrete or FRP and concrete to understand the effect of reinforcement on impact simulations or dynamic problems (seismic analysis, demolitions, etc…).

To fully develop confidence in the use of the proposed discrete element method for applications involving solids subjected to severe damage, small-scale validation experiments are required, so that numerical results can be compared to actual experimental results where both local and global damage can be seen and compared.